Electronic Supplementary Material (ESI) for Chemical Science.

Supplemental Information

Halogenated PETN Derivatives: Interplay Between Physical and Chemical Factors in Explosive Sensitivity

*Nicholas Lease [a] *, Kyle D. Spielvogel [a], Jack V. Davis [a], Jeremy T. Tisdale [a], Lisa M. Klamborowski [a], M. J. Cawkwell [b], Virginia W. Manner [a]*

[a] High Explosives Science and Technology, Los Alamos National Laboratory, Los Alamos, NM 87545

[b] Theoretical Division, Los Alamos National Laboratory, Los Alamos, NM, 87545

Table of Contents

Materials and Methods: Reagent 2-(bromomethyl)-2-(hydroxymethyl)propane-1,3-diol was purchased from TCI America and used as received. 2,2-bis(bromomethyl)propane-1,3-diol, 3-bromo-2,2-bis(bromomethyl)propan-1-ol, sodium iodide (99.99%), thionyl chloride and Trimethylolpropane were purchased from Sigma Aldrich and used as received. Pentaerythritol was purchased from Fisher Scientific and used as received. 2-(chloromethyl)-2-(hydroxymethyl)propane-1,3-diol was purchased from Aurora Fine Chemicals and used as received. Trifluoroacetic anhydride, nitric acid (70%), nitric acid (fuming) and sulfuric acid were purchased from Acros Chemical and used as received. Deuterated solvents (acetone d_6, chloroform d) were purchased from Acros chemical and Sigma Aldrich and used as received. ^{1}H-NMR and ^{13}C-NMR were recorded on a 400-MHz Bruker spectrometer. NMR signals were referenced to residual solvent signals in the deuterated solvents. Chromatography for certain derivatives was performed on a Standard CycloGraph™ Centrifugal Chromatography System A87-40 purchased from iChromatography using 2- and 4-mm silica plates.

Synthesis of PETN Derivatives:

3-chloro-2,2-bis(chloromethyl)propan-1-ol and 2,2-bis(chloromethyl)propane-1,3-diol: Materials were synthesized according to the following reference [1]. Isolation of the mono-chloride described was unsuccessful.

2,2-bis(iodomethyl)propane-1,3-diol (PEDI-I2-OH2): 2,2-bis(bromomethyl)propane-1,3-diol (1.68 g, 6.4 mmol), sodium iodide (7.5 g, 50 mmol) and 12 mL of DMF were added to a round bottom flask. The mixture was stirred at 100°C overnight, during that time the solution turns brown. The solution was cooled to room temperature (material solidifies) and transferred to a beaker containing a 10% by weight aqueous solution of sodium thiosulfate. The solution was stirred until all the brown color dissipates, leaving a white solid stirring in the water solution. The solid material is filtered and washed with water. Yield = (1.71 g) (75%). ^{1}H-NMR (400 MHz, $CDCl_3$) δ 1.98 (t, *J* = 5.45 Hz, 3H, *OH*), 3.29 (s, 4H, C*H*$_2$-I), 3.74 (d, *J* =5.6 Hz, 4H, C*H*$_2$-OH). ^{13}C{^{1}H}-NMR (100 MHz, $CDCl_3$) δ 11.5, 41.9, 65.0.

3-iodo-2,2-bis(iodomethyl)propan-1-ol (PEMI-I-OH3): 3-bromo-2,2-bis(bromomethyl)propan-1-ol (2.0 g, 6.2 mmol), sodium iodide (13 g, 87 mmol) and 16 mL of DMF were added to a round bottom flask. The

mixture was stirred at 115°C overnight, during that time the solution turns brown. The solution was cooled to room temperature (material solidifies) and transferred to a beaker containing a 10% by weight aqueous solution of sodium thiosulfate. The solution was stirred until all the brown color dissipates, leaving a clear oil in the stirring in the water solution. The solution was extracted with dichloromethane (3x). The combined organic layer was then washed with water (2x), dried on magnesium sulfate and filtered. The solvent was removed leaving a sticky solid material. Yield = (2.1 g) (72.5%). ^{1}H-NMR (400 MHz, $CDCl_3$) δ 3.36 (s, 6H, CH_2-I), 3.72 (d, *J* =5.6 Hz, 2H, CH_2-OH). ^{13}C{^{1}H}-NMR (100 MHz, $CDCl_3$) δ 11.0, 40.1, 64.1

General Procedure for Chloro/Bromo-PETN Derivatives: To a small beaker, fuming nitric acid (4 g) is added and cooled in an ice bath. To the cooled nitric acid, substrate (1 g) is added slowly, once fully added the solution is allowed to stir in the ice bath for 15 minutes. Sulfuric acid (4 g) is added to the suspension slowly (do not add quickly as temperature will increase rapidly). Once fully added the solution is stirred at 0°C for one hour, then warmed to room temperature and stirred for an additional hour. During the stirring white precipitate will form in the solution. After stirring the solution is poured into ice water and white precipitate can be seen floating in the water. The solid is filtered and washed with water, sodium bicarbonate solution and water again, the solid is then allowed to dry overnight. The solid is crashed into water and washed with weak base (K_2CO_3) as opposed to neutralizing the solution in solution due to the potential reaction of base with the liable nitrate ester functional groups.

2-(bromomethyl)-2-((nitrooxy)methyl)propane-1,3-diyl dinitrate (PETriN-Br): ^{1}H-NMR (400 MHz, $CDCl_3$) δ 3.53 (s, 2H, CH_2-Br), 4.58 (s, 6H, CH_2-OH). ^{13}C{^{1}H}-NMR (100 MHz, $CDCl_3$) δ 30.5, 42.2, 69.7

2,2-bis(bromomethyl)propane-1,3-diyl dinitrate (PEDN-Br2): ^{1}H-NMR (400 MHz, $CDCl_3$) δ 3.54 (s, 4H, CH_2-Br), 4.58 (s, 4H, CH_2-OH). ^{13}C{^{1}H}-NMR (100 MHz, $CDCl_3$) δ 32.2, 42.5, 70.4

3-bromo-2,2-bis(bromomethyl)propyl nitrate (PEMN-Br3): ^{1}H-NMR (400 MHz, $CDCl_3$) δ 3.56 (s, 6H, CH_2-Br), 4.59 (s, 2H, CH_2-OH). ^{13}C{^{1}H}-NMR (100 MHz, $CDCl_3$) δ 33.5, 42.9, 71.0.

2-(chloromethyl)-2-((nitrooxy)methyl)propane-1,3-diyl dinitrate (PETriN-Cl): *Starting material purchased contained 5% pentaerythritol impurity. After nitration, PETN impurity was removed by column chromatography (hexane/ethyl acetate, 95:5). ^{1}H-NMR (400 MHz, $CDCl_3$) δ 3.69 (s, 2H, CH_2-Cl), 4.58 (s,

6H, CH_2-ONO_2). $^{13}C\{^1H\}$-NMR (100 MHz, $CDCl_3$) δ 42.4, 43.1, 69.2

2,2-bis(chloromethyl)propane-1,3-diyl dinitrate (PEDN-Cl2): ^{1}H-NMR (400 MHz, $CDCl_3$) δ 3.69 (s, 4H, CH_2-Cl), 4.58 (s, 4H, CH_2-ONO_2). $^{13}C\{^1H\}$-NMR (100 MHz, $CDCl_3$) δ 43.0, 44.3, 69.52

3-chloro-2,2-bis(chloromethyl)propyl nitrate (PEMN-Cl3): ^{1}H-NMR (400 MHz, $CDCl_3$) δ 3.68 (s, 6H, CH_2-Cl), 4.57 (s, 2H, CH_2-ONO_2). $^{13}C\{^1H\}$-NMR (100 MHz, $CDCl_3$) δ 43.5, 45.5, 69.8

2,2-bis(iodomethyl)propane-1,3-diyl dinitrate (PEDN-I2) and 2-(iodomethyl)-2-((nitrooxy)methyl)propane-1,3-diyl dinitrate (PETriN-I): To a small beaker 70% nitric acid (3.0 mL) is added and then cooled to 0°C. Next trifluoroacetic anhydride (6.0 mL) dropwise and the solution is allowed to stir at 0°C for 15 min. Next 2,2-bis(iodomethyl)propane-1,3-diol (1.0 g) is added to the cooled solution slowly, upon addition of the material the solution turns a dark red. Once fully added the solution is allowed to stir at 0°C for 30 minutes and then at room temperature for 30 minutes during which precipitate can be seen forming in the solution. Next the suspension is poured into ice water resulting in an almost black precipitate. The solid is filtered and then washed with aqueous sodium bicarbonate solution. Next the solution is washed with 10% by weight sodium thiosulfate solution until the solid is white. The solid is dried and is approximately 50:50 (PEDN-I2) and (PETRIN-I). The two materials are separated using a cyclograph chromatography apparatus in which the substrates are dissolved in acetone to spot on the plate followed by a gradient of hexane and ethyl acetate to separate the materials. **(PEDN-I2)**: Yield = (0.6 g), **(PETRIN-I)**: Yield = (0.6 g). **(PEDN-I2):** ^{1}H-NMR (400 MHz, $CDCl_3$) δ 3.33 (s, 4H, CH_2-I), 4.53 (s, 4H, CH_2-ONO_2). $^{13}C\{^1H\}$-NMR (100 MHz, $CDCl_3$) δ 7.6, 39.9, 71.3. **(PETRIN-I):** ^{1}H-NMR (400 MHz, $CDCl_3$) δ 3.32 (s, 2H, CH_2-I), 4.55 (s, 6H, CH_2-ONO_2). $^{13}C\{^1H\}$-NMR (100 MHz, $CDCl_3$) δ 3.5, 41.0, 70.5

3-iodo-2,2-bis(iodomethyl)propyl nitrate (PEMN-I3): To a small beaker 70% nitric acid (3.0 mL) is added and then cooled to 0°C. Next trifluoroacetic anhydride (6.0 mL) dropwise and the solution is allowed to stir at 0°C for 15 min. Next 2,2-bis(iodomethyl)propane-1,3-diol (1.0 g) is added to the cooled solution slowly, upon addition of the material the solution turns a dark red. Once fully added the solution is allowed to stir at 0°C for 30 minutes and then at room temperature for 30 minutes during which precipitate can be seen forming in the solution. Next the suspension is poured into ice water resulting in an almost

black precipitate. The solid is filtered and then washed with aqueous sodium bicarbonate solution. Next the solution is washed with 10% by weight sodium thiosulfate solution until the solid is white. The solid is dried and is approximately 1:3:2 (PEMN-I3):(PEDN-I2):(PETRIN-I). The materials are separated using a cyclograph chromatography apparatus in which the substrates are dissolved in acetone to spot on the plate followed by a gradient of hexane and ethyl acetate to separate the materials. Yield = (0.2 g)**.** **(PEMN-I3):** ^{1}H-NMR (400 MHz, $CDCl_3$) δ 3.38 (s, 6H, C*H*$_2$-I), 4.57 (s, 2H, C*H*$_2$-ONO_2). ^{13}C{^{1}H}-NMR (100 MHz, $CDCl_3$) δ 9.6, 38.7, 72.3.

2-ethyl-2-((nitrooxy)methyl)propane-1,3-diyl dinitrate (PETriN-Methyl): To a small beaker, fuming nitric acid (4 g) is added and cooled in an ice bath. To the cooled nitric acid, 2-Ethyl-2-(hydroxymethyl)-1,3-propanediol (1 g) is added slowly, once fully added the solution is allowed to stir in the ice bath for 15 minutes. Sulfuric acid (4 g) is added to the suspension slowly. Once fully added the solution is stirred at 0°C for one hour, then warmed to room temperature and stirred for an additional hour. During the stirring the solution becomes cloudy white. The solution is then poured into ice water and a precipitate is observed however hard to filter. The suspension is extracted with dichloromethane (3x) and the combined organic layer is washed with water (3x). The organic layer is dried on $MgSO_4$ and then filtered. The solvent is removed under reduced pressure leaving a clear crystalline solid. Yield = (1.74 g) (87%). ^{1}H-NMR (400 MHz, $(CD_3)_2CO$) δ 1.05 (t, 3H, *J* = 7.6 Hz, C*H*$_3$) 1.72 (q, 2H, *J* = 7.6 Hz, CH_2-CH_3), 4.69 (s, 6H, C*H*$_2$-ONO_2). ^{13}C{^{1}H}-NMR (100 MHz, $(CD_3)_2CO$) δ 7.6, 24.0, 41.6, 72.8.

2,2-diethylpropane-1,3-diyl dinitrate (PEDN-Methyl2): To a small beaker 70% nitric acid (3.0 mL) is added and then cooled to 0°C. Next trifluoroacetic anhydride (6.0 mL) dropwise and the solution is allowed to stir at 0°C for 15 min. Next 2,2-diethylpropane-1,3-diol (1.0 g) is added to the cooled solution slowly. Once fully added the solution is allowed to stir at 0°C for 2 hours and then at room temperature for 2 hours during which the solution appears to become cloudy. The suspension is then poured into ice water resulting in a biphasic mixture of oil in the water. The oil is extracted from the water with diethyl ether (3x) and the resulting organic phase is washed with water (2x), aqueous bicarbonate solution (4x) and water (2x) again. The organic phase is dried on $MgSO_4$, filtered and the solvent is then removed leaving a clear oil. Yield = (1.52 g) (90%). ^{1}H-NMR (400 MHz, $(CD_3)_2CO$) δ 0.93 (t, 6H, *J* = 7.6 Hz, C*H*$_3$)

1.52 (q, 4H, *J* = 7.6 Hz, CH_2-CH_3), 4.69 (s, 4H, C*H*$_2$-ONO_2). $^{13}C\{^1H\}$-NMR (100 MHz, $(CD_3)_2CO$) δ 7.2, 24.0, 40.6, 74.8.

NMR Data:

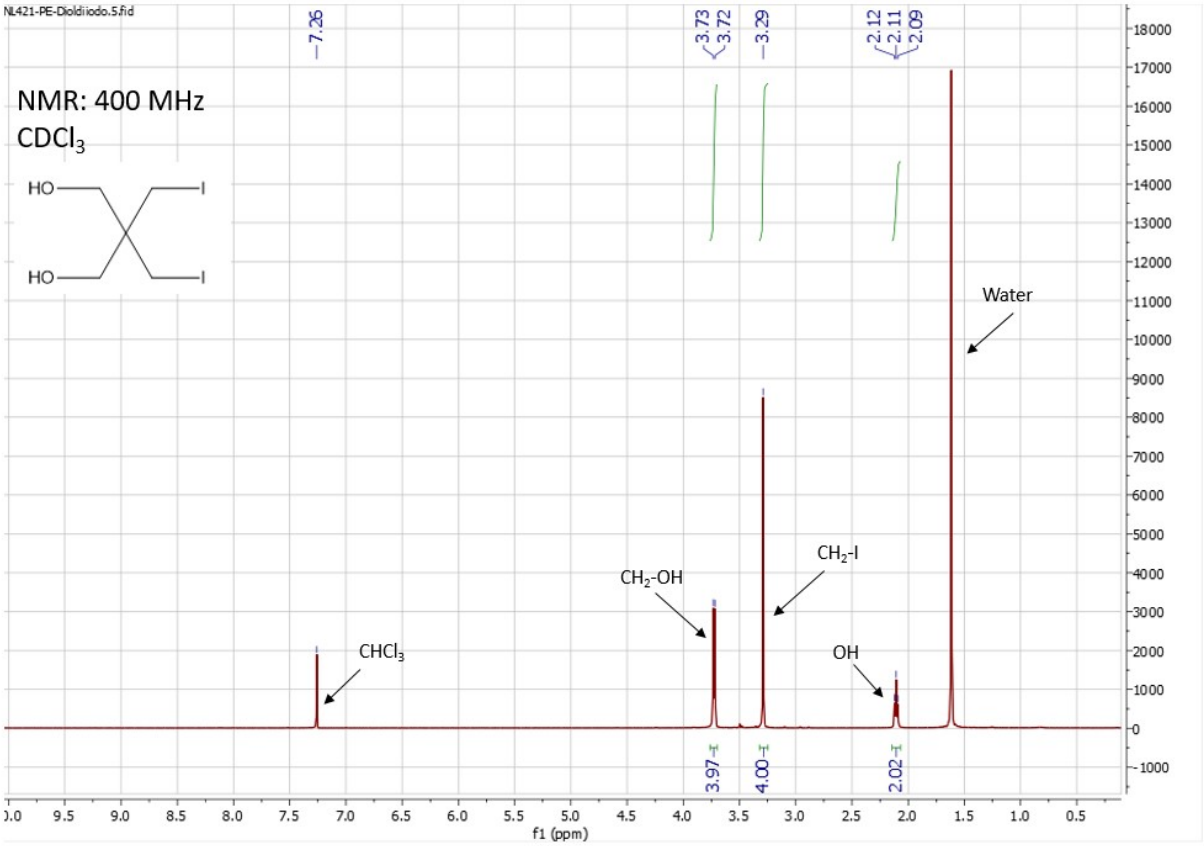

Figure S1: ^{1}H-NMR of compound (**PEDI-I2-OH2**)

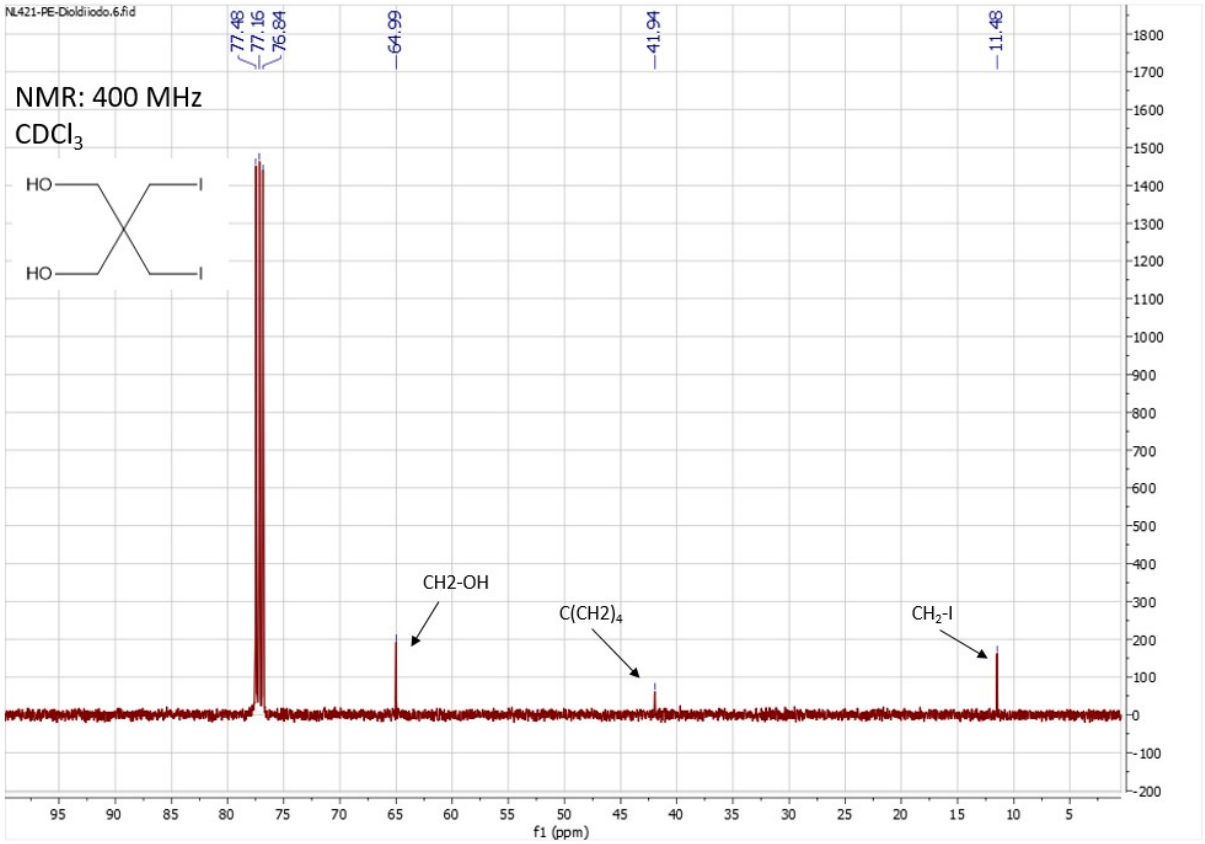

Figure S2: ^{13}C-NMR of compound (**PEDI-I2-OH2**)

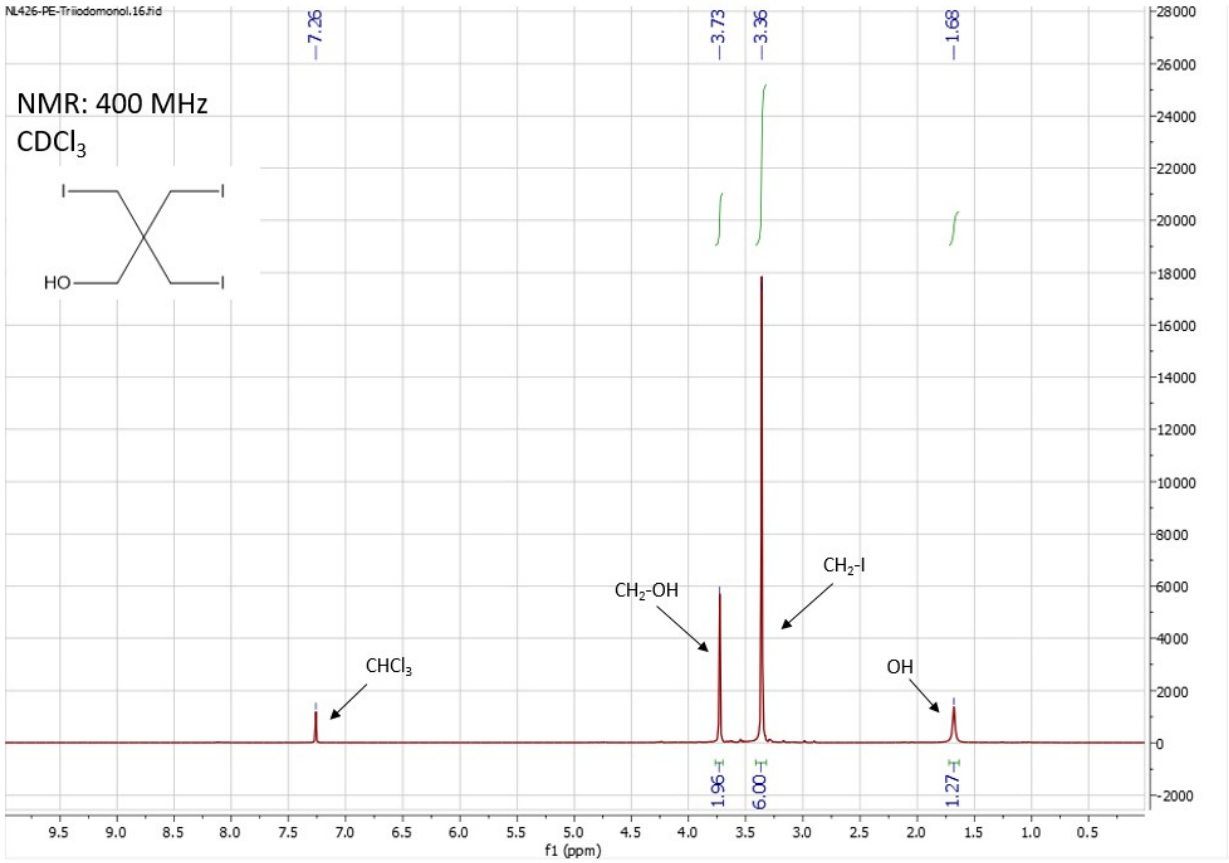

Figure S3: ^{1}H-NMR of compound **(PEMI-I-OH3)**

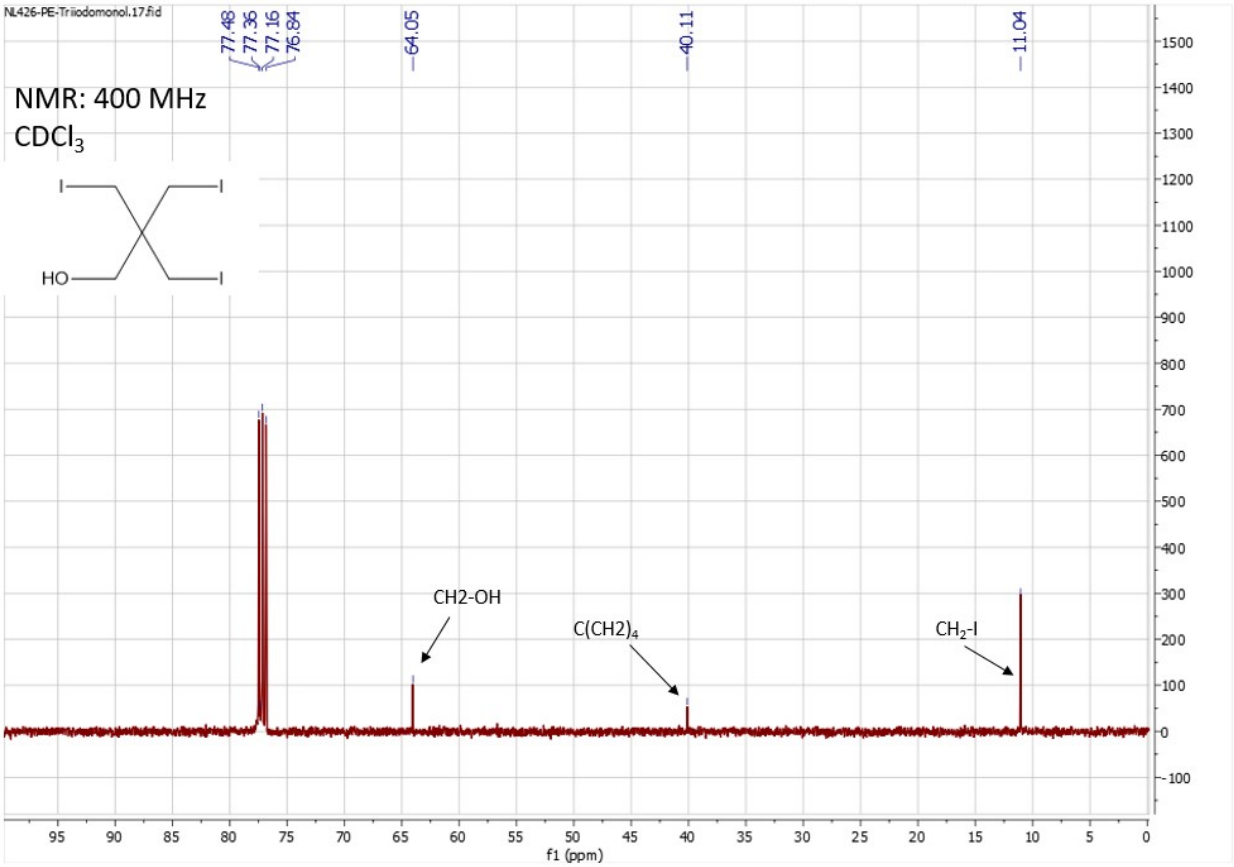

Figure S4: ^{13}C-NMR of compound **(PEMI-I-OH3)**

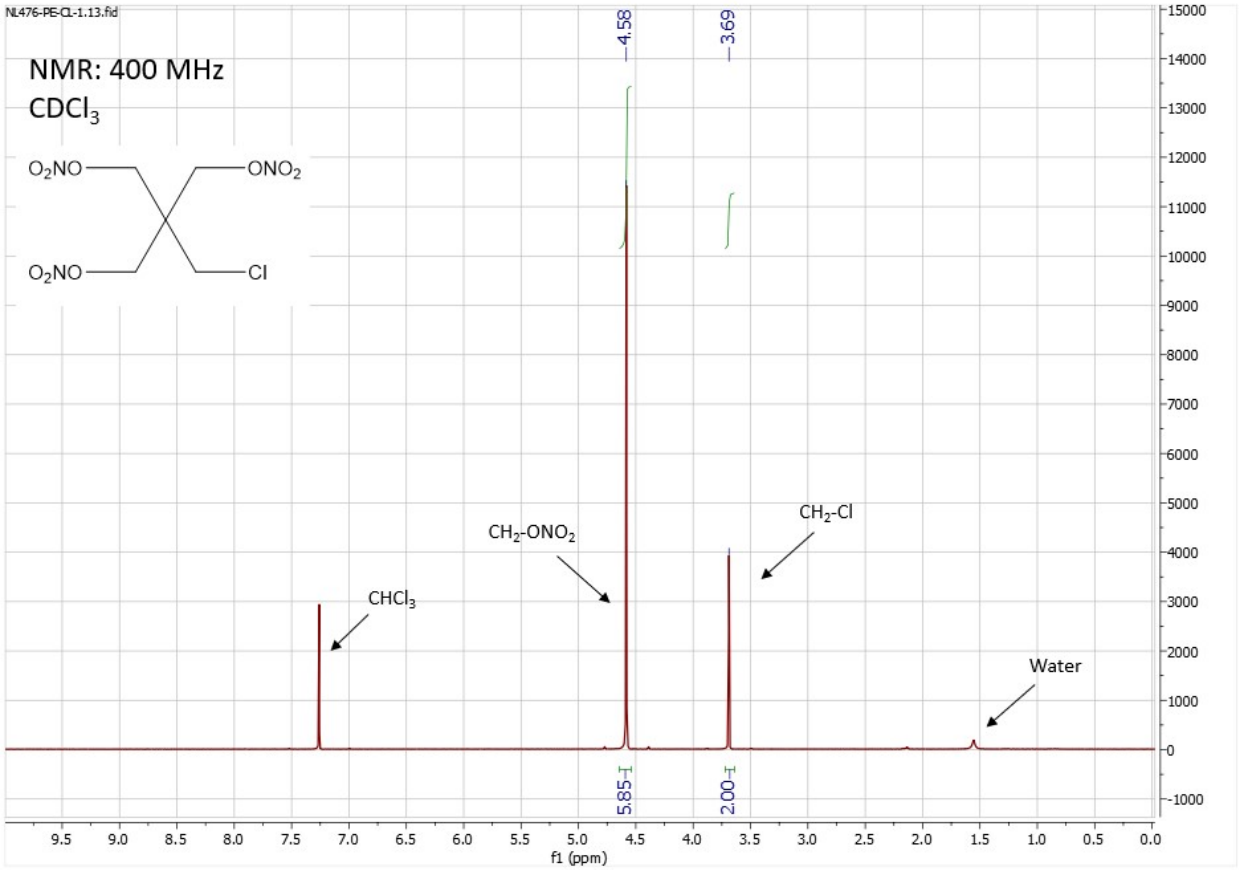

Figure S5: ^{1}H-NMR of compound (**PETriN-Cl**)

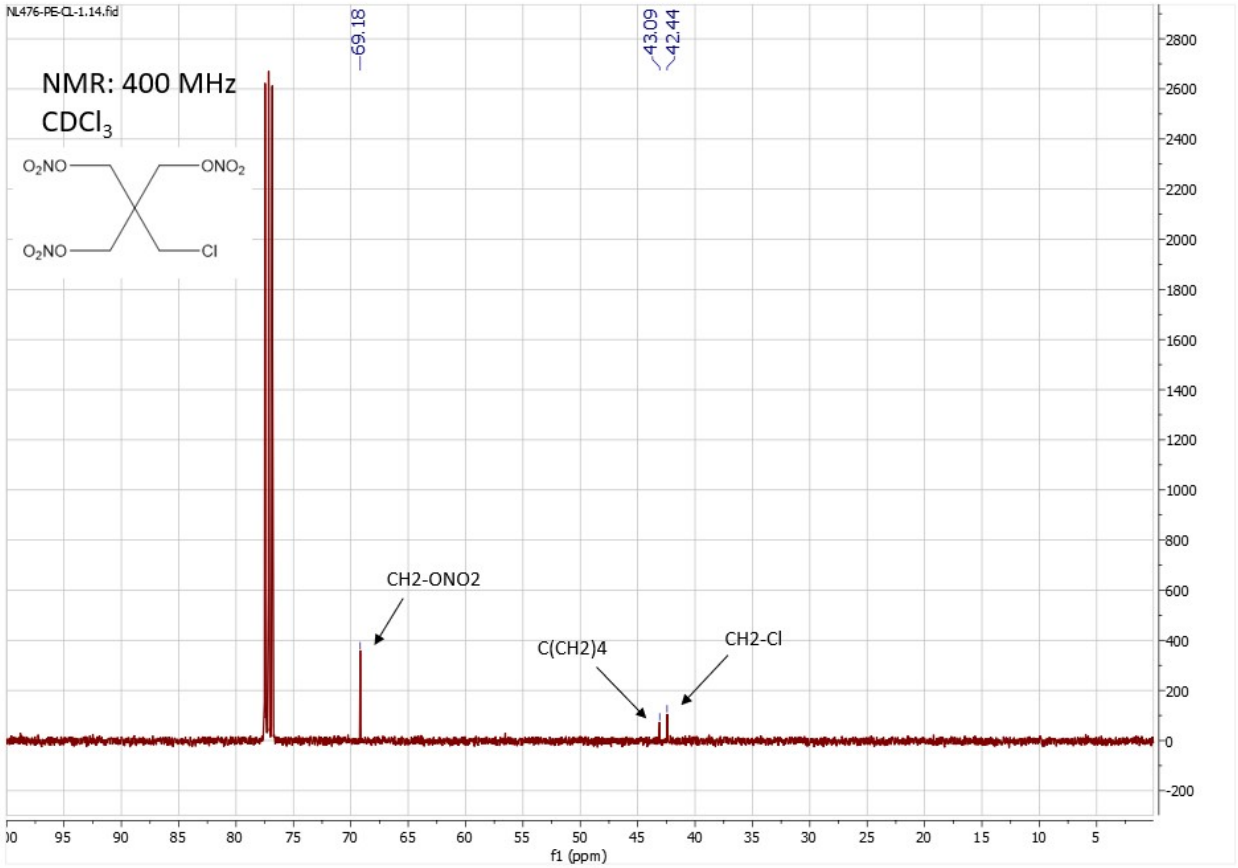

Figure S6: ^{13}C-NMR of compound (**PETriN-Cl**)

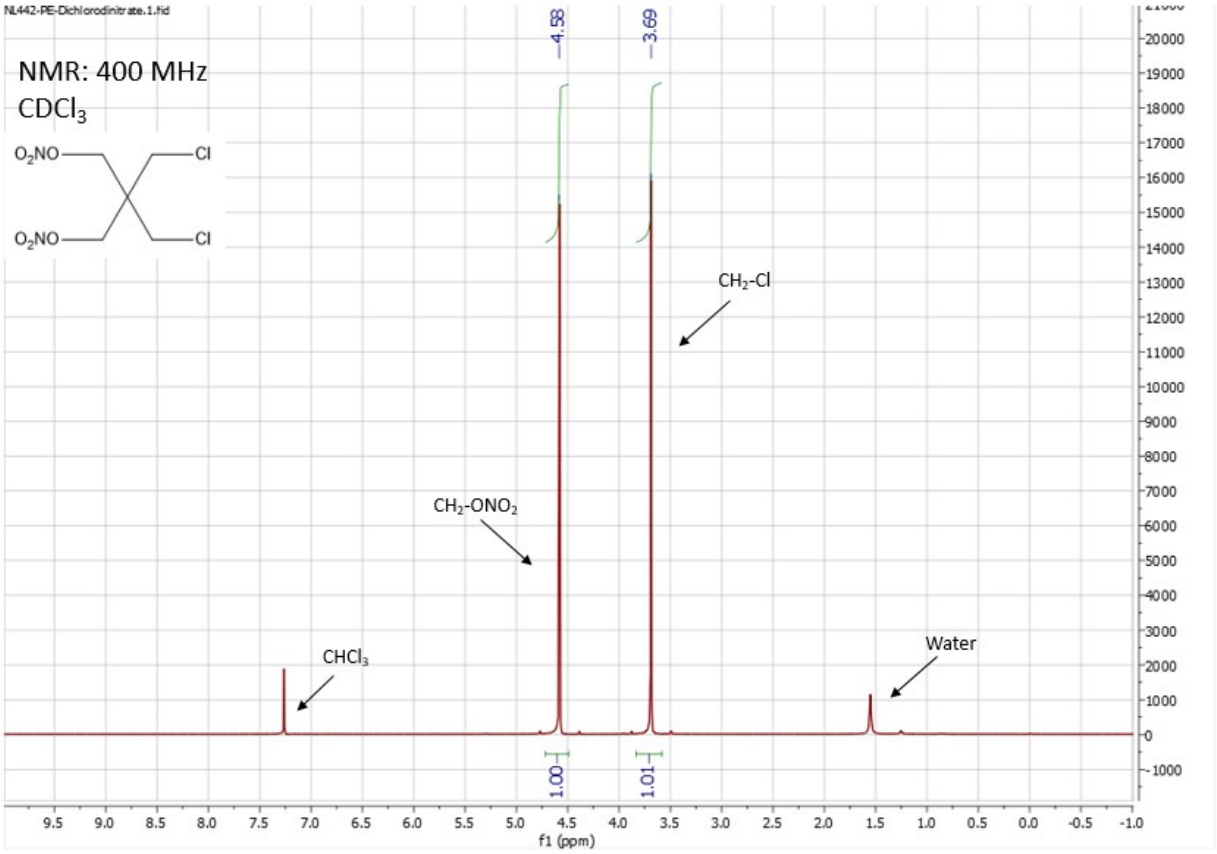

Figure S7: ^{1}H-NMR of compound (**PEDN-Cl2**)

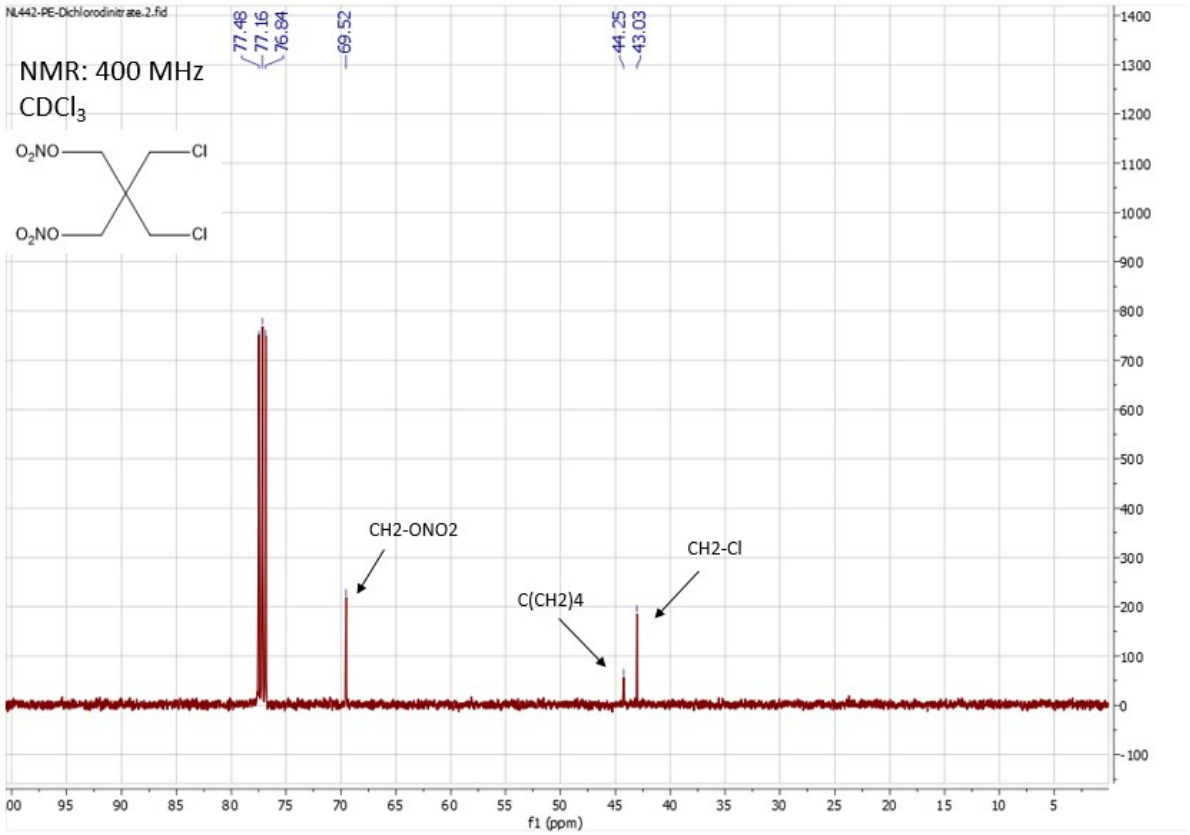

Figure S8: ^{13}C-NMR of compound (**PEDN-Cl2**)

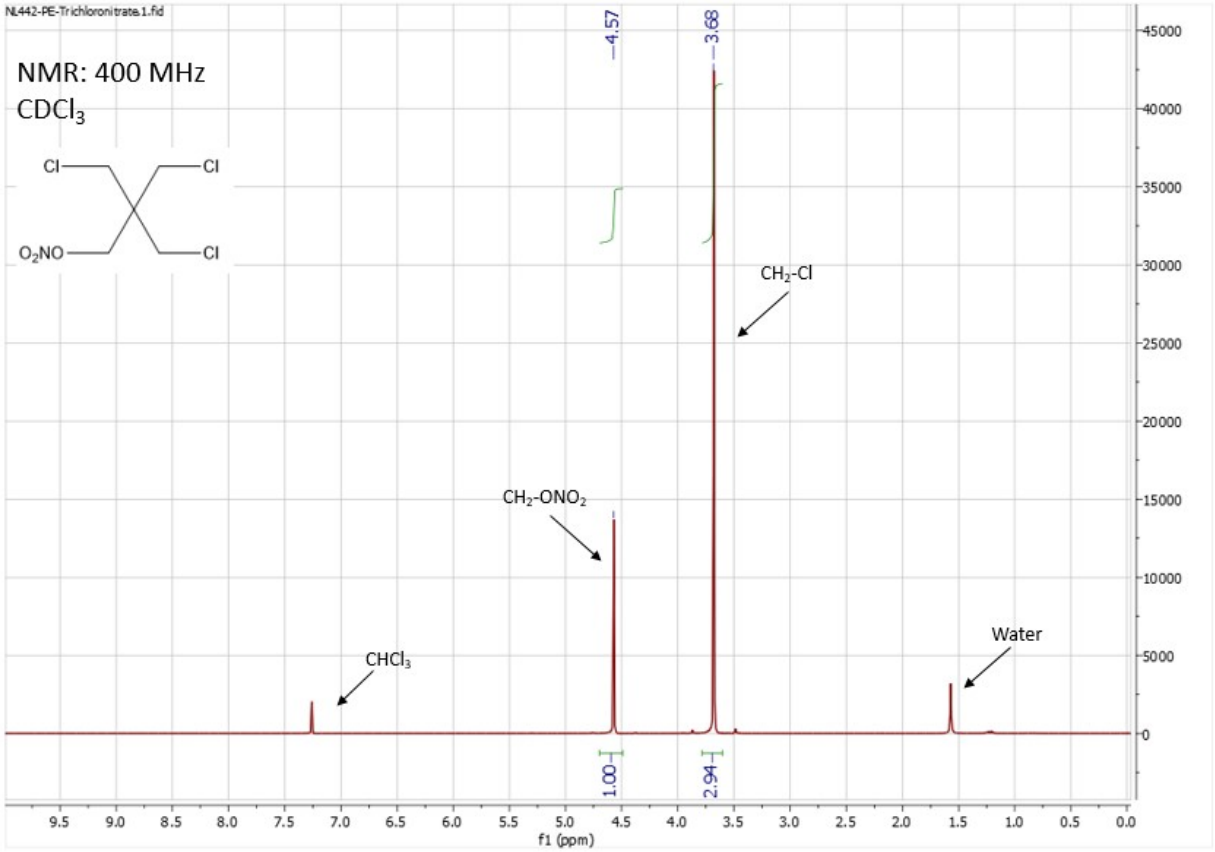

Figure S9: ^{1}H-NMR of compound (**PEMN-Cl3**)

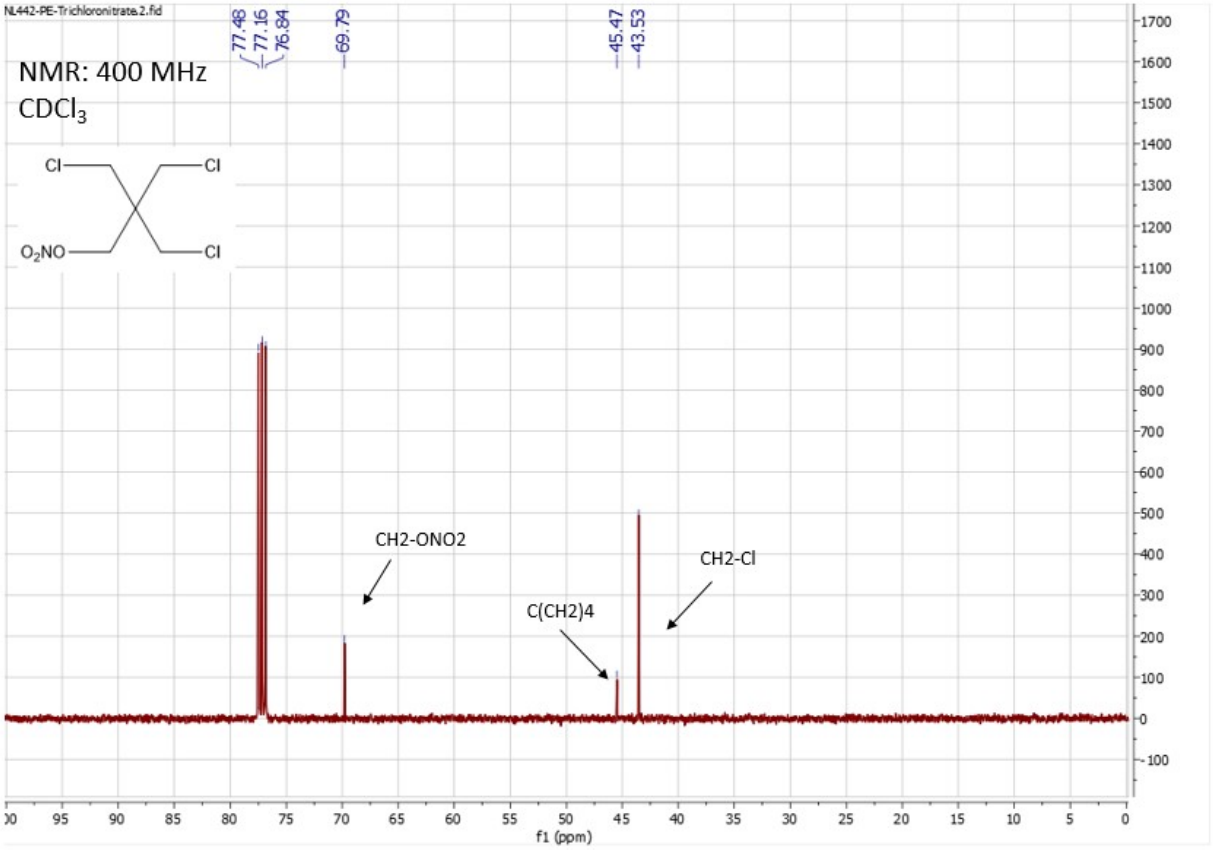

Figure S10: ^{13}C-NMR of compound (**PEMN-Cl3**)

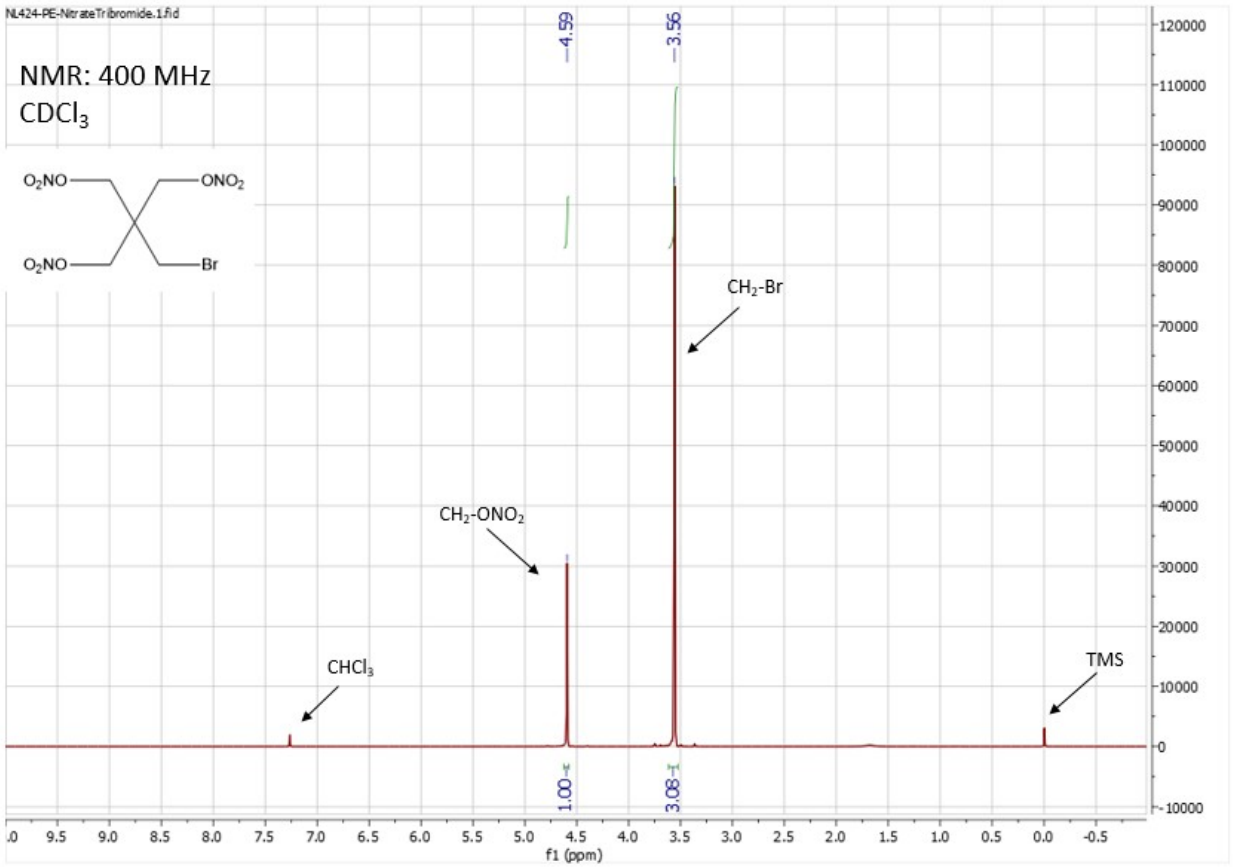

Figure S11: ^{1}H-NMR of compound (**PETriN-Br**)

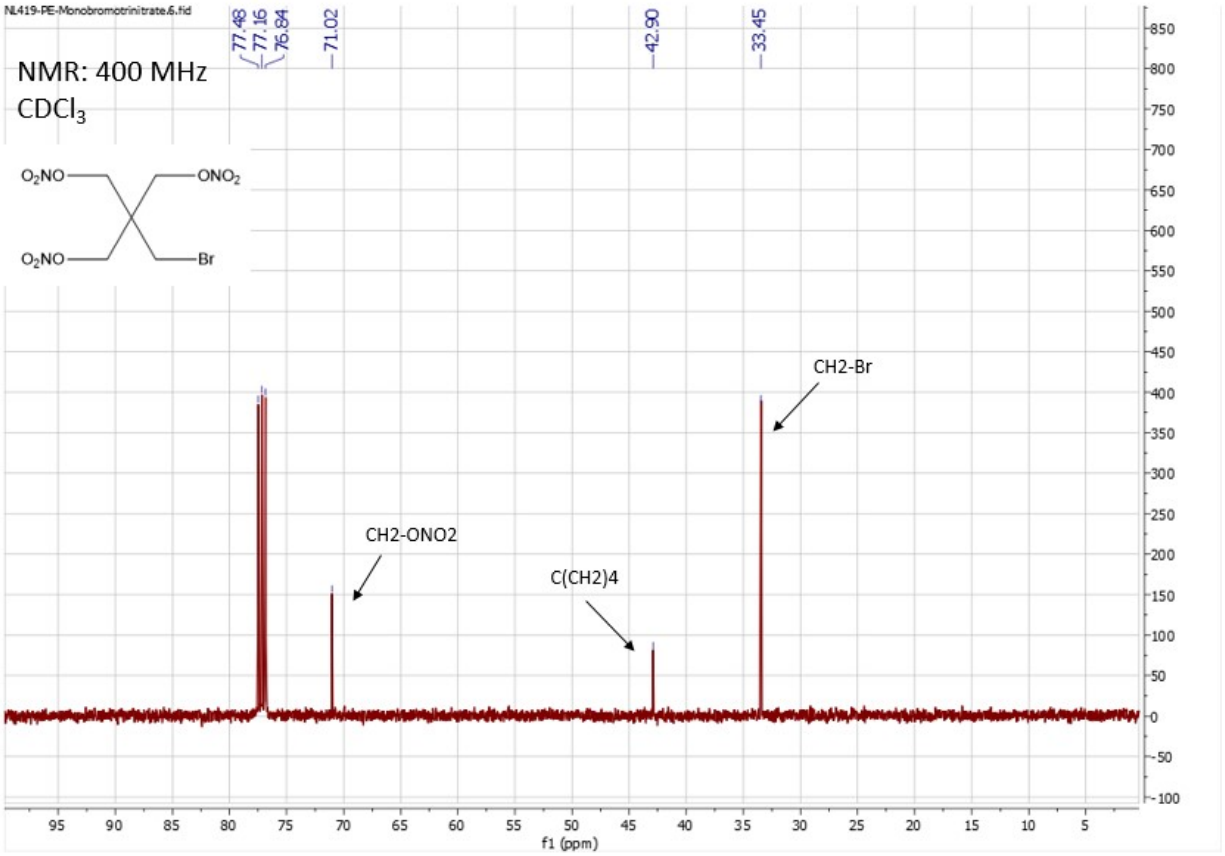

Figure S12: ^{13}C-NMR of compound (**PETriN-Br**)

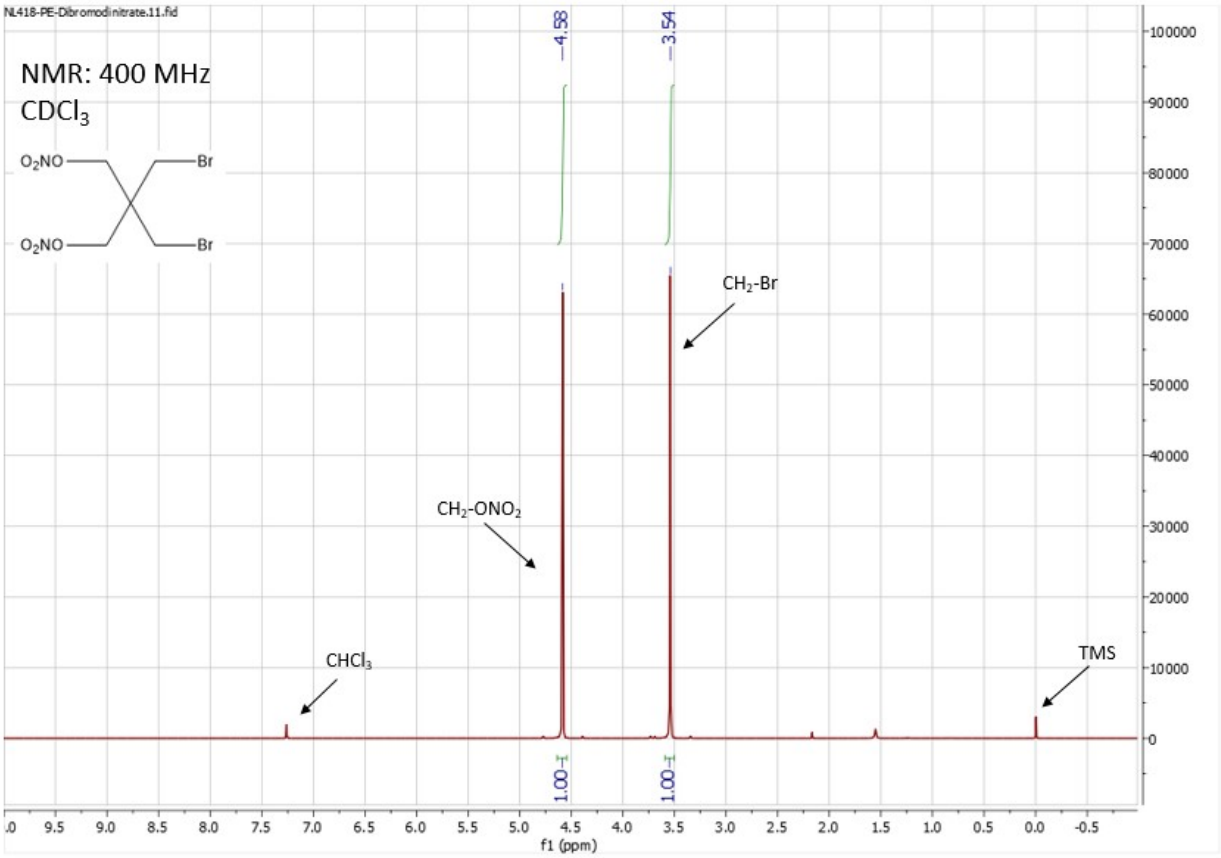

Figure S13: ^{1}H-NMR of compound (**PEDN-Br2**)

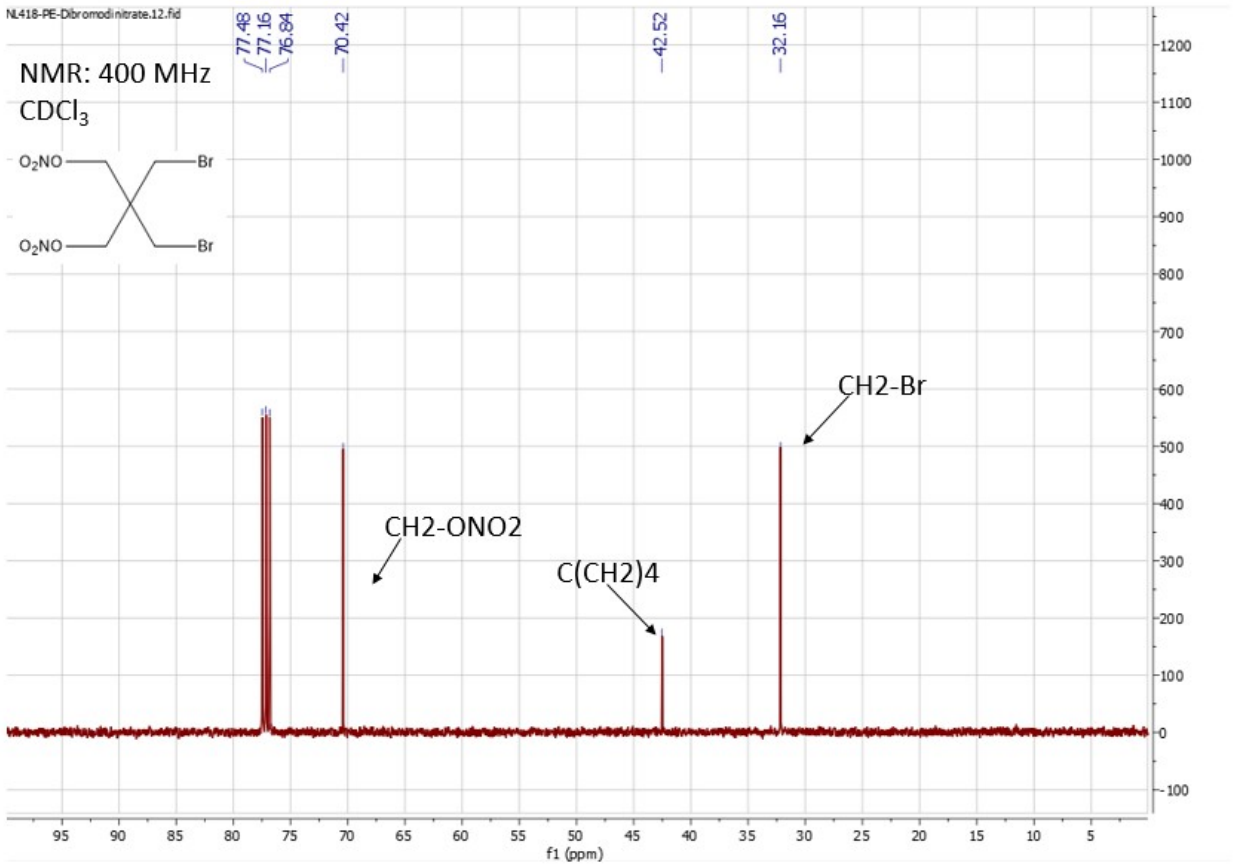

Figure S14: ^{13}C-NMR of compound (**PEDN-Br2**)

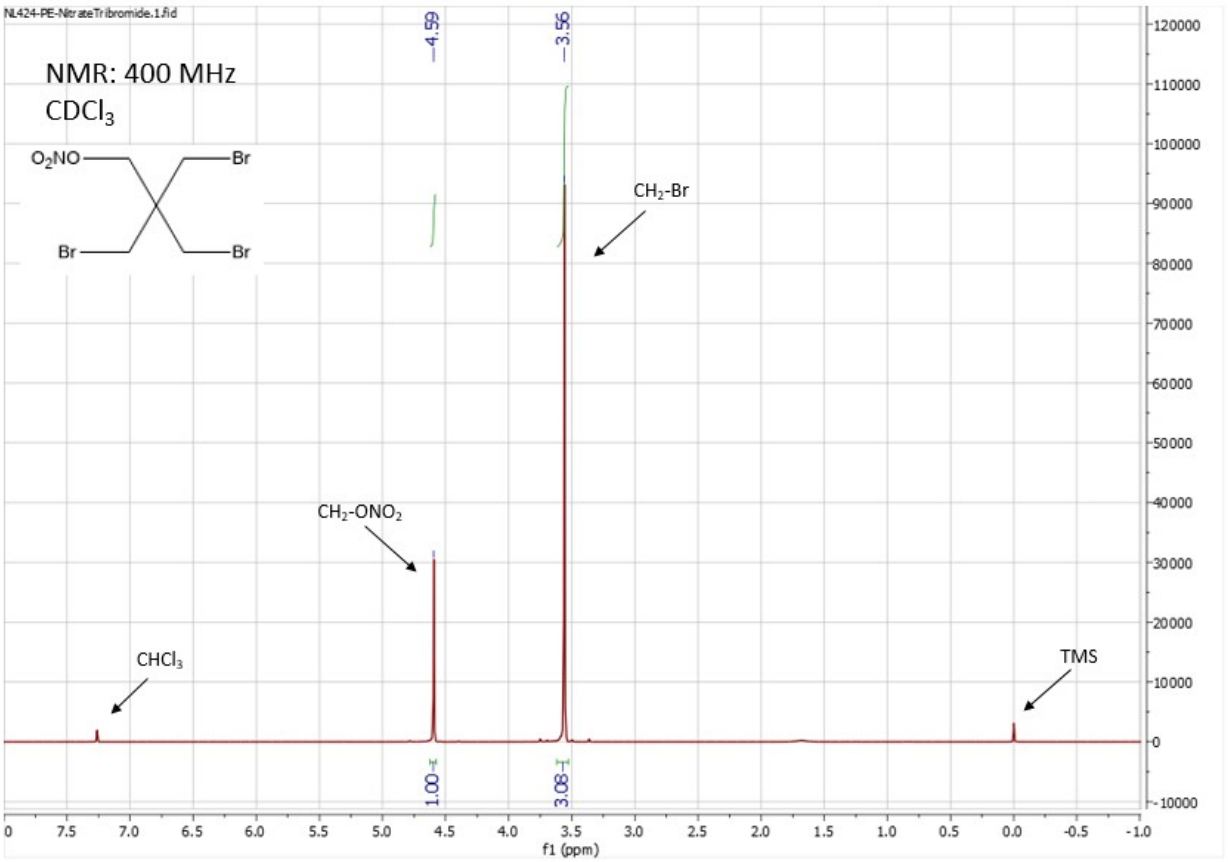

Figure S15: ^{1}H-NMR of compound (**PEMN-Br3**)

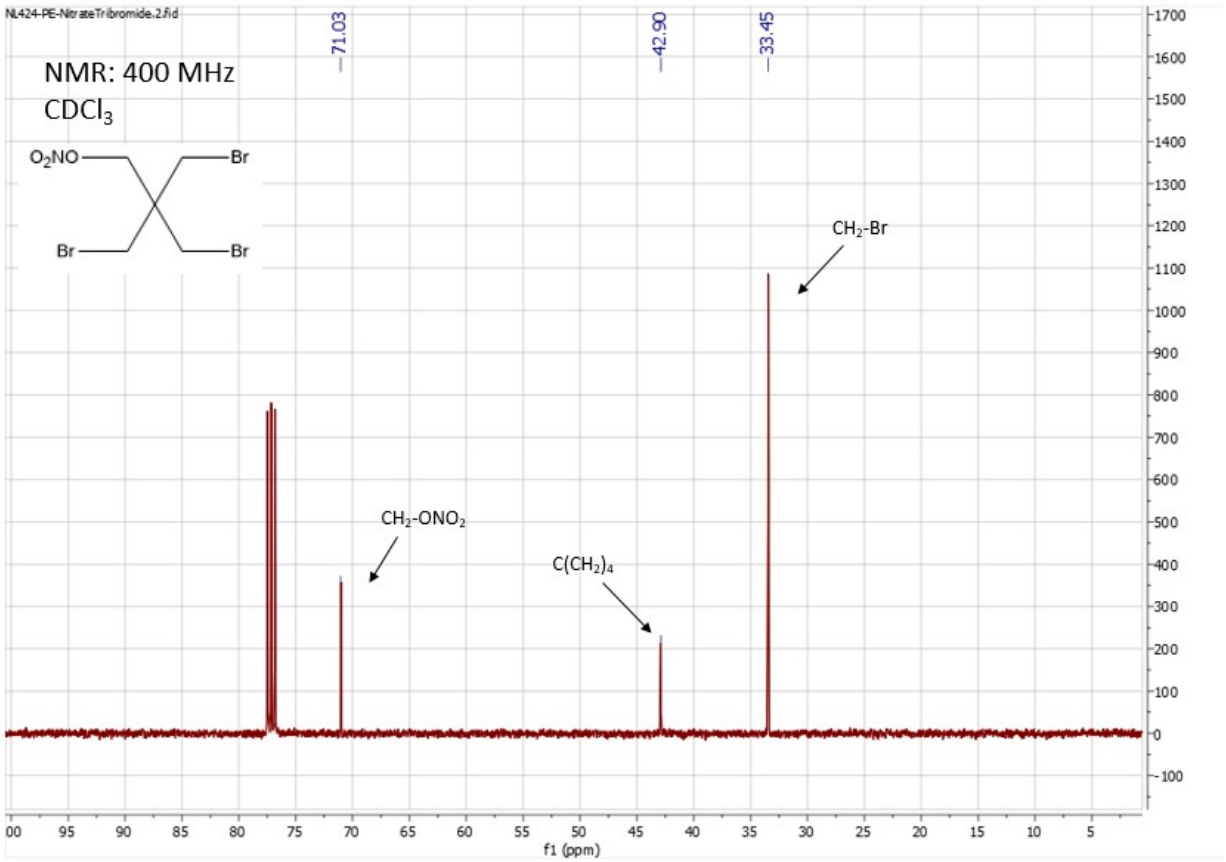

Figure S16: ^{13}C-NMR of compound (**PEMN-Br3**)

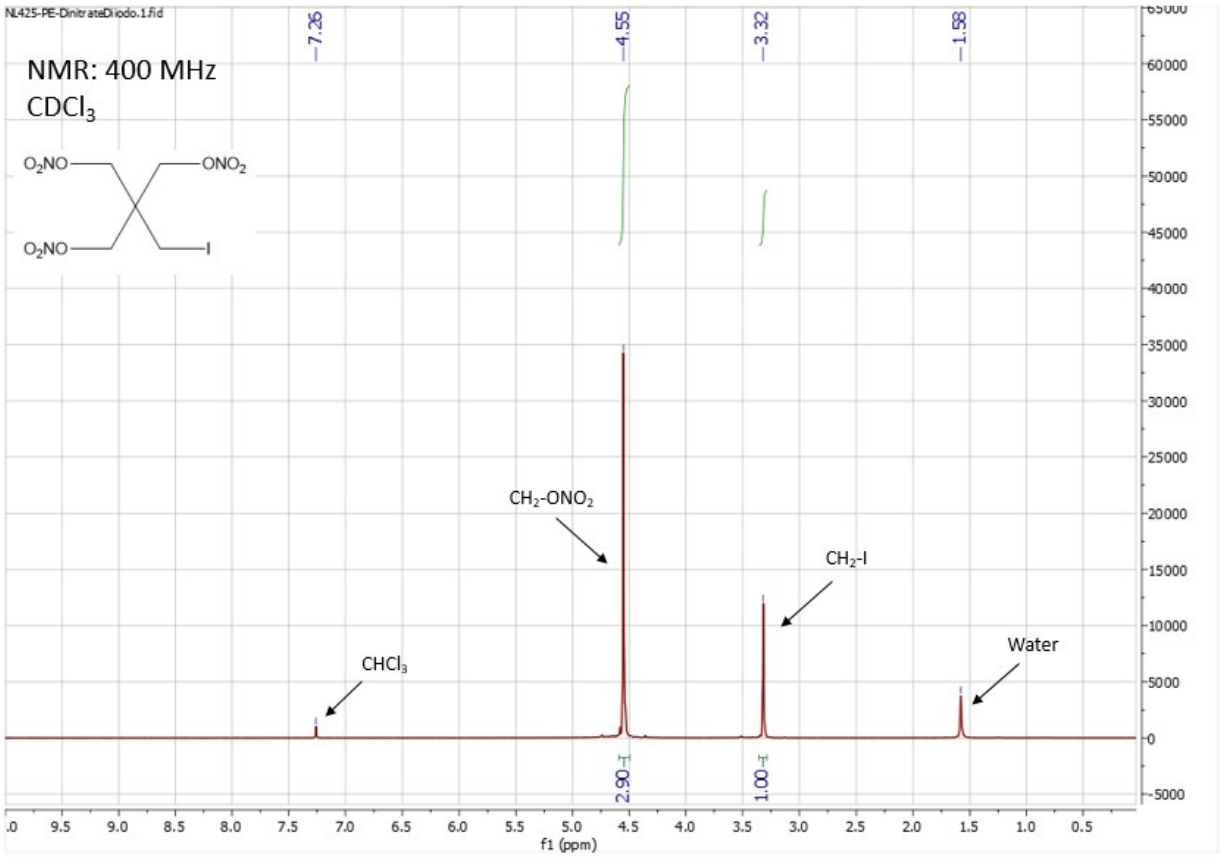

Figure S17: ^{1}H-NMR of compound (**PETRIN-I**)

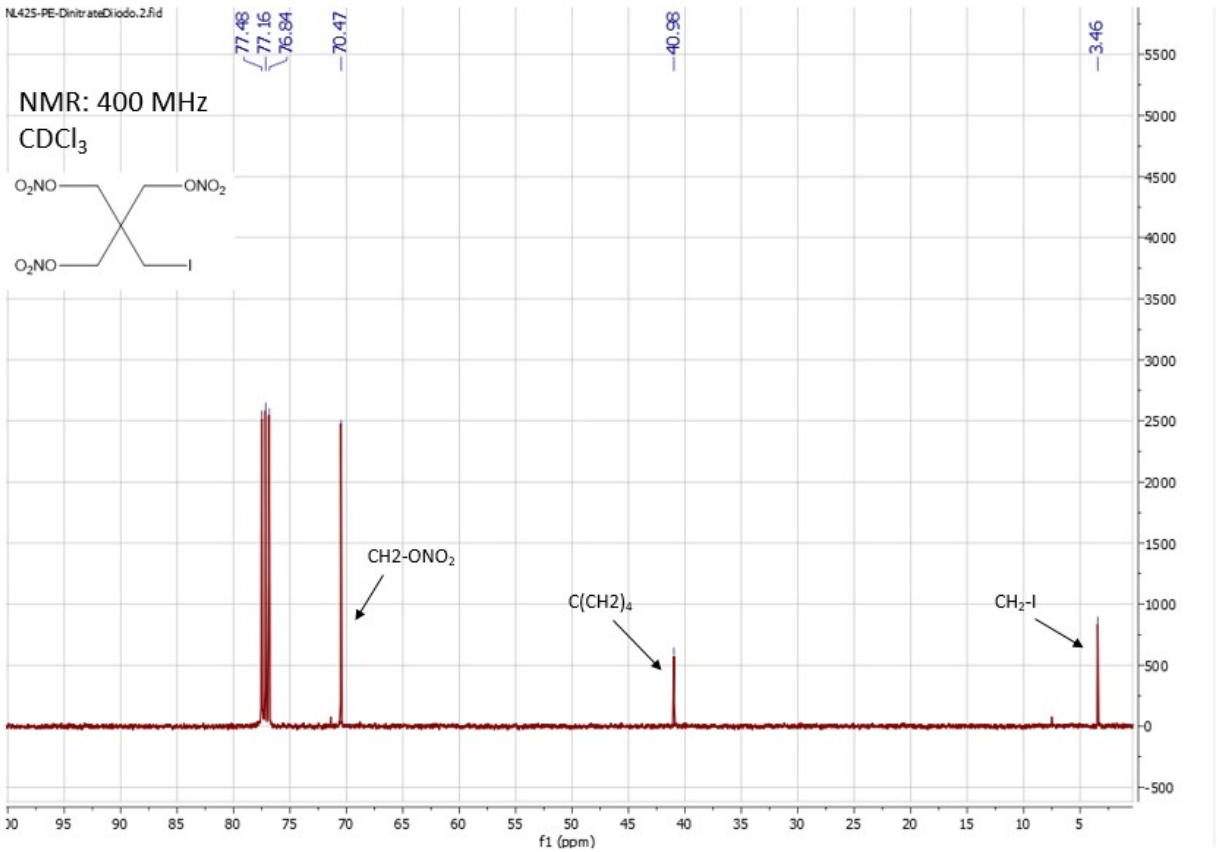

Figure S18: ^{13}C-NMR of compound (**PETRIN-I**)

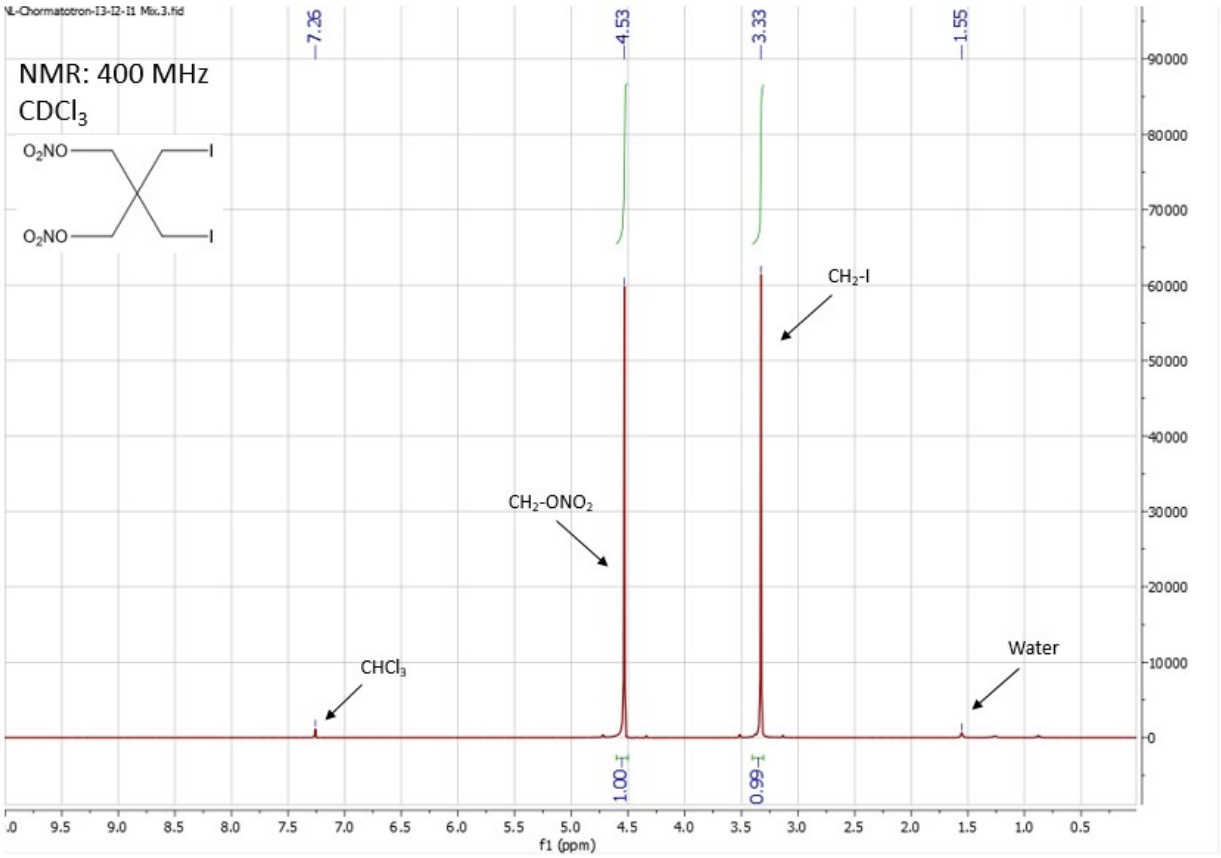

Figure S19: ^{1}H-NMR of compound (**PEDN-I2**)

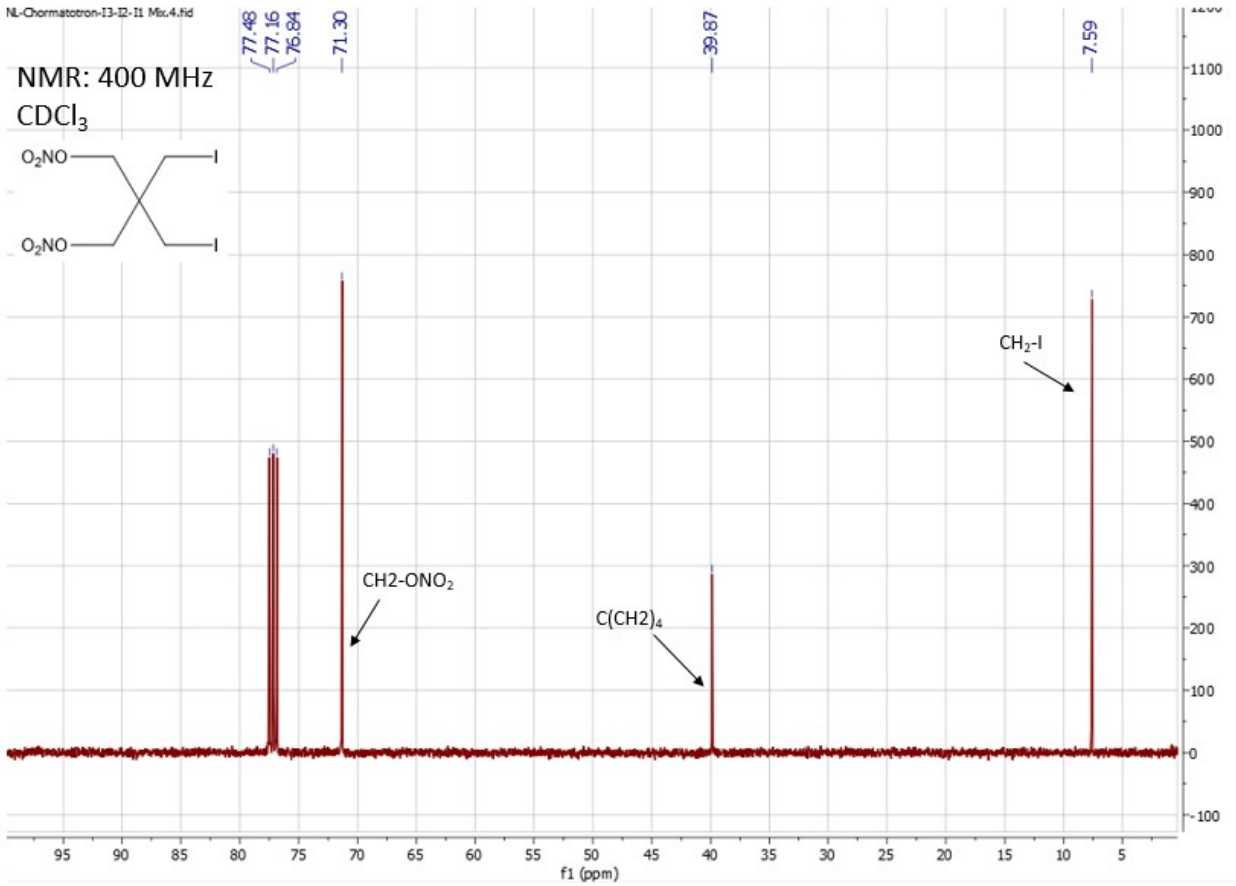

Figure S20: ^{13}C-NMR of compound (**PEDN-I2**)

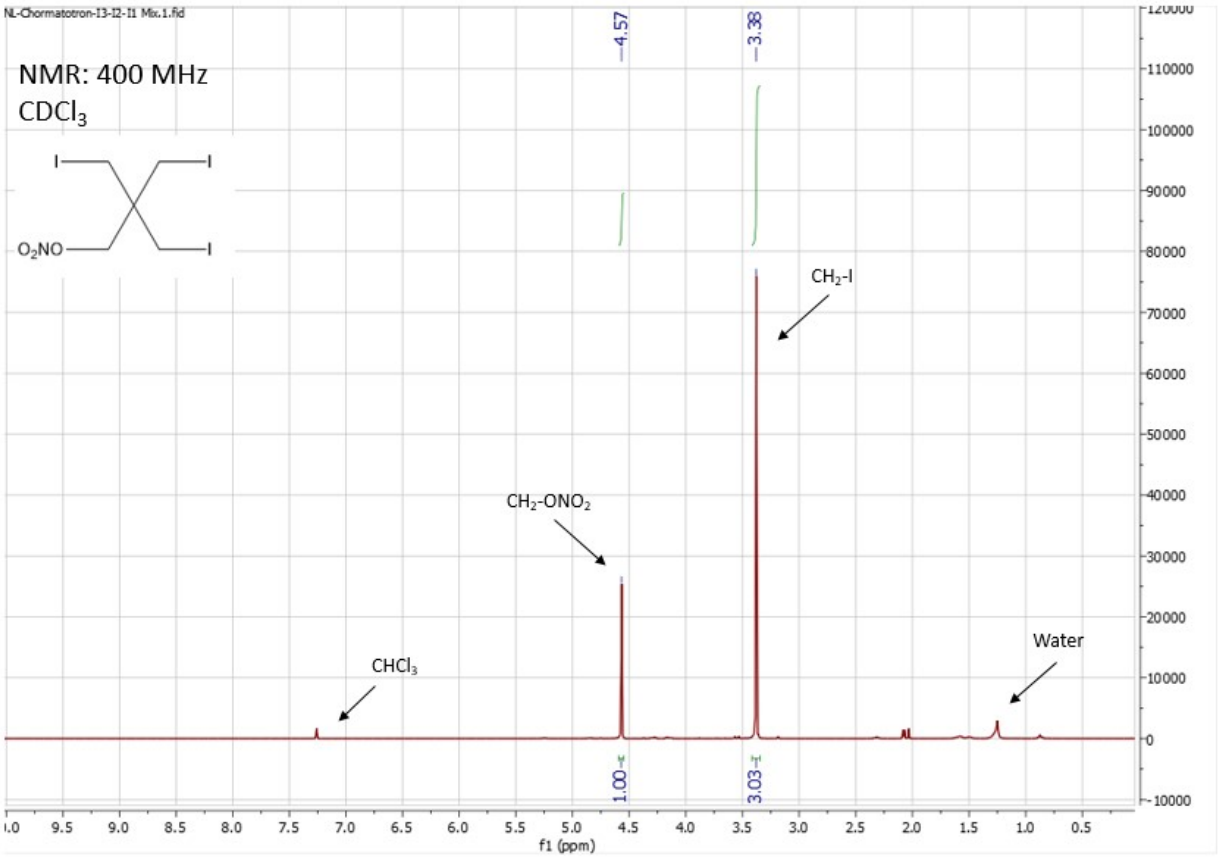

Figure S21: ^{1}H-NMR of compound (**PEMN-I3**)

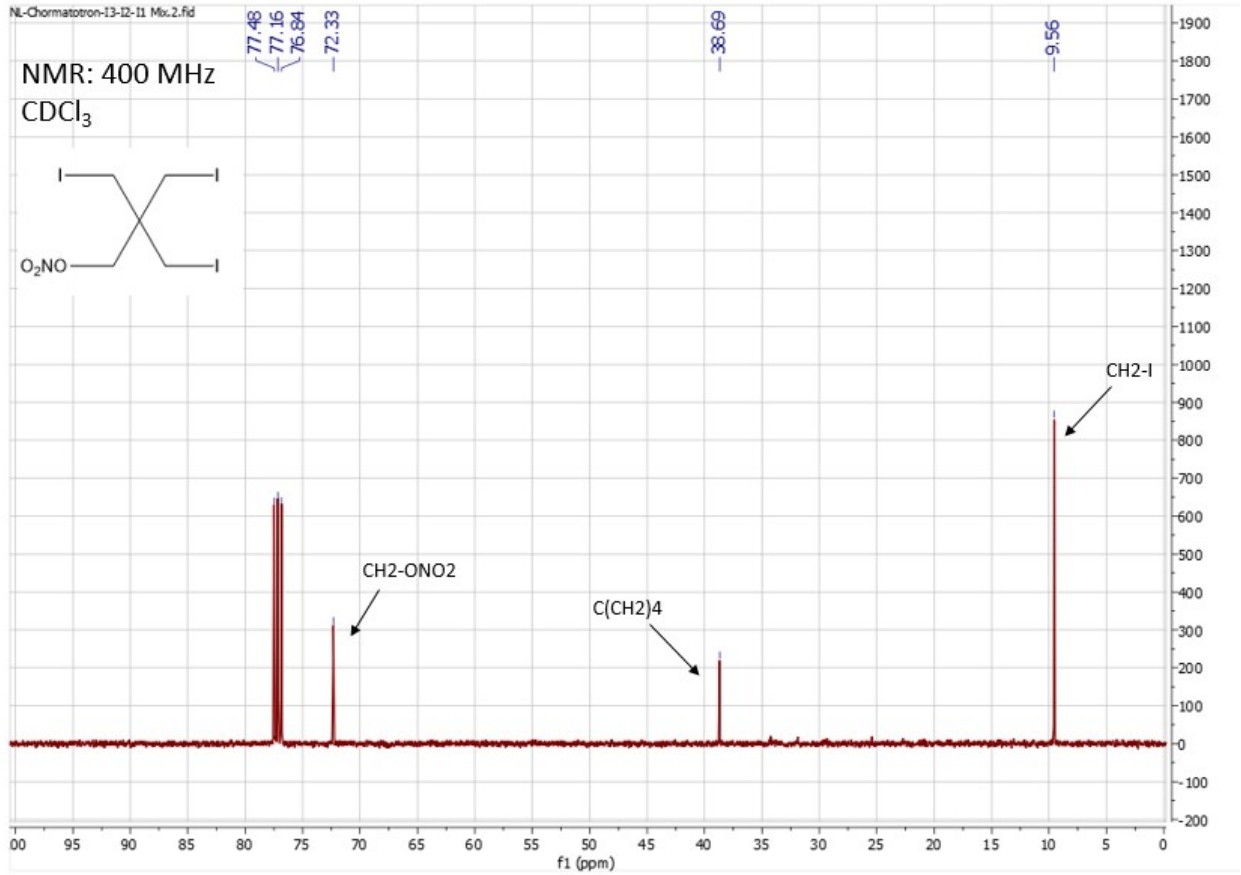

Figure S22: ^{13}C-NMR of compound (**PEMN-I3**)

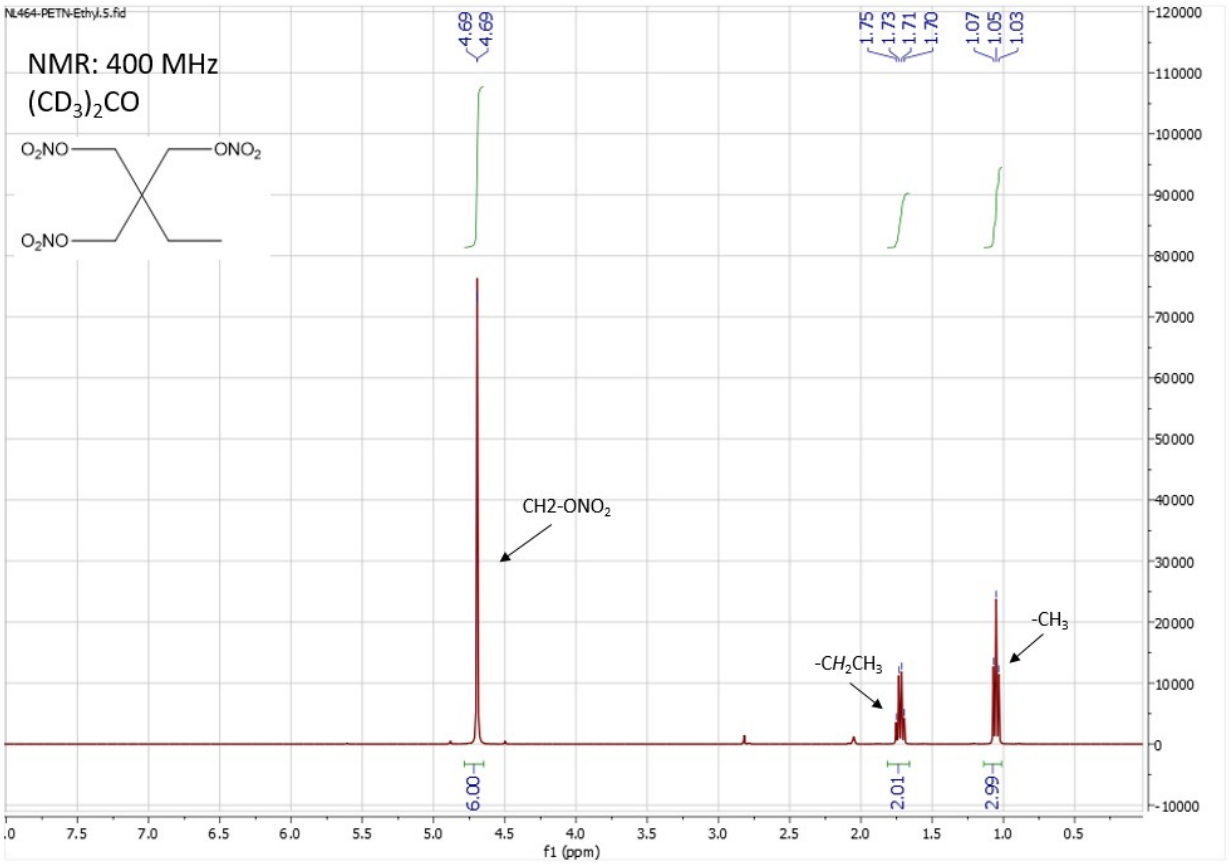

Figure S23: ^{1}H-NMR of compound (**PETriN-Methyl**)

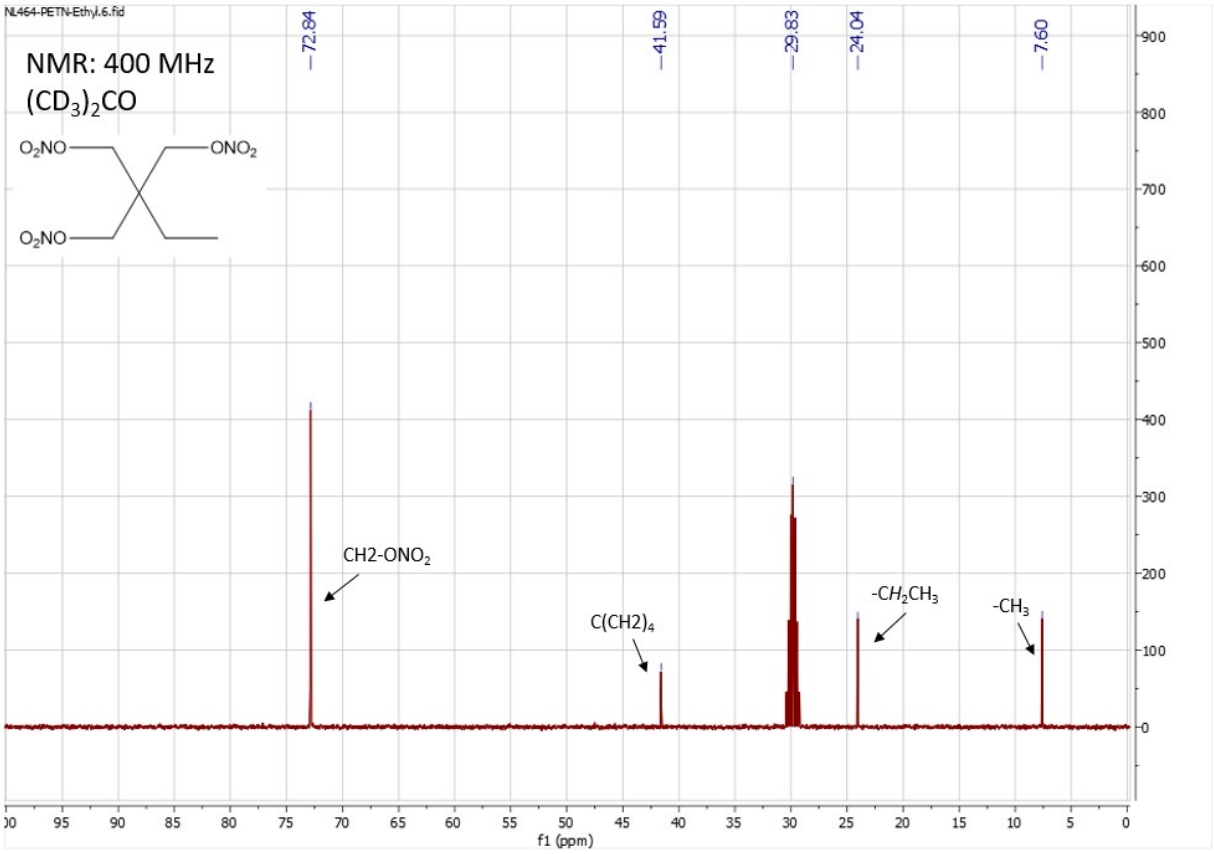

Figure S24: ^{13}C-NMR of compound (**PETriN-Methyl**)

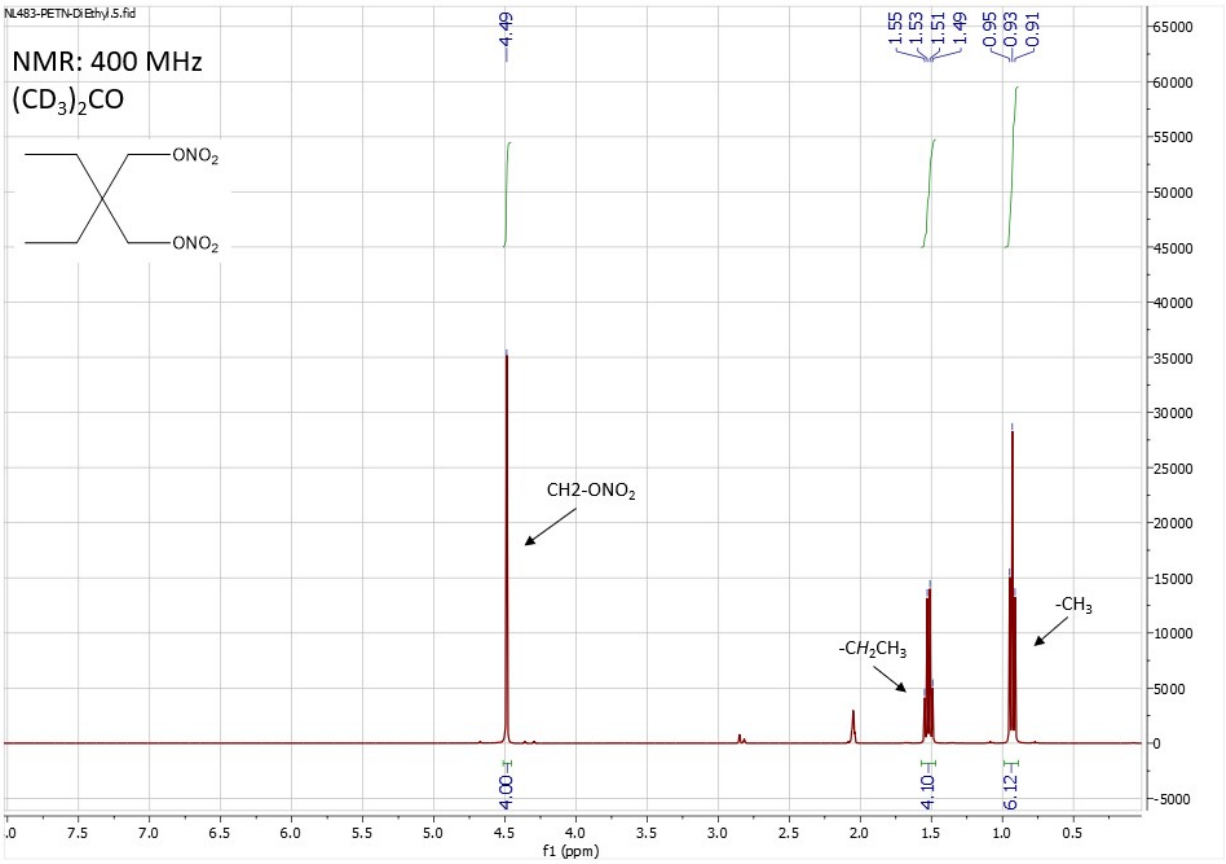

Figure S25: ^{1}H-NMR of compound (**PEDN-Methyl2**)

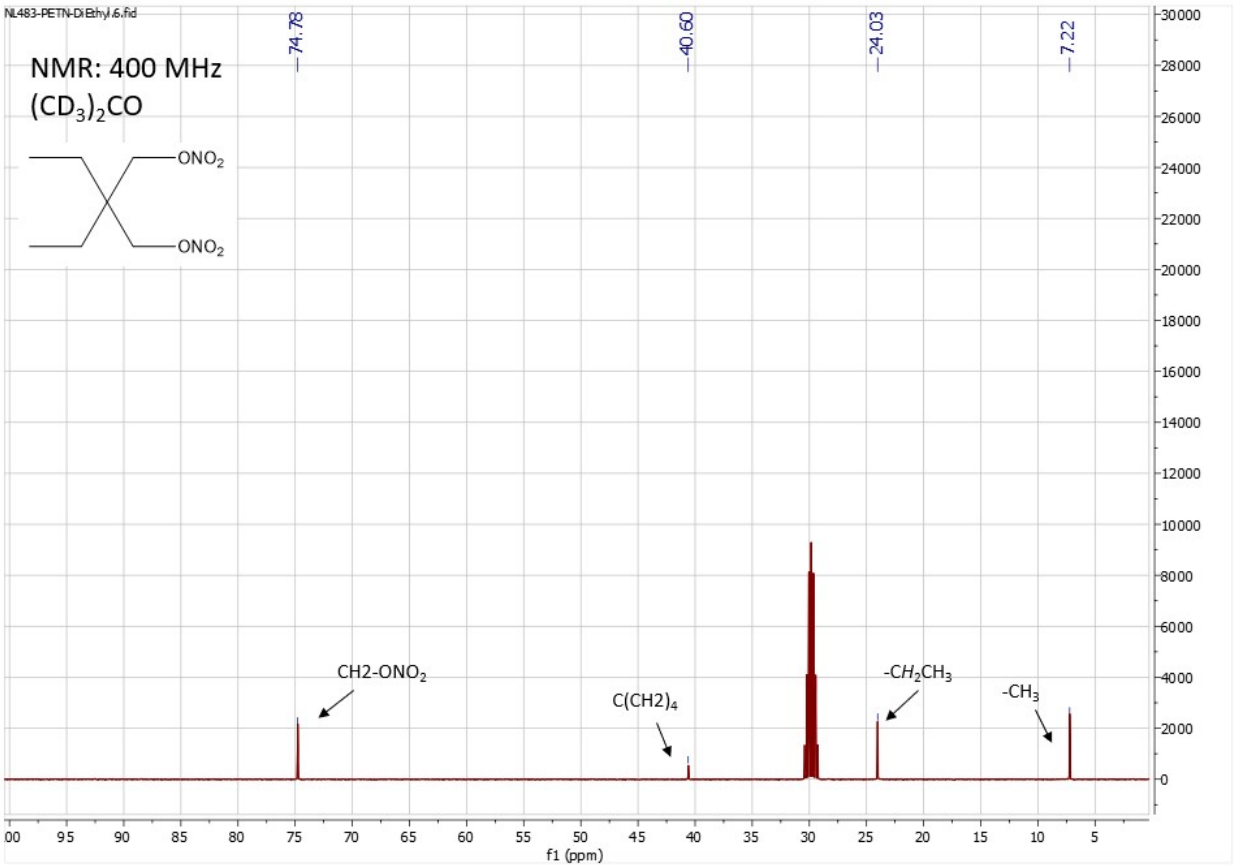

Figure S26: ^{13}C-NMR of compound (**PEDN-Methyl2**)

Impact Sensitivity Data:

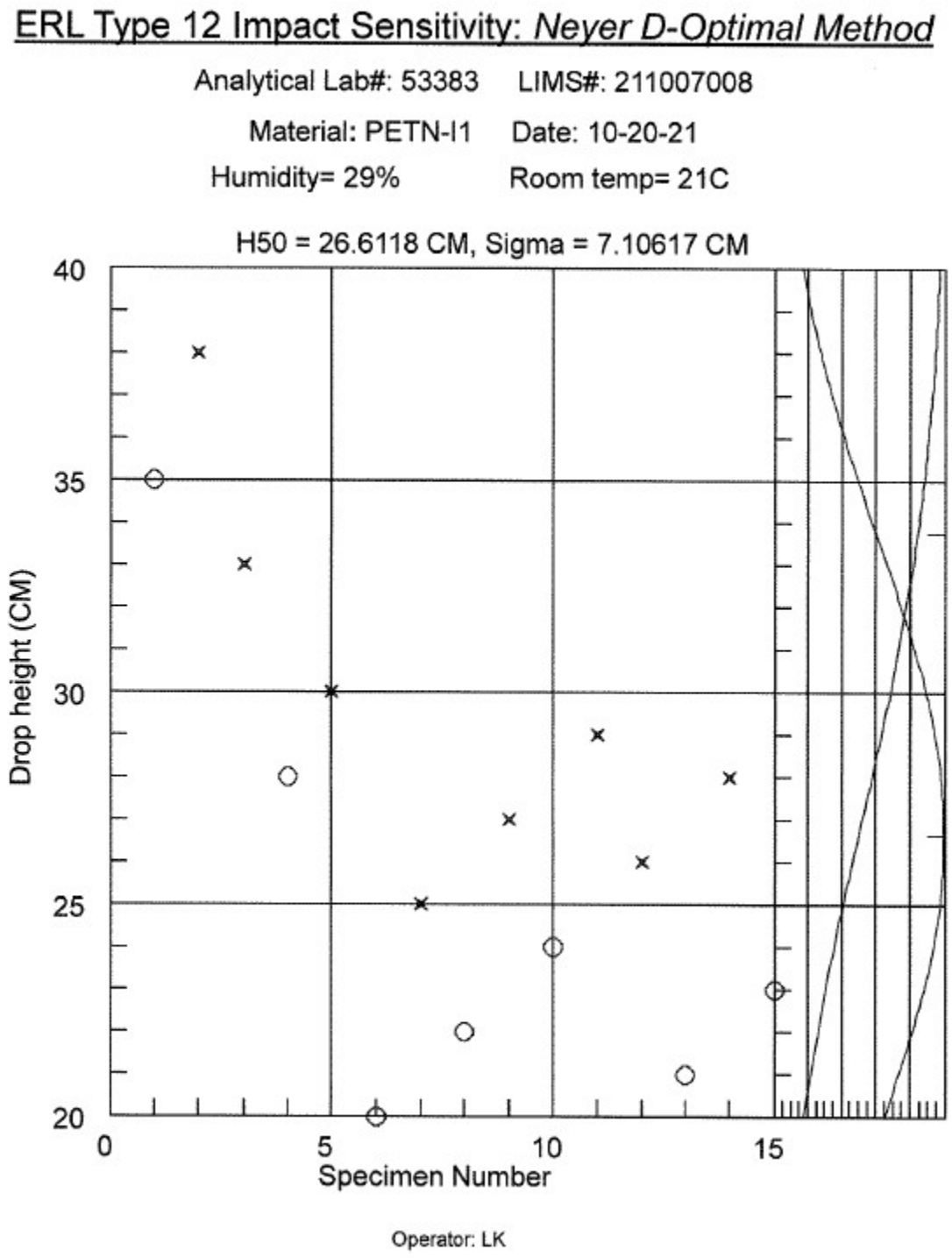

Figure S27: Impact sensitivity data for PETriN-I

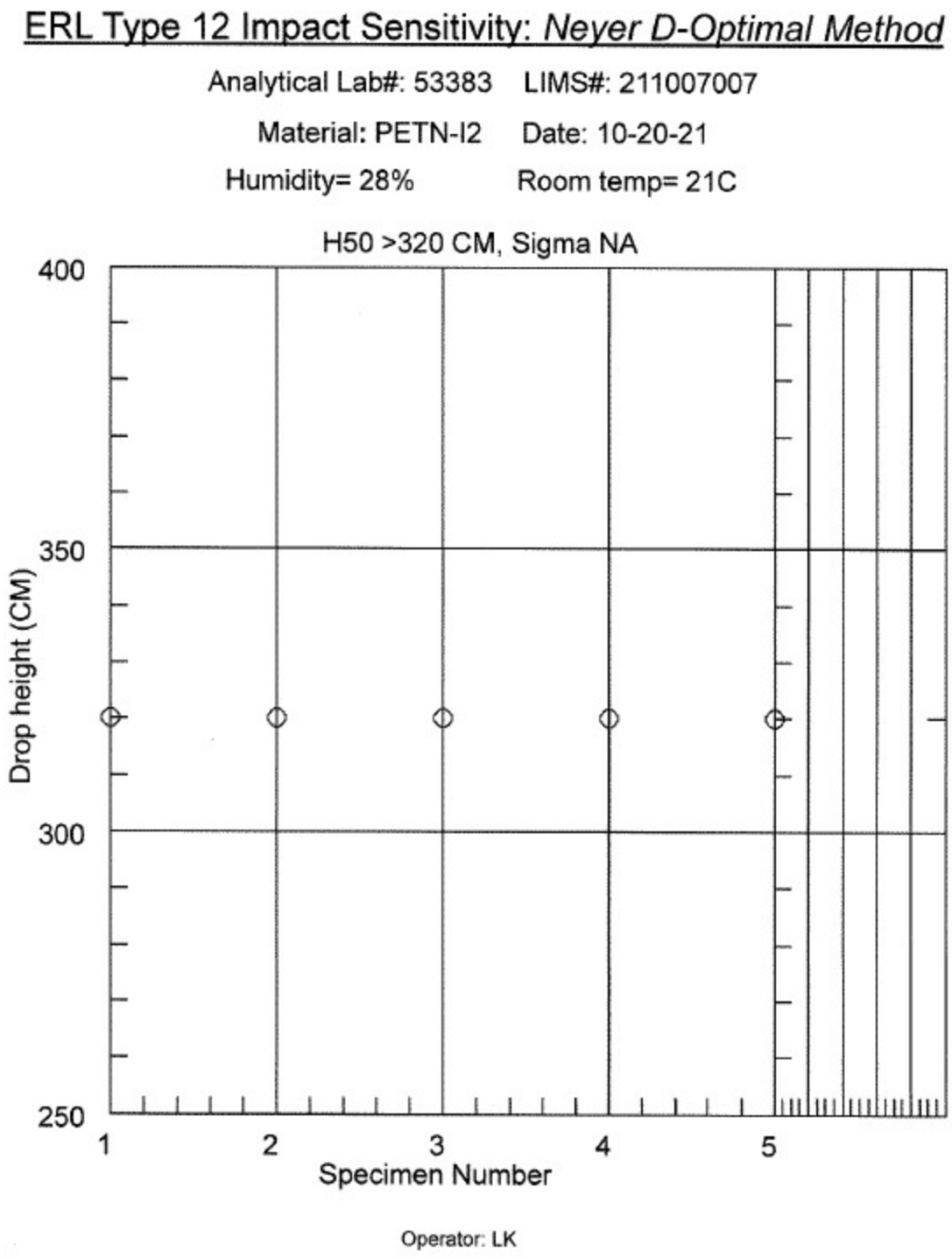

Figure S28: Impact sensitivity data for PEDN-I2

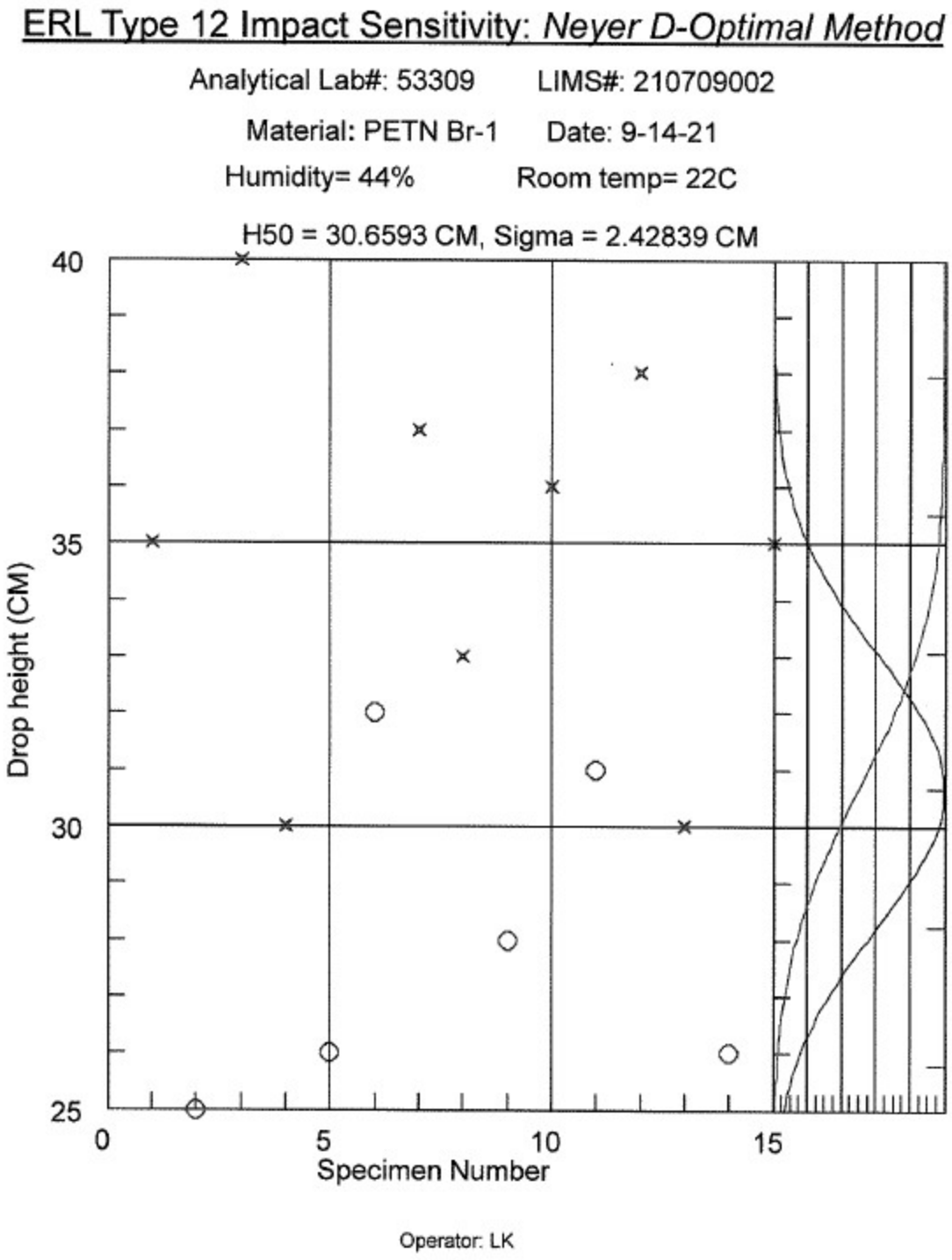

Figure S29: Impact sensitivity data for PETriN-Br

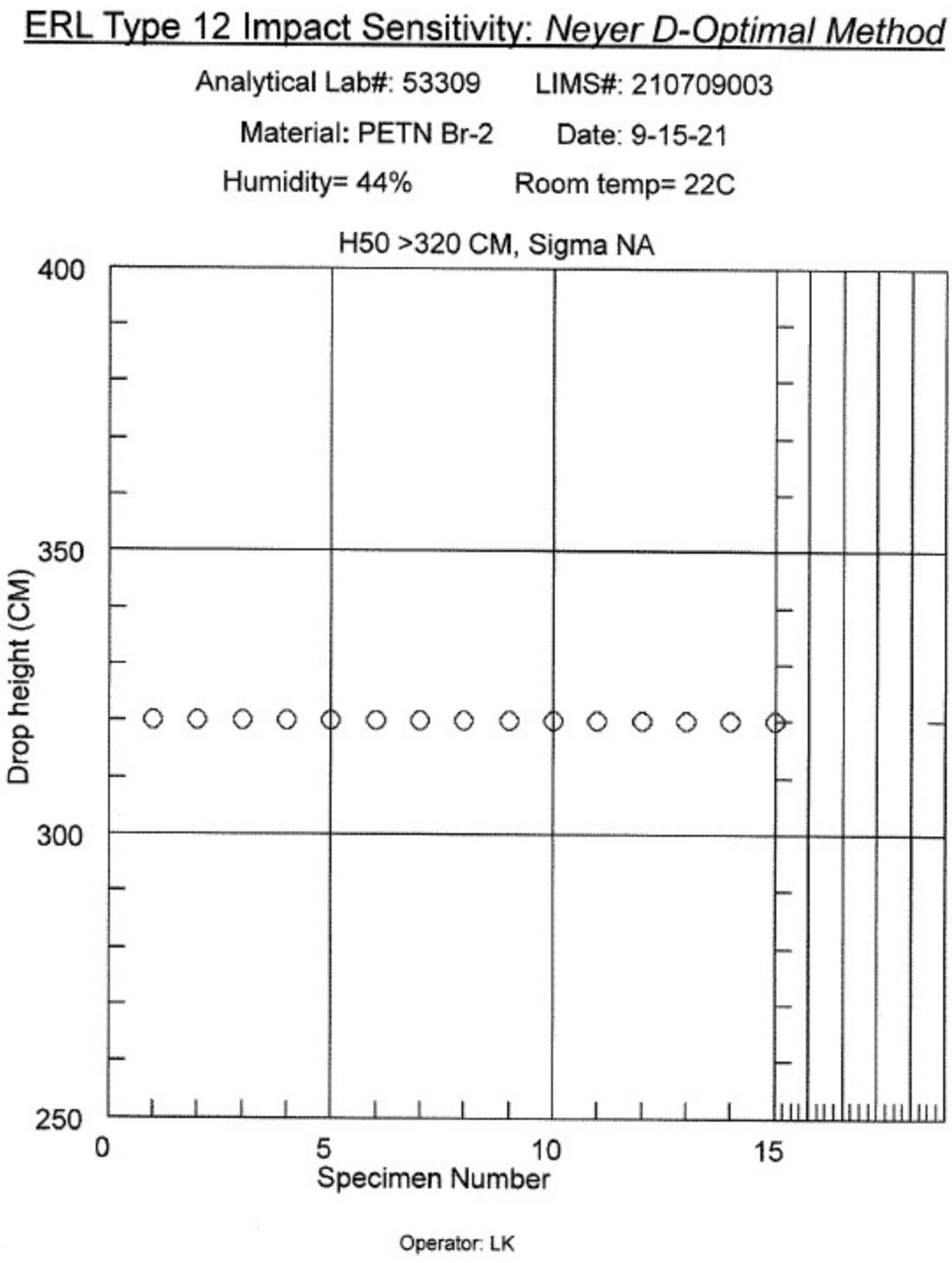

Figure S30: Impact sensitivity data for PEDN-Br2

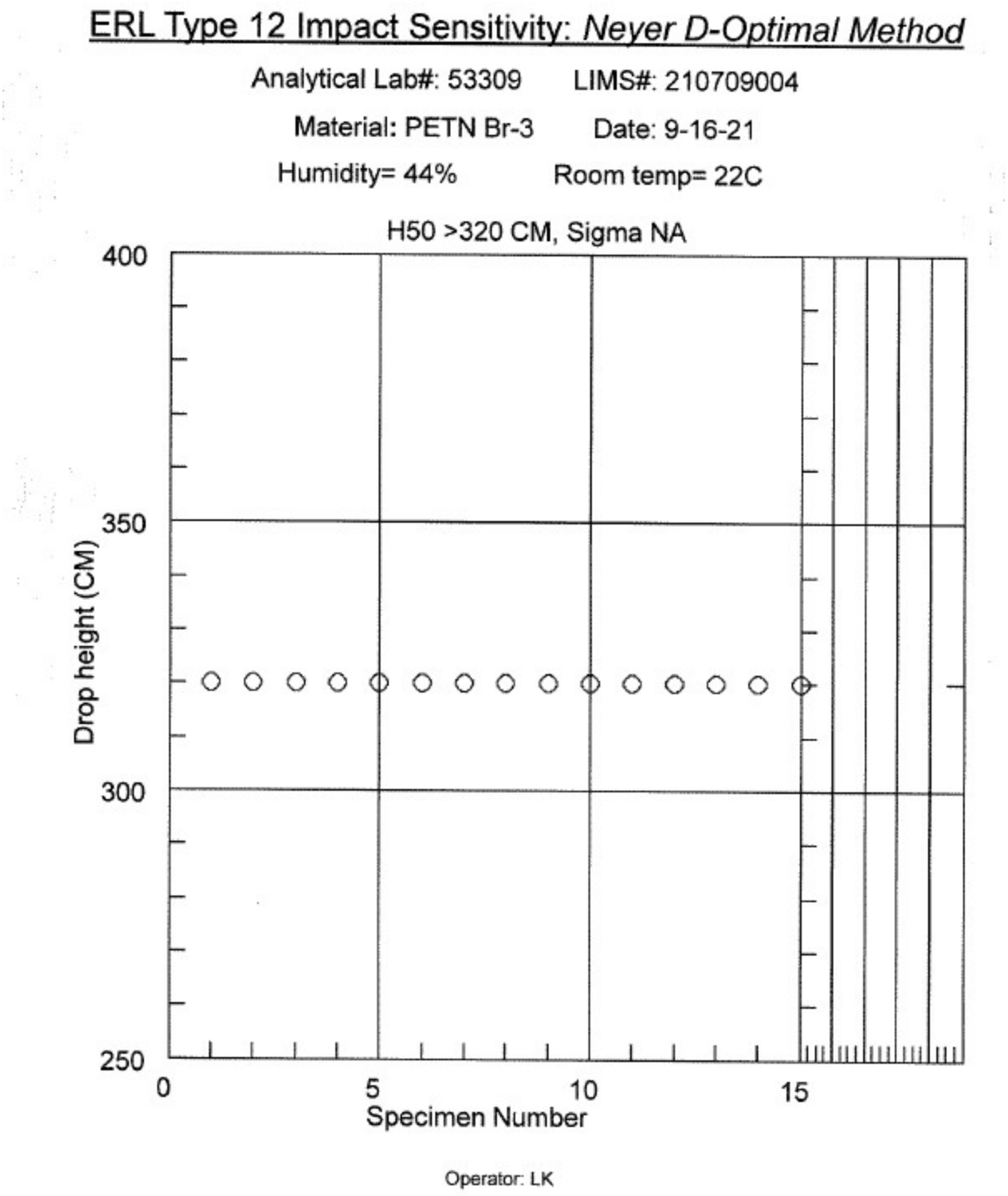

Figure S31: Impact sensitivity data for PEMN-Br3

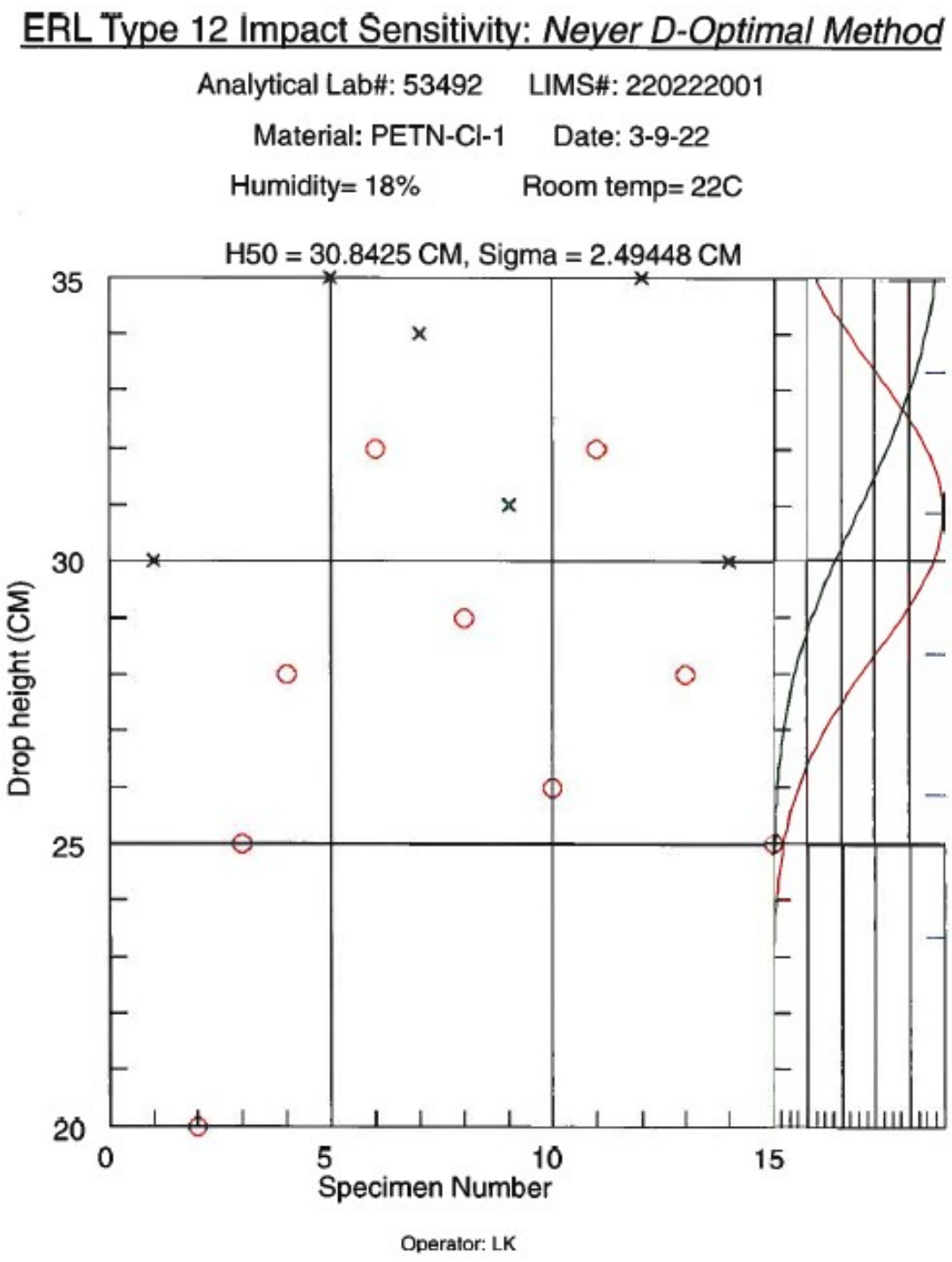

Figure S32: Impact sensitivity data for PETriN-Cl

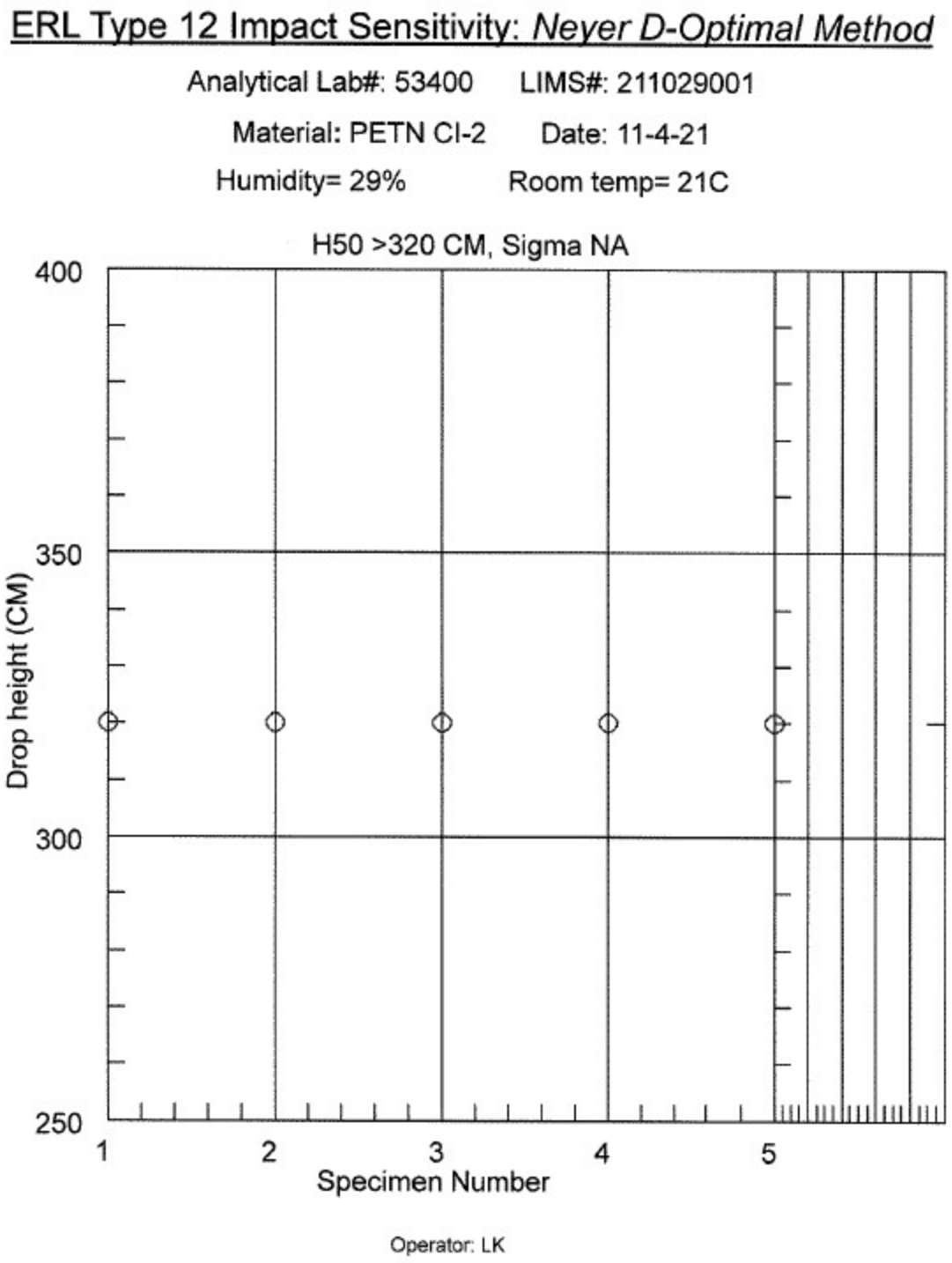

Figure S33: Impact sensitivity data for PEDN-Cl2

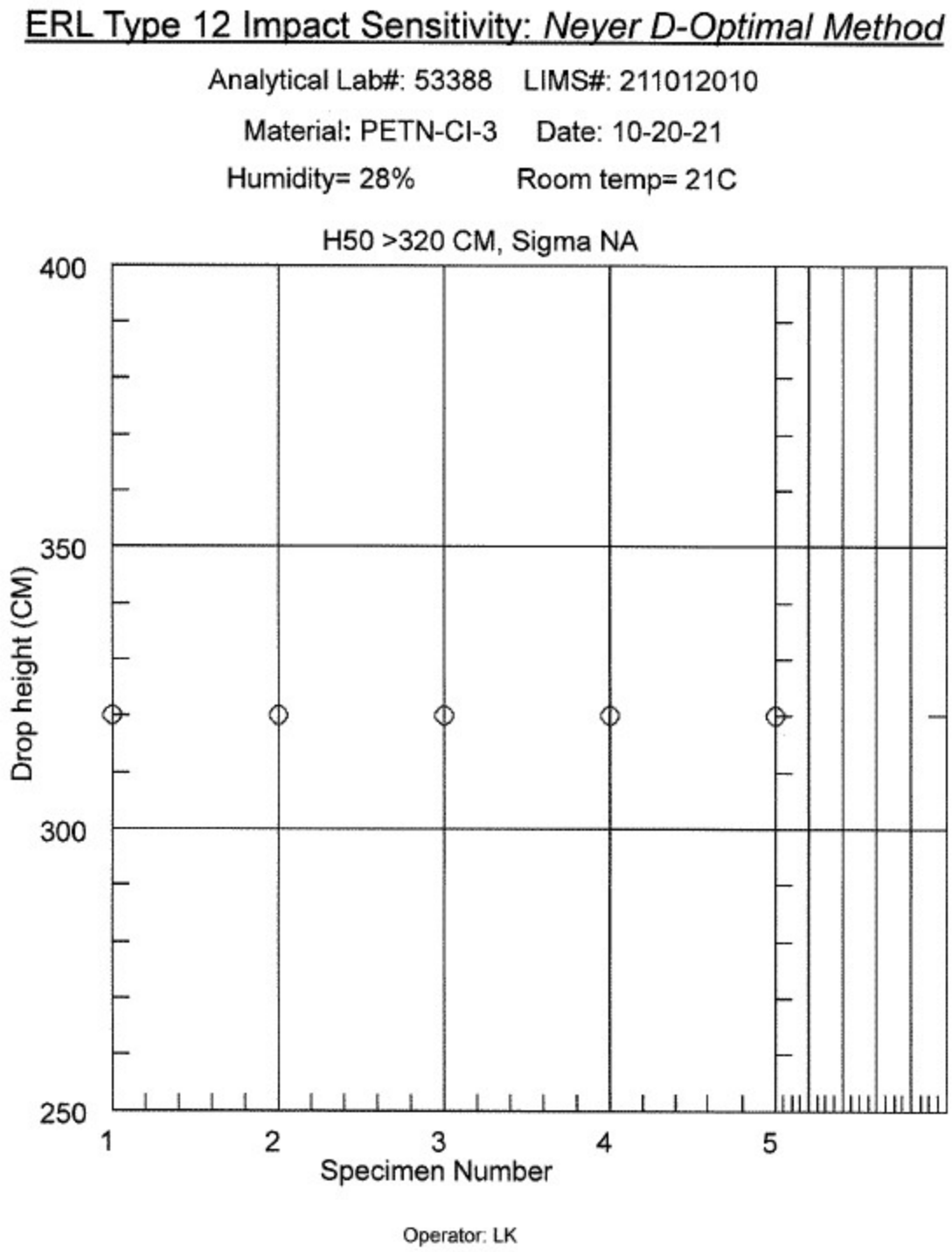

Figure S34: Impact sensitivity data for PEMN-Cl3

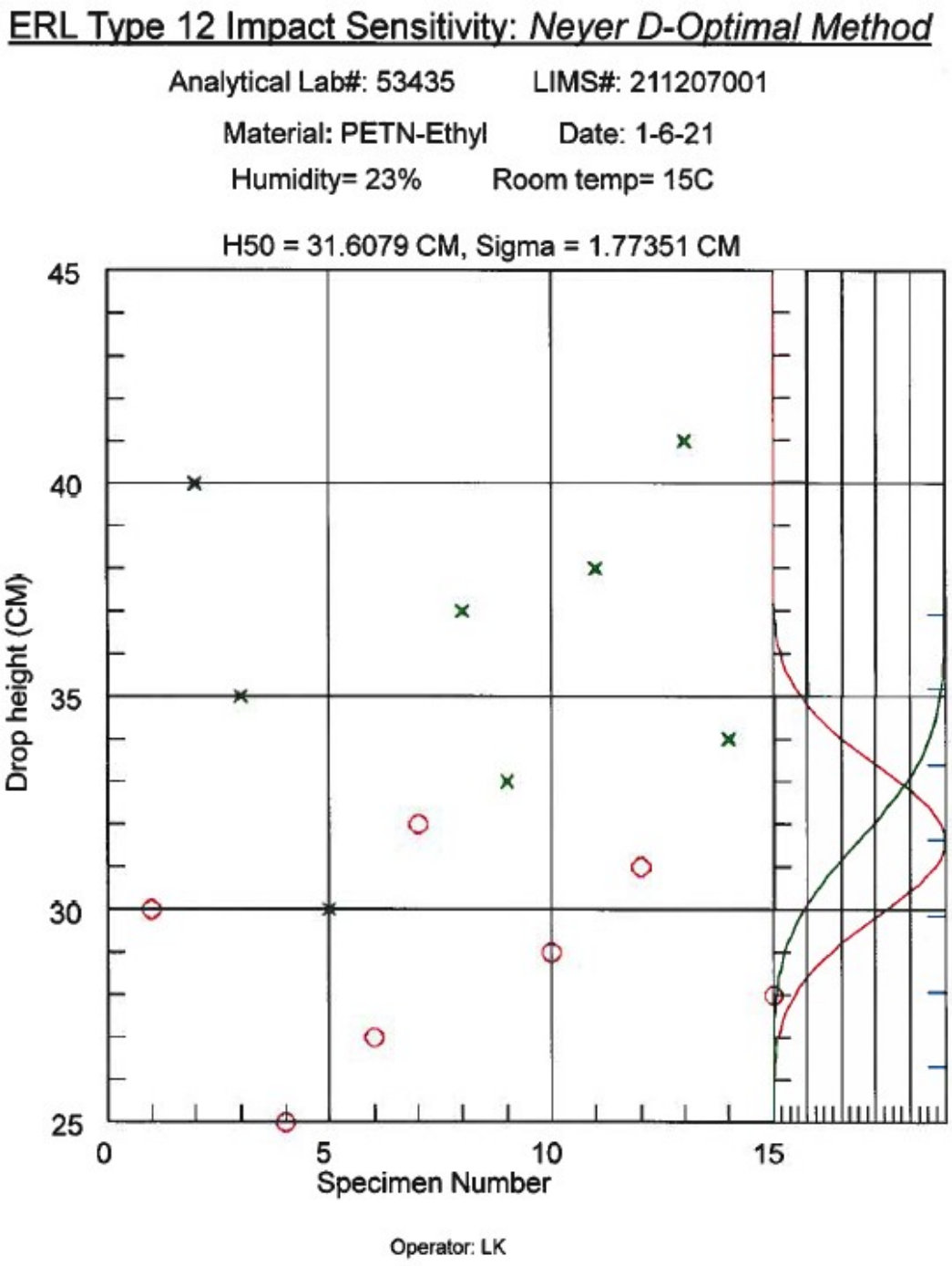

Figure S35: Impact sensitivity data for PETriN-Methyl

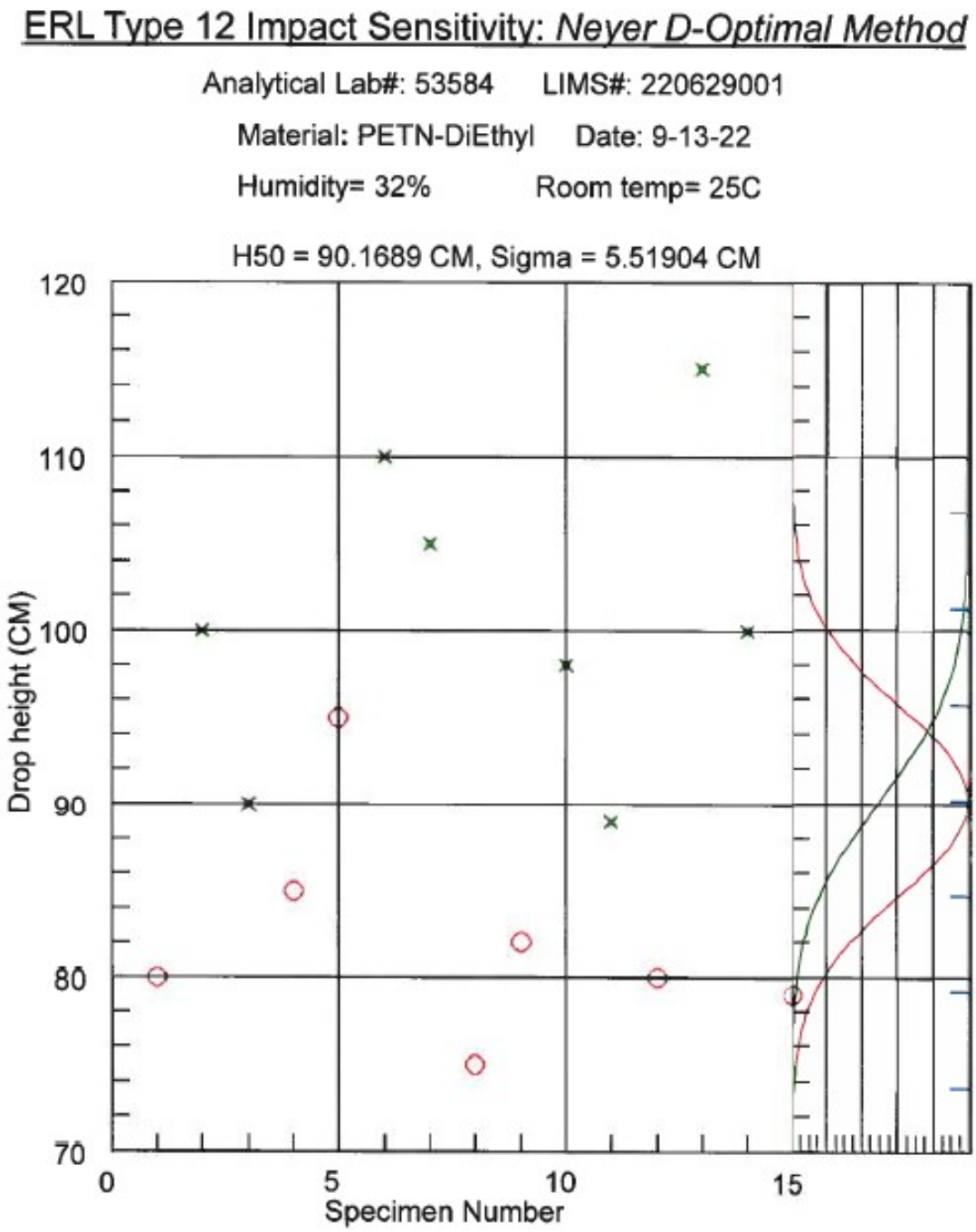

Figure S36: Impact sensitivity data for PEDN-Methyl2

Friction Sensitivity Data:

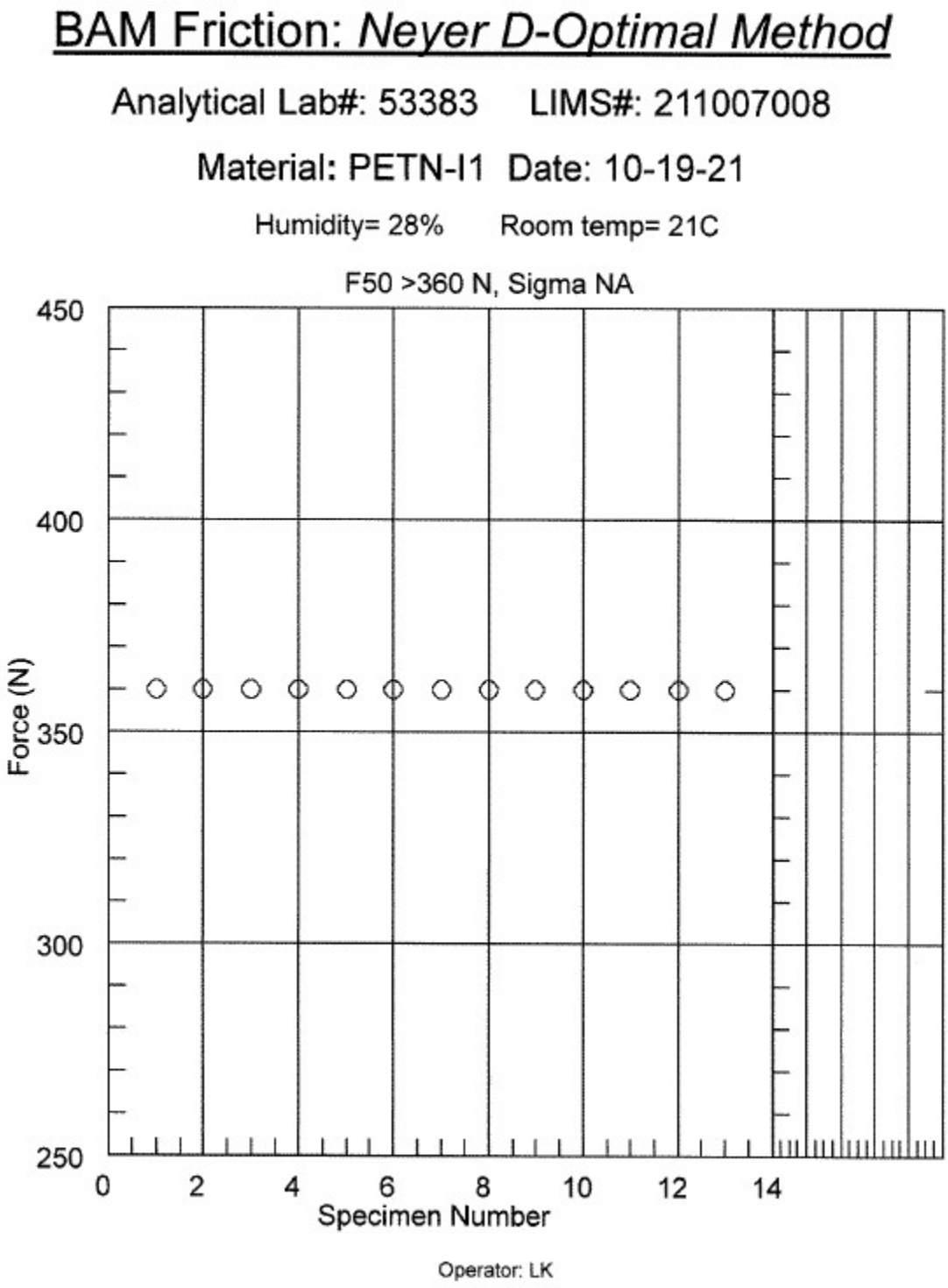

Figure S37: Friction sensitivity data for PETriN-I

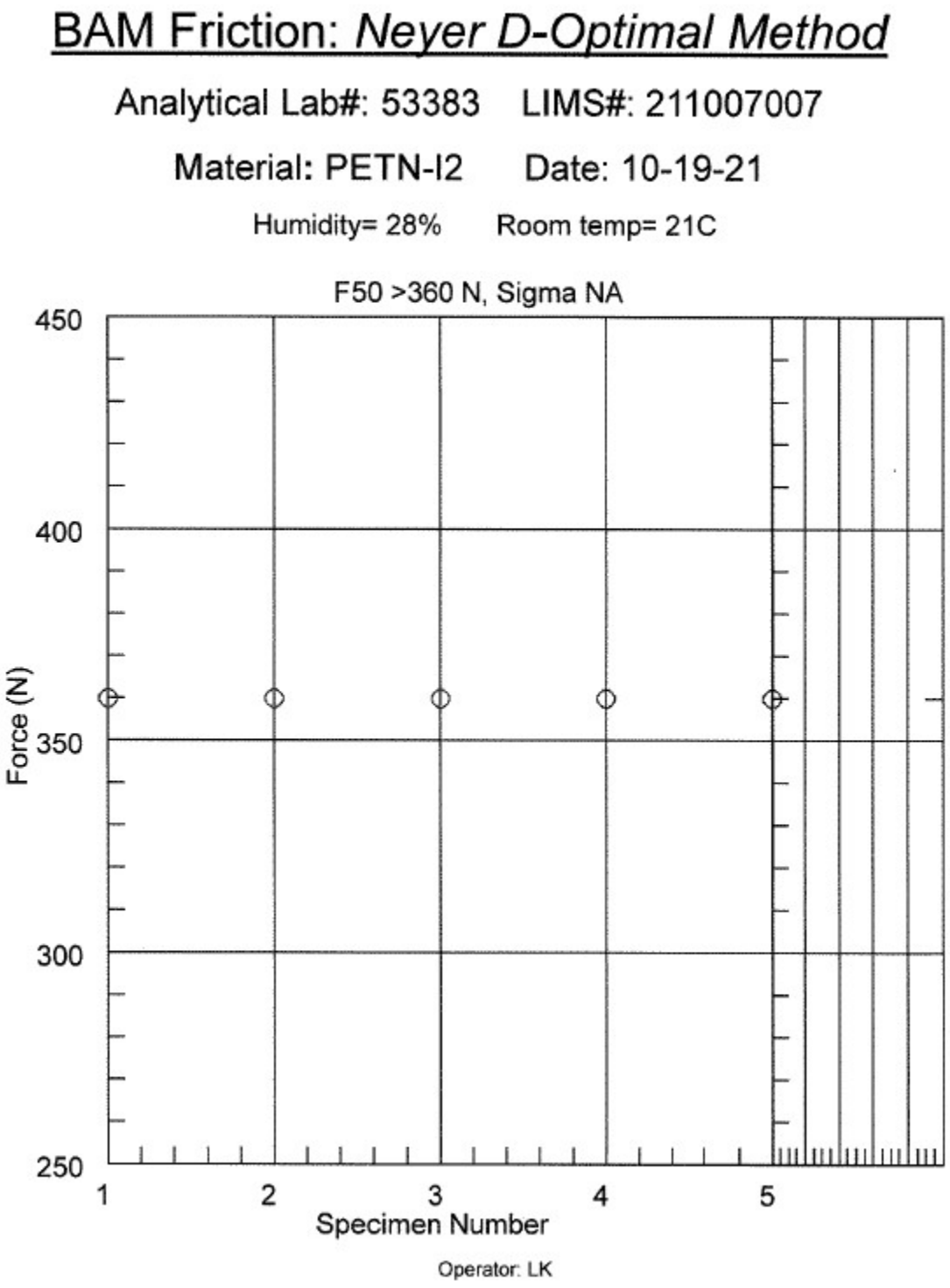

Figure S38: Friction sensitivity data for PEDN-I2

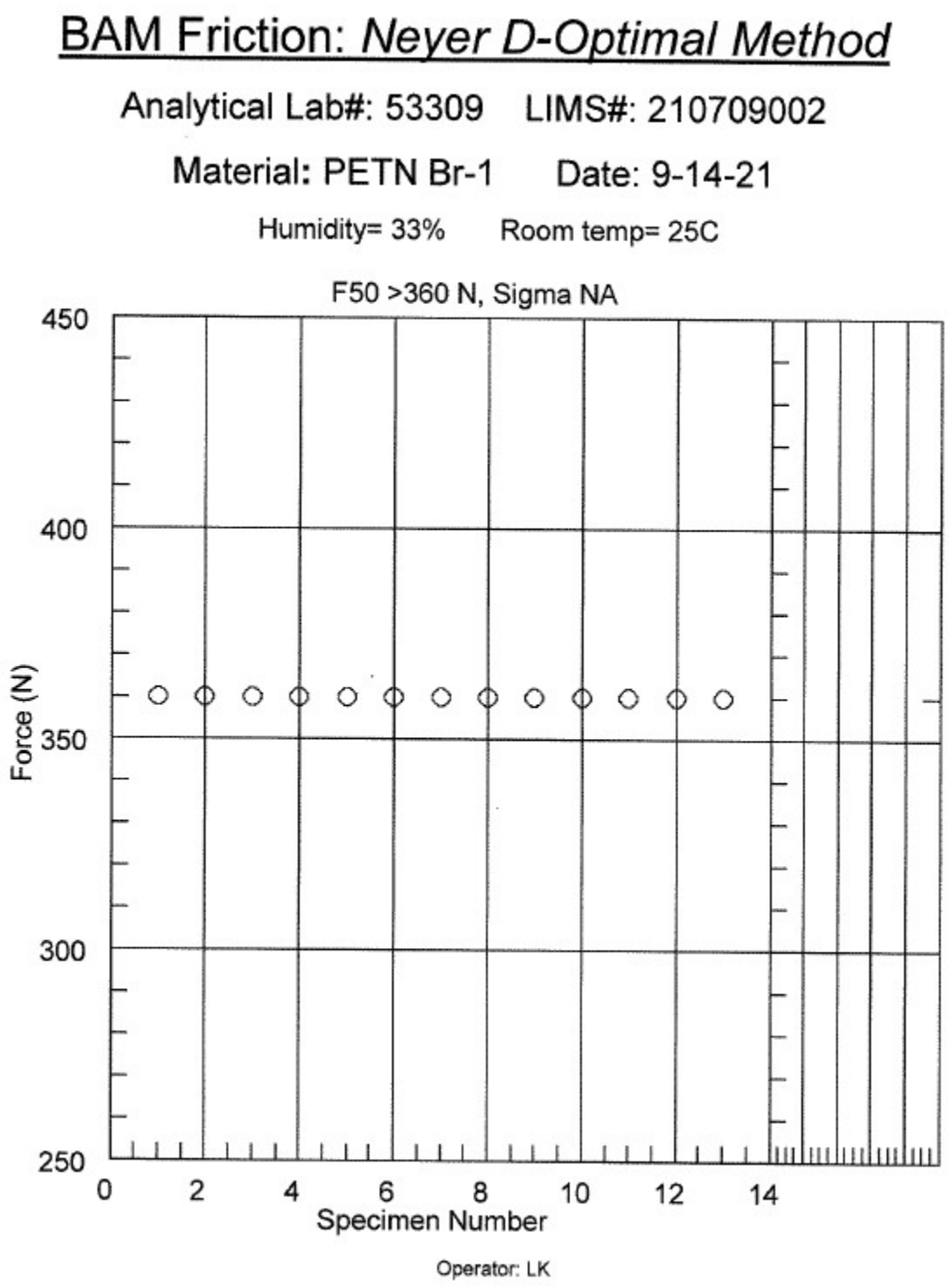

Figure S39: Friction sensitivity data for PETriN-Br

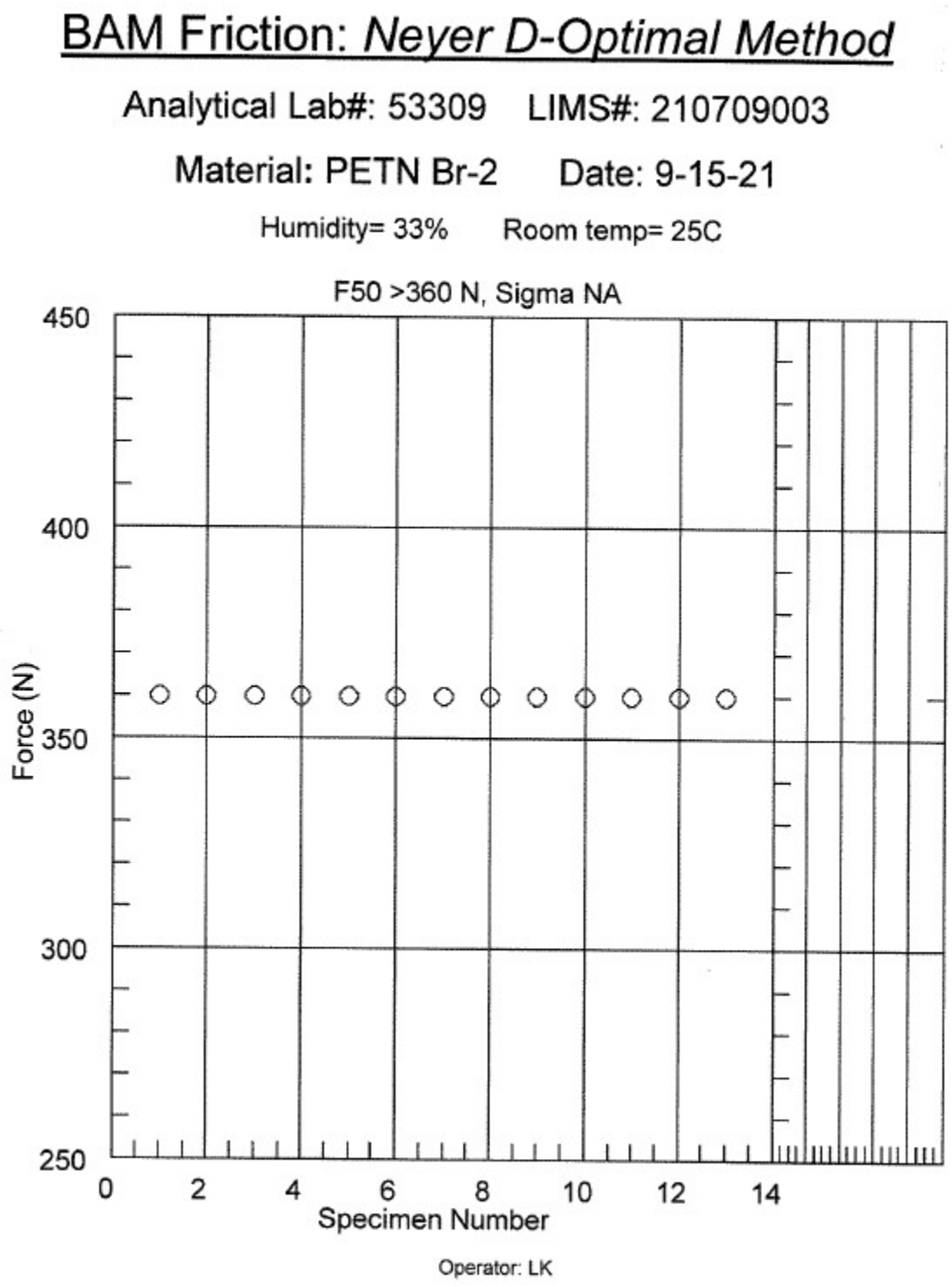

Figure S40: Friction sensitivity data for PEDN-Br2

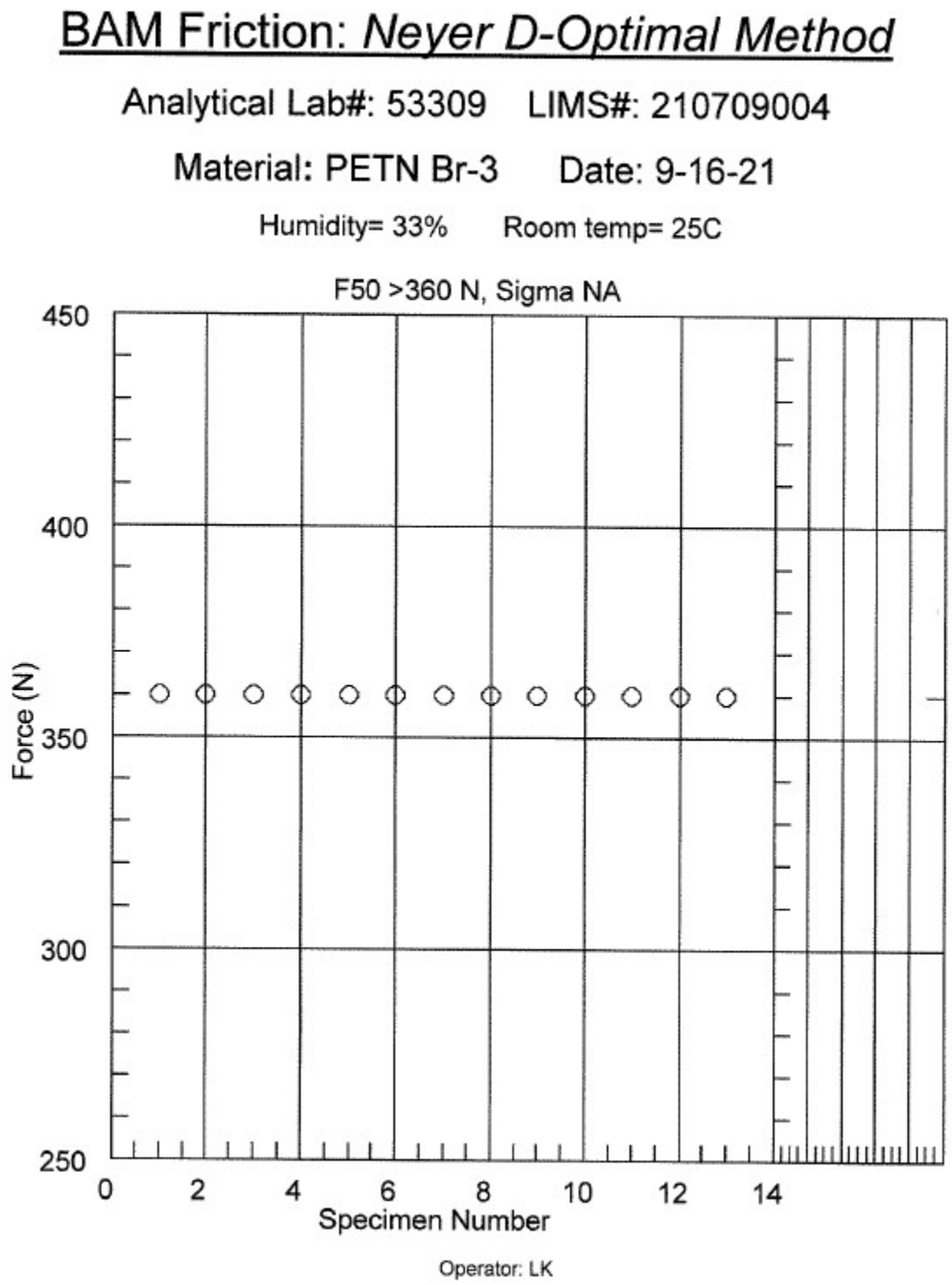

Figure S41: Friction sensitivity data for PEMN-Br3

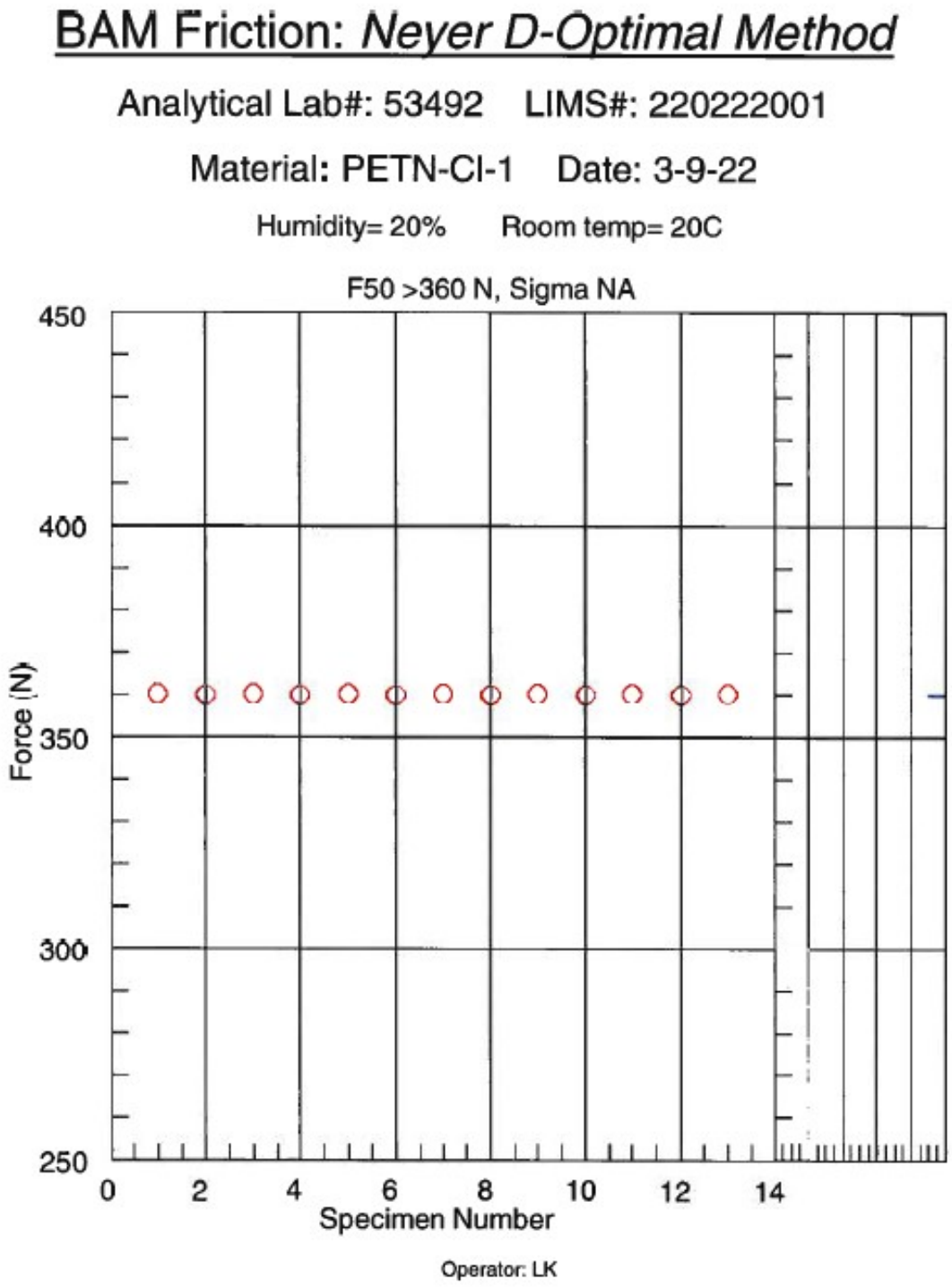

Figure S42: Friction sensitivity data for PETriN-Cl

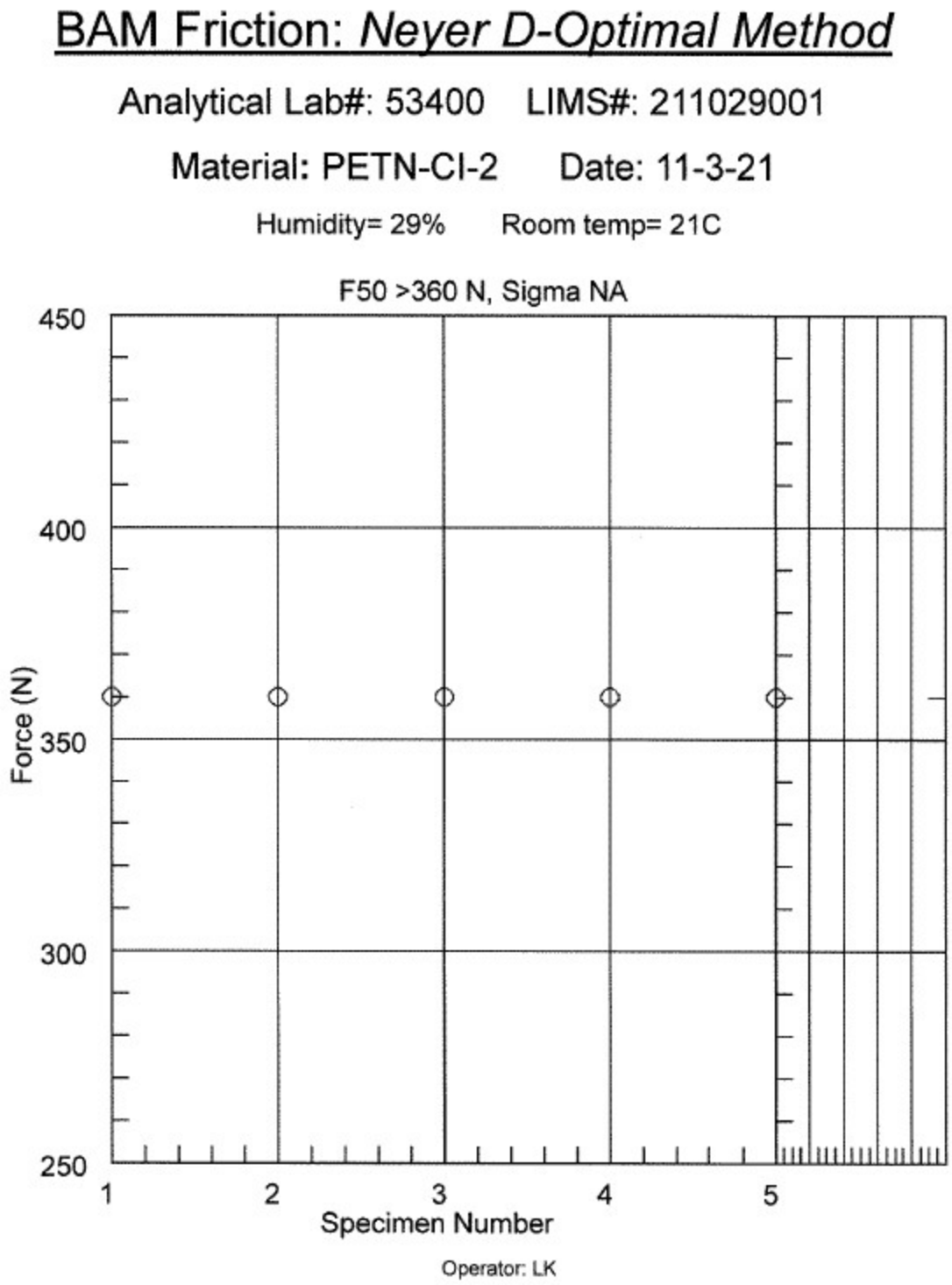

Figure S43: Friction sensitivity data for PEDN-Cl2

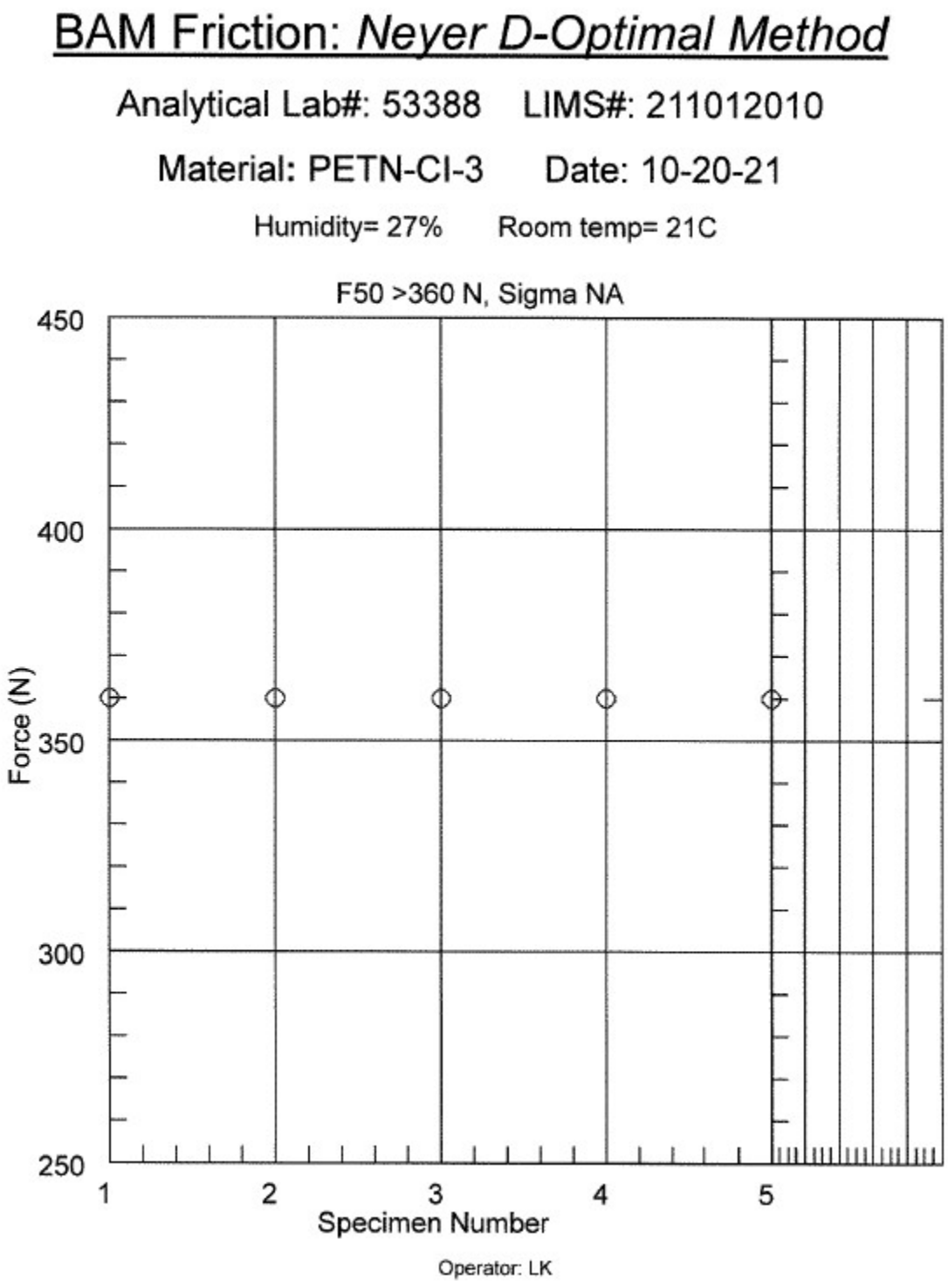

Figure S44: Friction sensitivity data for PEMN-Cl3

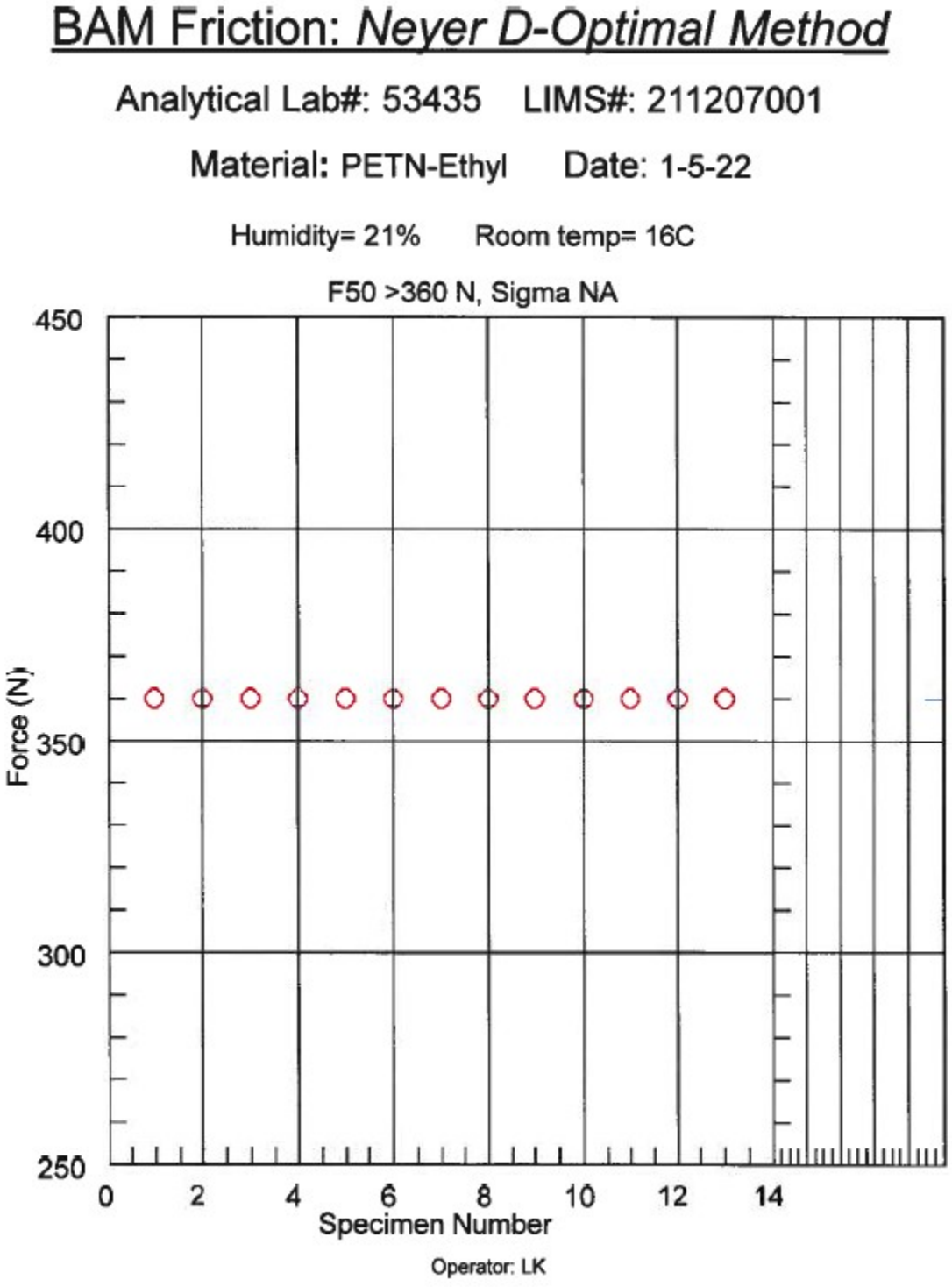

Figure S45: Friction sensitivity data for PETriN-Methyl

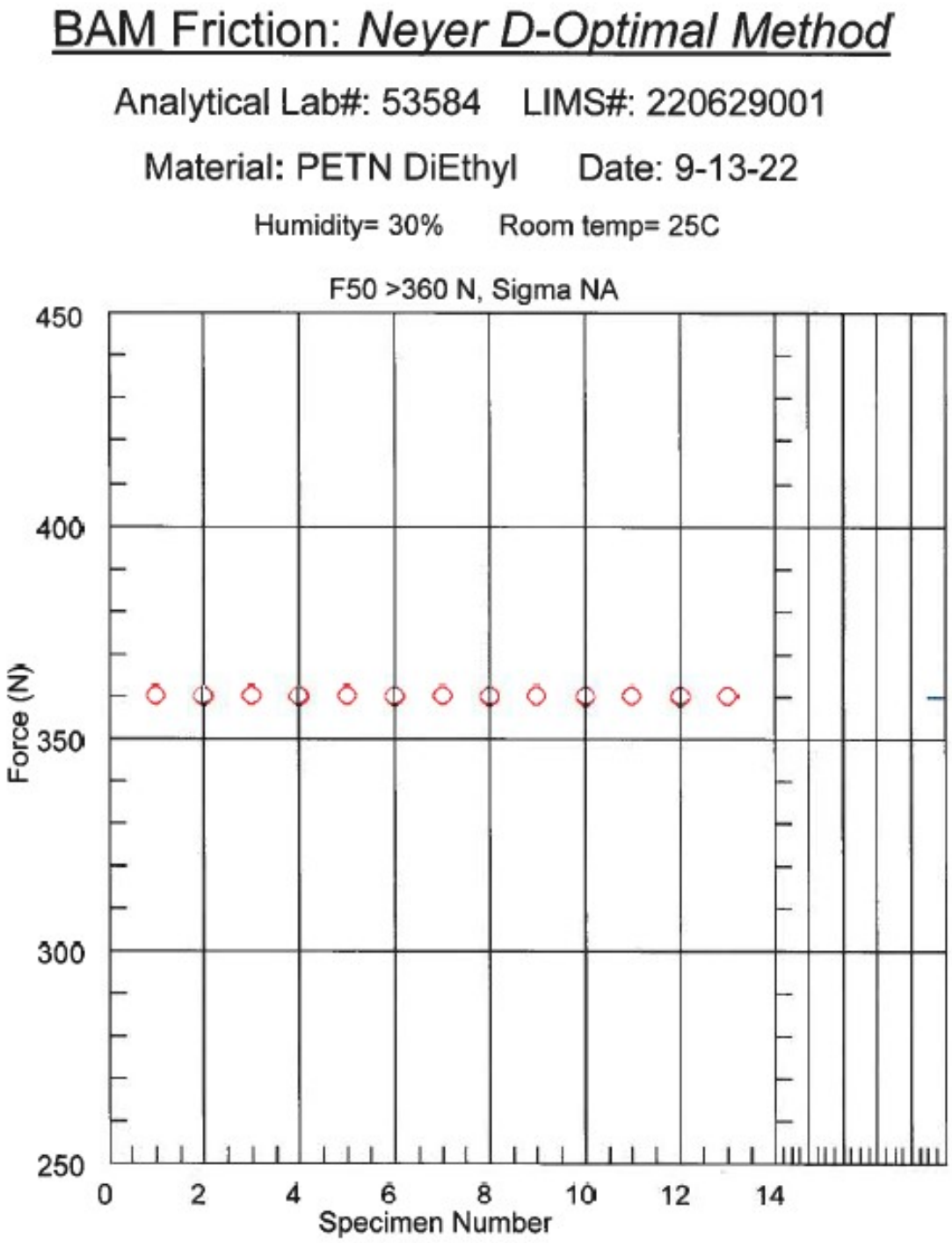

Figure S46: Friction sensitivity data for PEDN-Methyl2

Electrostatic Discharge Sensitivity Data:

Test Results

Discharge Level	1	2	3	4	5	6	7	8	9	10
0.25 Joules	N	E								
0.125 Joules	N	N	E							
0.0625 Joules	N	N	N	N	N	N	N	N	N	N
0.025 Joules										

Test Results (continued)

Discharge Level	11	12	13	14	15	16	17	18	19	20
0.25 Joules										
0.125 Joules										
0.0625 Joules	N	N	N	N	N	N	N	N	N	N
0.025 Joules										

Figure S47: ESD sensitivity data for PETriN-I

Test Results

Discharge Level	1	2	3	4	5	6	7	8	9	10
0.25 Joules	E									
0.125 Joules	E									
0.0625 Joules	N	N	N	N	N					
0.025 Joules										

Figure S48: ESD sensitivity data for PEDN-I2

Test Results

Discharge Level	1	2	3	4	5	6	7	8	9	10
0.25 Joules	N	N	E							
0.125 Joules	N	N	N	N	N	N	N	N	N	N
0.0625 Joules										
0.025 Joules										

Test Results (continued)

Discharge Level	11	12	13	14	15	16	17	18	19	20
0.25 Joules										
0.125 Joules	N	N	N	N	N	N	N	N	N	N
0.0625 Joules										
0.025 Joules										

Figure S49: ESD sensitivity data for PETriN-Br

Test Results

Discharge Level	1	2	3	4	5	6	7	8	9	10
0.25 Joules	N	E								
0.125 Joules	N	N	N	N	N	N	N	N	N	N
0.0625 Joules										
0.025 Joules										

Test Results (continued)

Discharge Level	11	12	13	14	15	16	17	18	19	20
0.25 Joules										
0.125 Joules	N	N	N	N	N	N	N	N	N	N
0.0625 Joules										
0.025 Joules										

Figure S50: ESD sensitivity data for PEDN-Br2

Test Results

Discharge Level	1	2	3	4	5	6	7	8	9	10
0.25 Joules	N	N	E							
0.125 Joules	N	N	N	N	N	N	N	N	N	N
0.0625 Joules										
0.025 Joules										

Test Results (continued)

Discharge Level	11	12	13	14	15	16	17	18	19	20
0.25 Joules										
0.125 Joules	N	N	N	N	N	N	N	N	N	N
0.0625 Joules										
0.025 Joules										

Figure S51: ESD sensitivity data for PEMN-Br3

Test Results

Discharge Level	1	2	3	4	5	6	7	8	9	10
0.25 Joules	E									
0.125 Joules	E									
0.0625 Joules	N	N	N	N	N	N	N	N	N	N
0.025 Joules										

Test Results (continued)

Discharge Level	11	12	13	14	15	16	17	18	19	20
0.25 Joules										
0.125 Joules										
0.0625 Joules	N	N	N	N	N	N	N	N	N	N
0.025 Joules										

Figure S52: ESD sensitivity data for PETriN-Cl

	Test Results									
Discharge Level	1	2	3	4	5	6	7	8	9	10
0.25 Joules	E									
0.125 Joules	N	N	N	N	N					
0.0625 Joules										
0.025 Joules										

Figure S53: ESD sensitivity data for PEDN-Cl2

	Test Results									
Discharge Level	1	2	3	4	5	6	7	8	9	10
0.25 Joules	E									
0.125 Joules	N	N	N	N	N					
0.0625 Joules										
0.025 Joules										

Figure S54: ESD sensitivity data for PEMN-Cl3

Discharge Level	1	2	3	4	5	6	7	8	9	10
0.25 Joules	E									
0.125 Joules	E									
0.0625 Joules	N	N	N	N	N	N	N	N	N	N
0.025 Joules										

	Test Results (continued)									
Discharge Level	11	12	13	14	15	16	17	18	19	20
0.25 Joules										
0.125 Joules										
0.0625 Joules	N	N	N	N	N	N	N	N	N	N
0.025 Joules										

Figure S55: ESD sensitivity data for PETriN-Methyl

	Test Results									
Discharge Level	1	2	3	4	5	6	7	8	9	10
0.25 Joules	N	N	E							
0.125 Joules	N	E								
0.0625 Joules	N	N	E							
0.025 Joules	N	N	N	N	N	N	N	N	N	N

	Test Results (continued)									
Discharge Level	11	12	13	14	15	16	17	18	19	20
0.25 Joules										
0.125 Joules										
0.0625 Joules										
0.025 Joules	N	N	N	N	N	N	N	N	N	N

Figure S56: ESD sensitivity data for PEDN-Methyl2

Differential Scanning Calorimetry (DSC) Data:

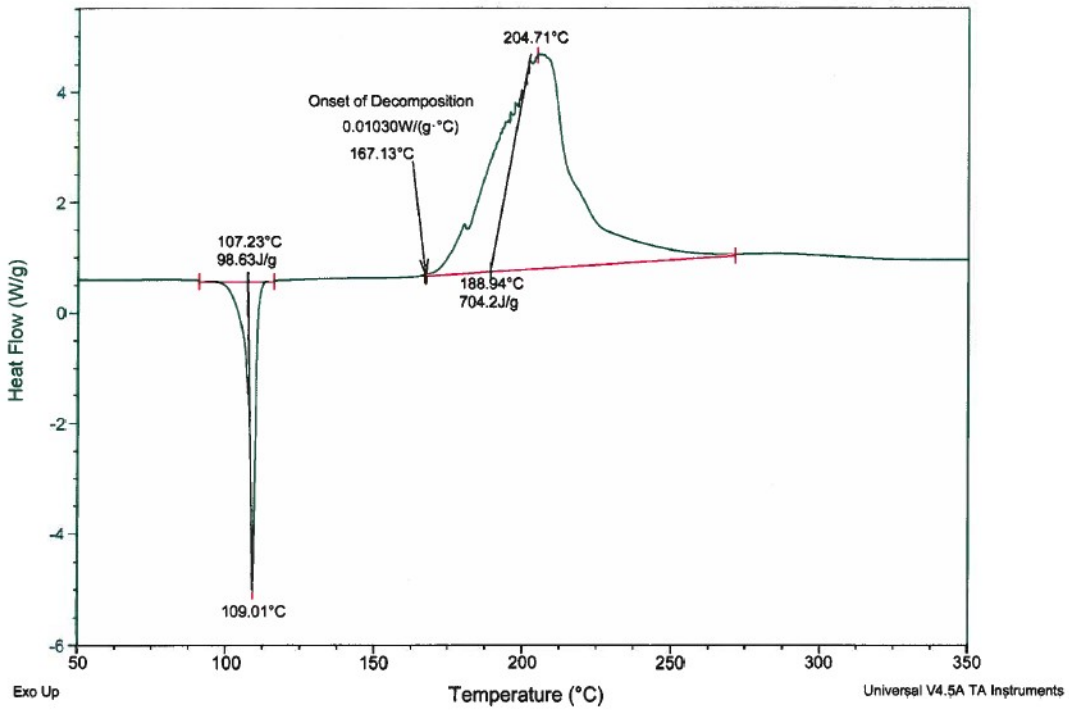

Figure S57: DSC data for PETriN-I

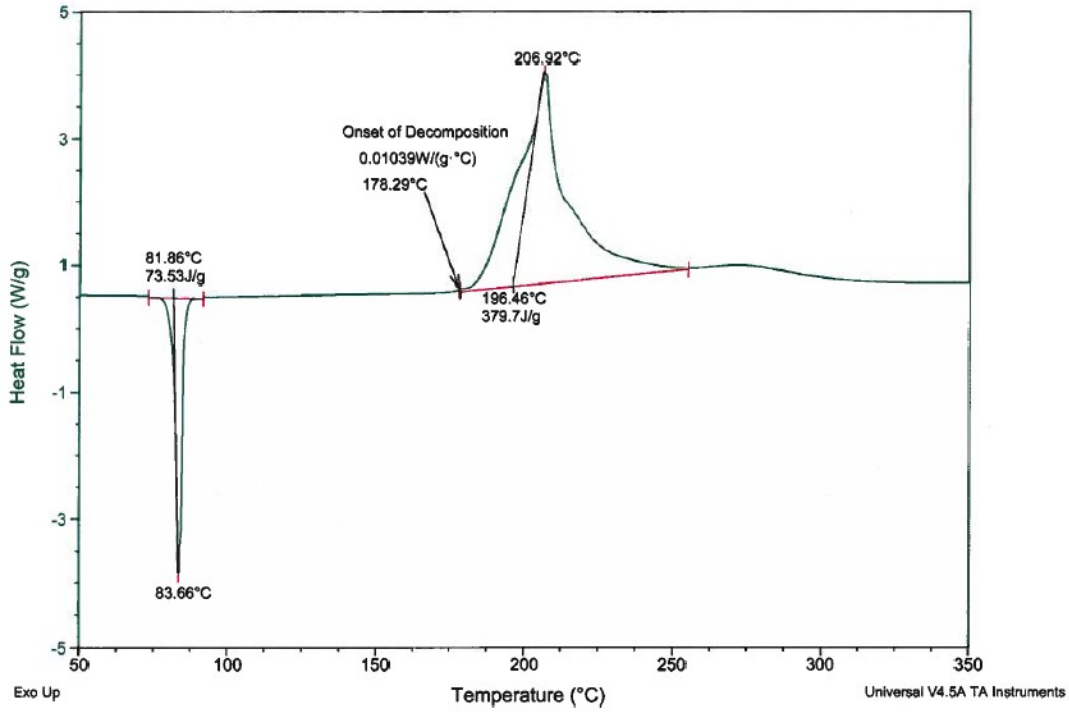

Figure S58: DSC data for PEDN-I2

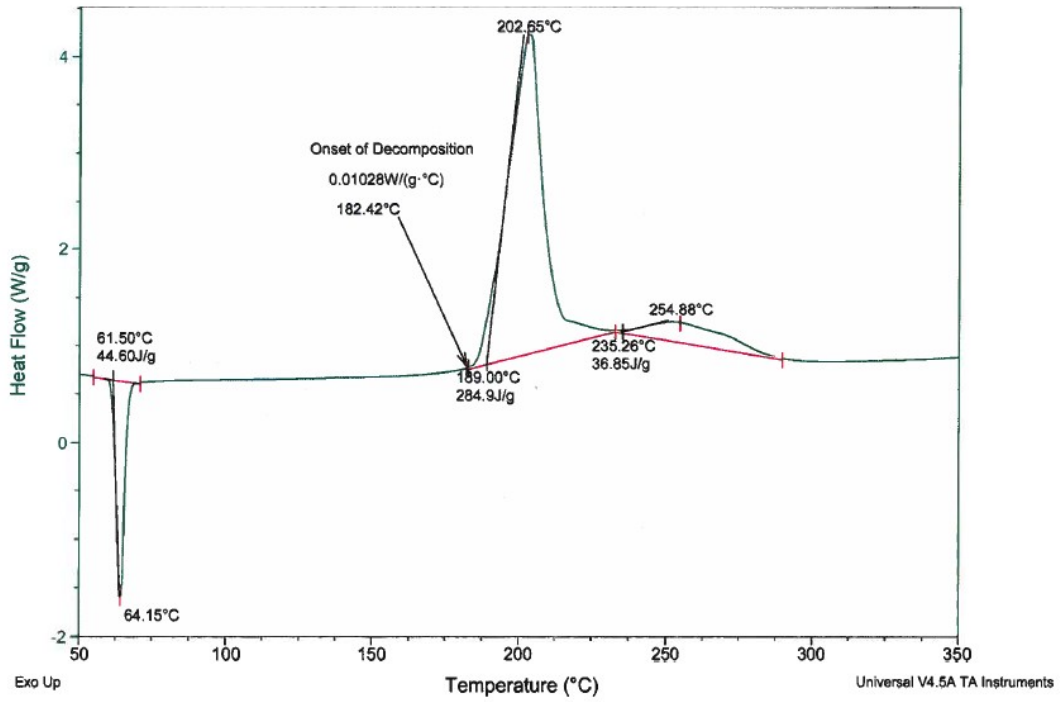

Figure S59: DSC data for PEMN-I3

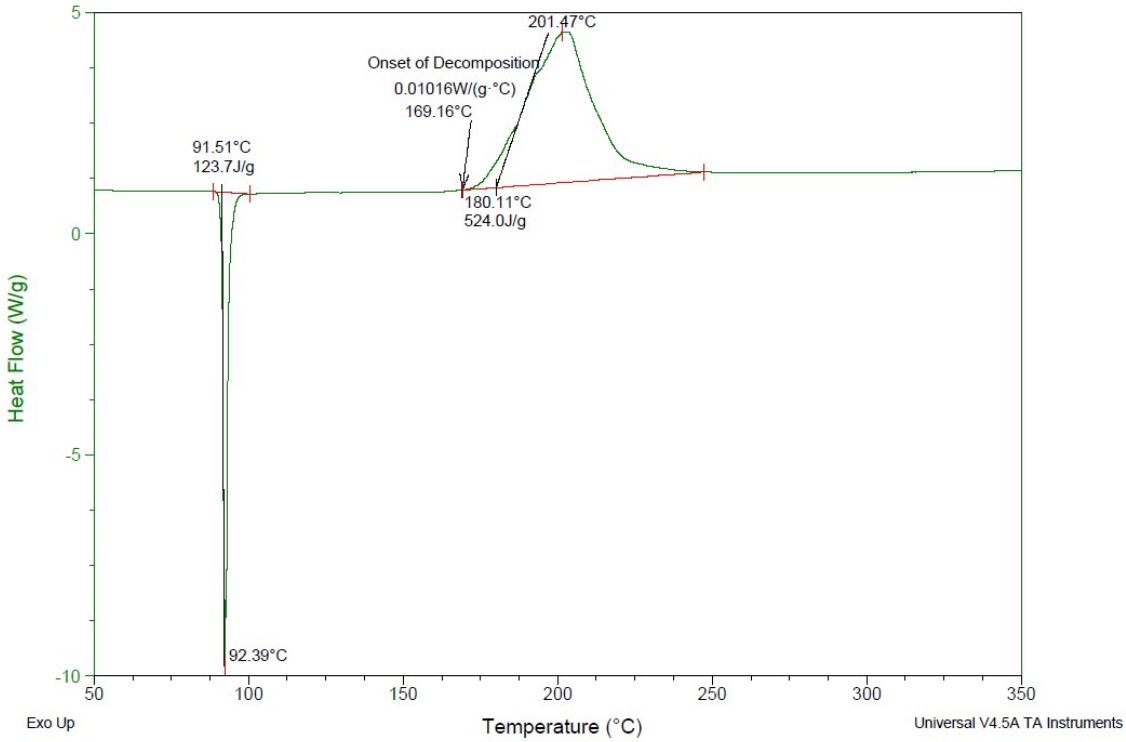

Figure S60: ^{13}C-NMR of compound PETriN-Br

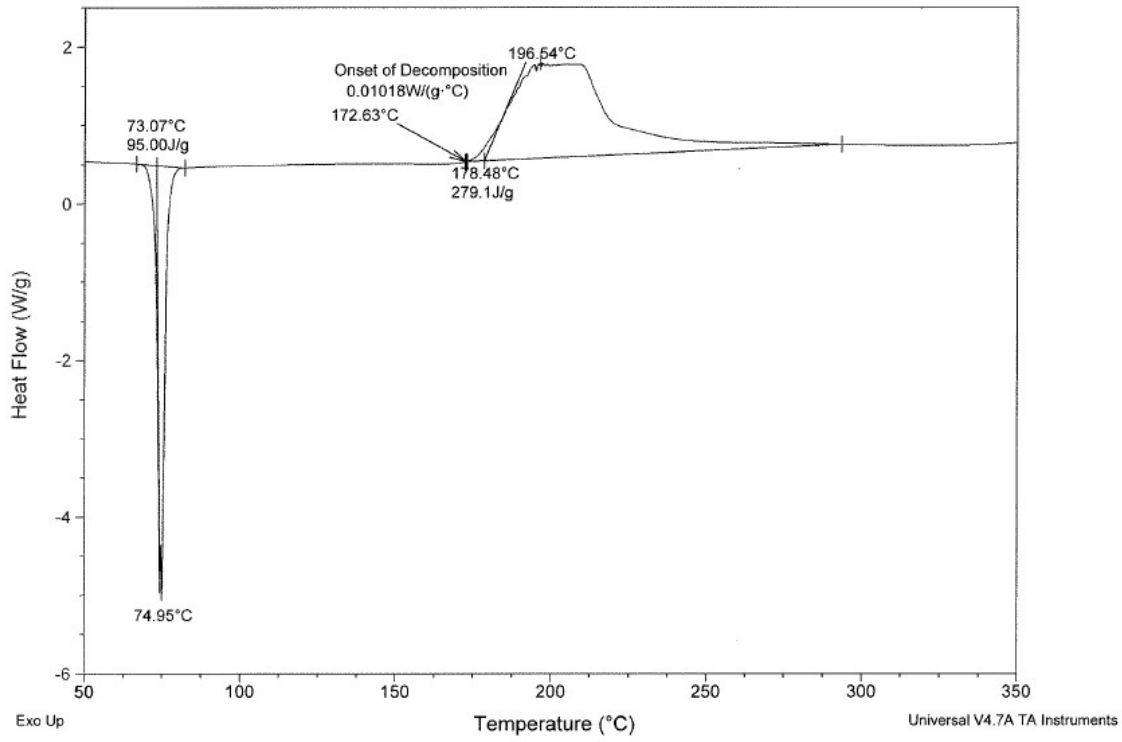

Figure S61: DSC data for PEDN-Br2

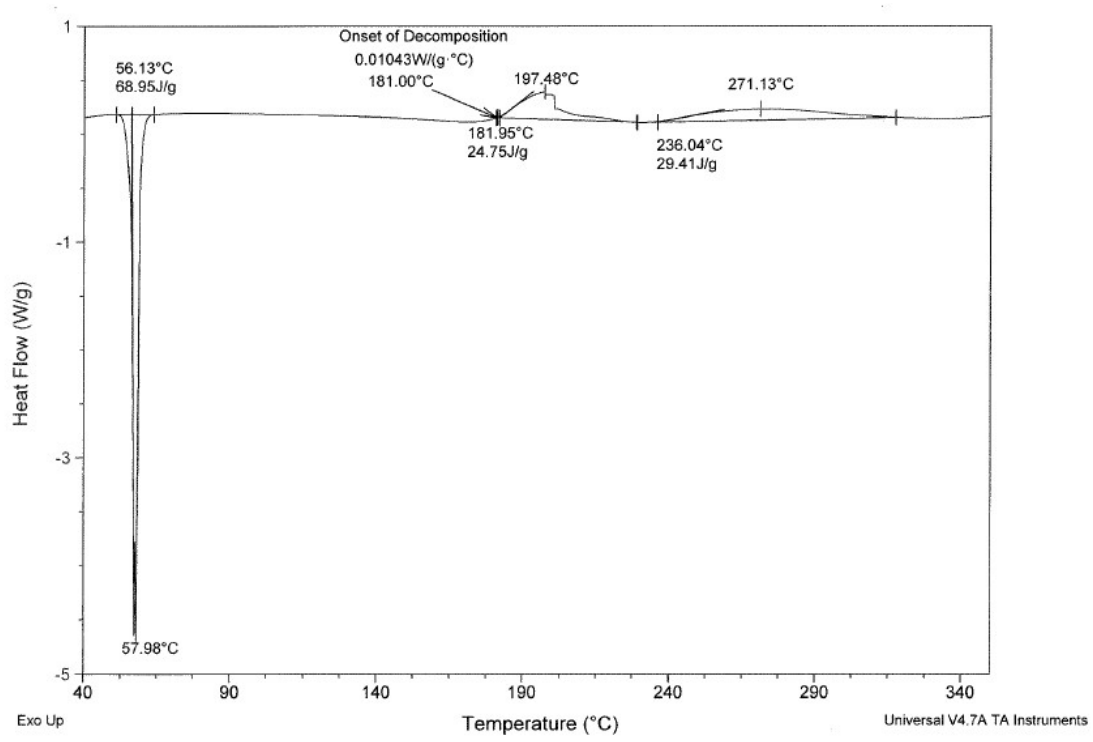

Figure S62: DSC data for PEMN-Br3

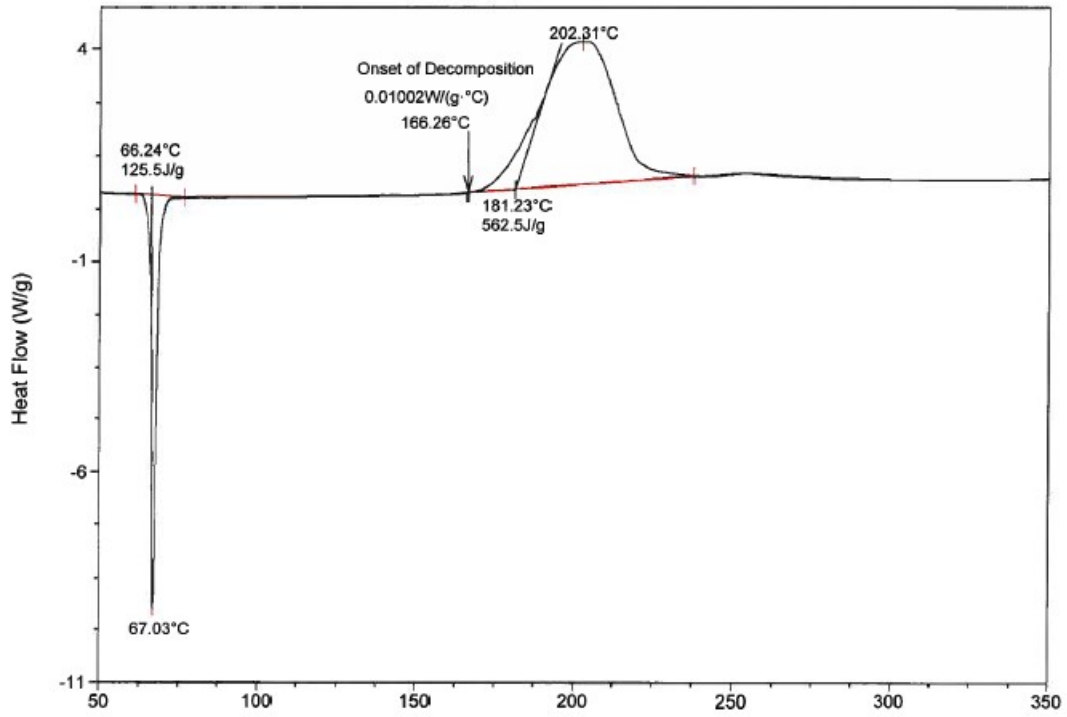

Figure S63: DSC data for PETriN-Cl

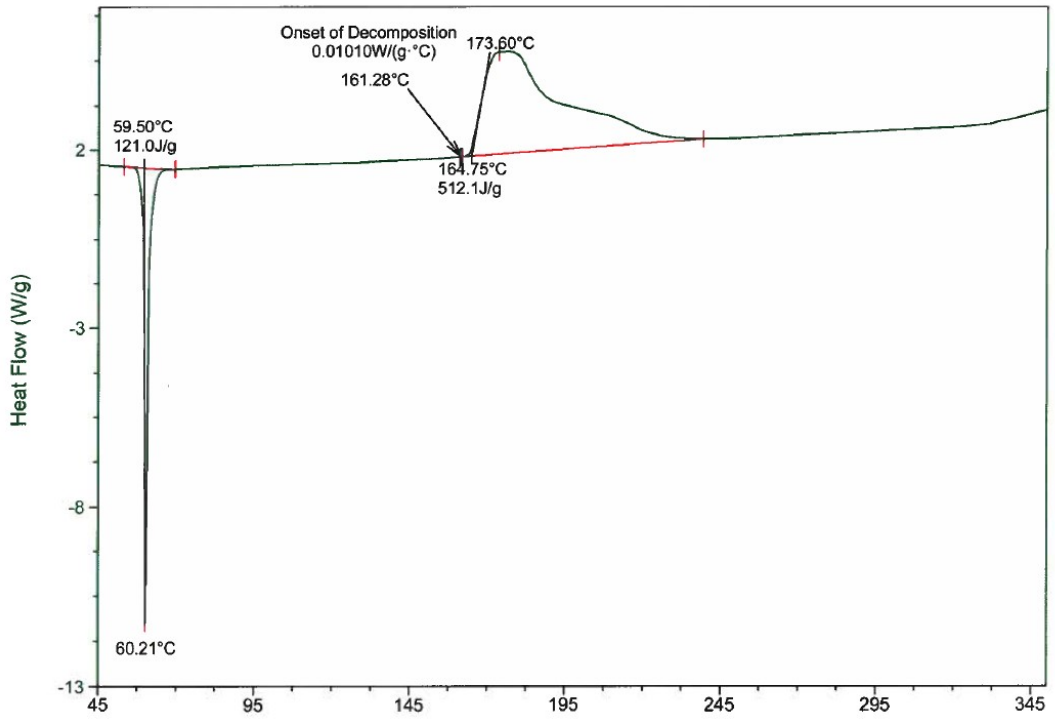

Figure S64: DSC data for PEDN-Cl2

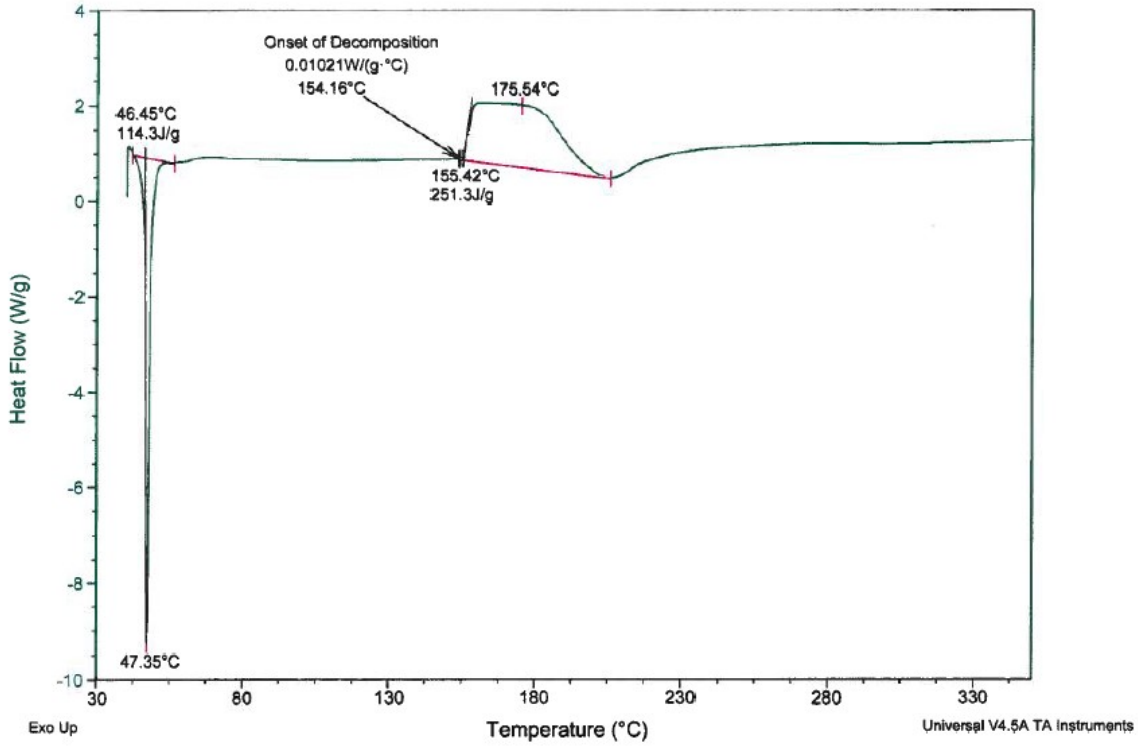

Figure S65: DSC data for PEMN-Cl3

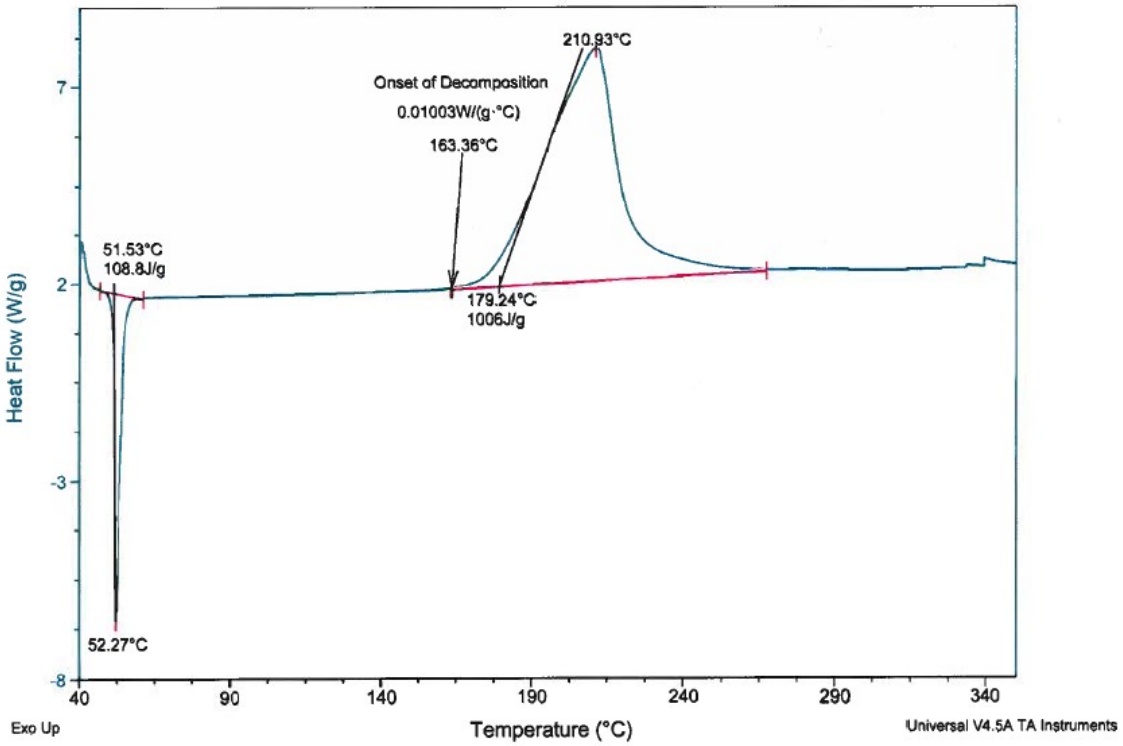

Figure S66: DSC data for PETriN-Methyl

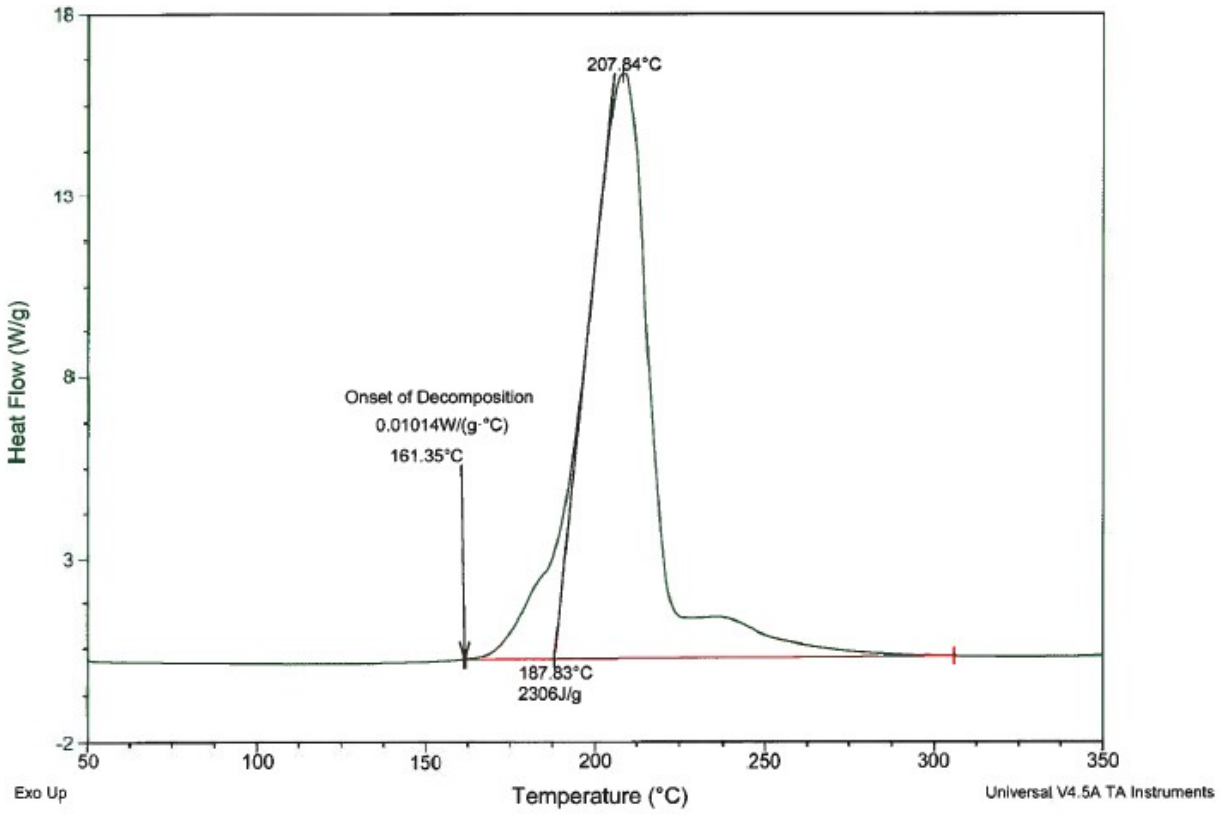

Figure S67: DSC data for PEDN-Methyl2

VIII. DFT Heat of formation calculations for CHNO-X

Atom equivalent energies for the estimation of the heat of formation of organic energetic molecules containing halogens

The heat of formation, ΔH_f, of an energetic molecule is used to estimate its enthalpy of explosion,

$$Q = \frac{-1}{\text{Mol. Wt.}}\left(\sum_j n_j (\Delta H_f^p)_j - \Delta H_f \right) \qquad \text{* MERGEFORMAT (1.1)}$$

where n_j is the number of moles of product species, j, with heats of formation, ΔH_f^p, derived from one mole of reactants [4-5]. The amounts, n, and types of product molecules can be derived from the stoichiometry of the reactant via a set of prescribed oxidation priorities, as in Ref [6]. The specific enthalpy of explosion characterizes the performance and theoretical maximum energy release of an energetic material. It is also correlated with handling safety because high-performance explosives tend to be relatively sensitive to accidental initiation, and vice versa [7-9]

Owing to the importance of the enthalpy of explosion, Q, to the development and characterization of new energetic materials, a number of computational approaches have been developed to rapidly estimate the ΔH_f for reactant species [10-15]. Here, it should be noted that the calorimetry techniques used to quantify ΔH_f experimentally may not be feasible during the earliest stages of synthesis owing to the limited quantities of material available. Rather than develop from scratch a new model for the ΔH_f of the CHNO-X explosives synthesized in this work, where X = F, Cl, Br, I, we have instead chosen to extend the density functional theory-based approach of Byrd and Rice [16] to organic molecules containing halogens.

The Byrd and Rice scheme for energetic molecules, which has become *de rigueur* within the field, is based on a set of atom-equivalent energies, ϵ, that map the total energy, u, from a high-level density functional theory (DFT) calculation to the corresponding heat of formation,

$$\Delta H_f = u - \sum_l \eta_l \epsilon_l \qquad \text{* MERGEFORMAT (1.2)}$$

where η_l is the number of atoms of type l in the molecule. The set of atom equivalent energies is parameterized to minimize the error between the ΔH_f obtained via Eq. 2 and a set of standard reference values from experiment. To improve accuracy and transferability, the Byrd and Rice scheme distinguishes between C, N, and O atoms in single and multiply-bonded environments, resulting in a set of seven atom equivalent energies for molecules containing only C, H, N, and O. We have extended the Byrd and Rice scheme by parameterizing new atom equivalent energies, ϵ_l, for $l =$ F, Cl, Br, and I. We used the same B3LYP exchange-correlation functional [17] and the 6-31G* and 6-311++G(2df,2p) basis sets for the structural optimization and total energy calculations, respectively, that were employed in the original model [16]. However, the calculations on iodine-containing molecules used the standard 6-311G and 6-311G(d,p) basis sets for the I atoms and the 6-311++G(2df,2p)//6-31G* basis sets for all other elements. All DFT calculations were performed using the Gaussian 16 package [18].

As described in Ref. [15], the counts of C, N, and O atoms forming only single bonds (η_C, η_N, η_O) versus those forming double, triple, or resonant bonds etc. ($\eta_{C'}$, $\eta_{N'}$, $\eta_{O'}$) were obtained by the calculation of bond-orders, or Wiberg bond indices, B_{ij}, between pairs of atoms i and j from the self-consistent density matrix, P, in the orthogonalized representation,

$$B_{ij} = \sum_{\alpha \in i} \sum_{\beta \in j} (2P^{\perp}_{i\alpha, j\beta})^2 \qquad \text{* MERGEFORMAT (1.3)}$$

where α and β label electronic orbitals [19-20]. The density matrices were computed using minimal basis density functional tight binding theory [21] with the *lanl*31 parameter set [22]. These calculations were performed by substituting halogen atoms for H atoms because *lanl*31 lacks parameters for those elements. This procedure was found to be effective because H, like the halogens, can form only single bonds. The numbers of H and halogen atoms were determined from the stoichiometry of each molecule, which are provided with the Supplementary Material.

The MS Excel spreadsheet included with the Supplementary Materials provides the training data for the CHNO-X molecules for X = F, Cl, Br, and I. All of the reference ΔH_f values were obtained from the NIST Chemistry WebBook [23]. This resource also provided the IUPAC International Chemical Identifier (InChI) for each molecule, which we translated using the Open Babel package [24] into SMILES and 3D atomic coordinates suitable for DFT and DFTB calculations. The four atom equivalent energies for the halogens were fitted using 5-fold cross validation to these data sets. The atom equivalent energies for C, H, N, O, C', N', and O' were taken from Ref. [16] without modification. The best fit atom equivalent energies, root-mean-square errors, and maximum deviations are provided in Table S1. Correlation plots of the computed versus reference ΔH_f values are provided in Figures S68-S71.

Table S1. Best-fit atom equivalent energies for the halogens F, Cl, Br, and I for the extended Byrd and Rice model. The root mean square error and maximum deviations are derived from the best-fit energies and the four sets of training data provided with the Supplementary Material.

	ϵ_X (Hartree)	RMS error (kcal/mol)	Max. Deviation (kcal/mol)
F	-99.792760	7.50	39.44
Cl	-460.209040	4.44	15.48
Br	-2574.142934	2.98	7.79
I	-6919.549033	3.99	10.29

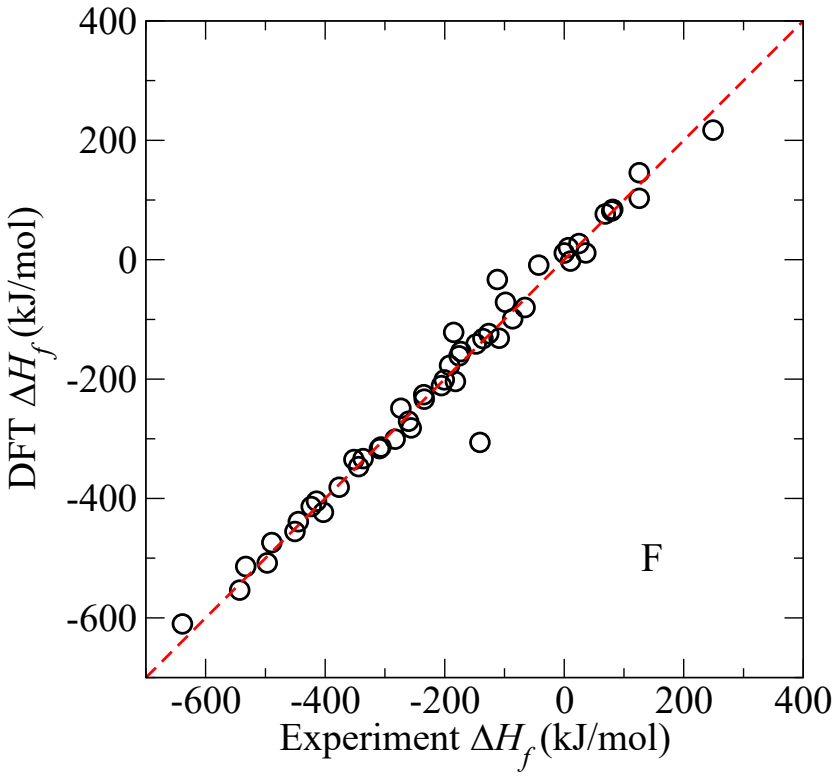

Figure S68. Correlation plot for ΔH_f computed using the extended atom equivalent energy model vs standard reference data for 50 CHNO+F compounds.

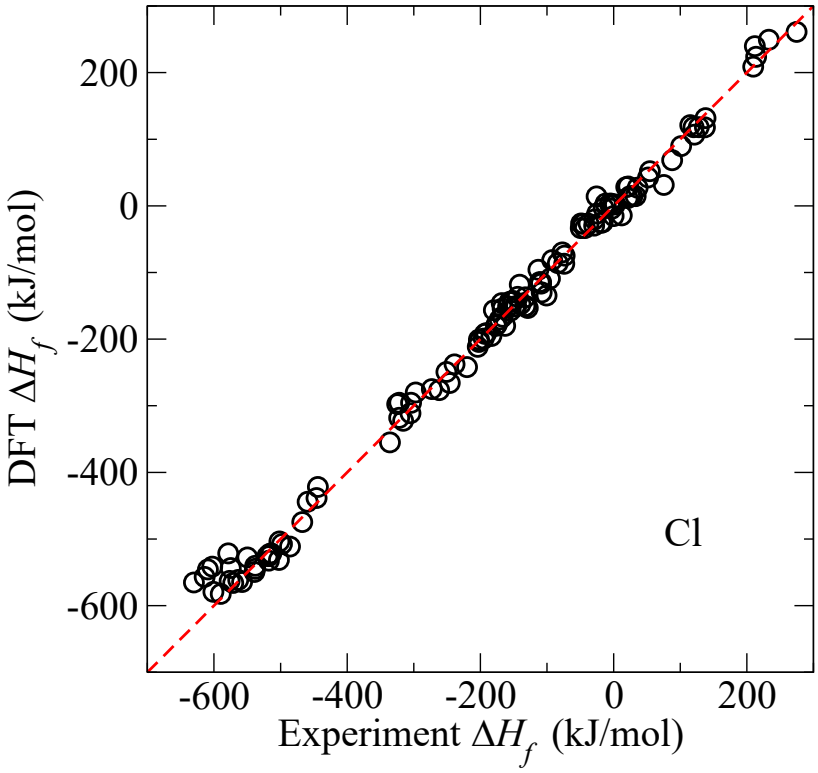

Figure S69. Correlation plot for ΔH_f computed using the extended atom equivalent energy model vs standard reference data for 127 CHNO+Cl compounds.

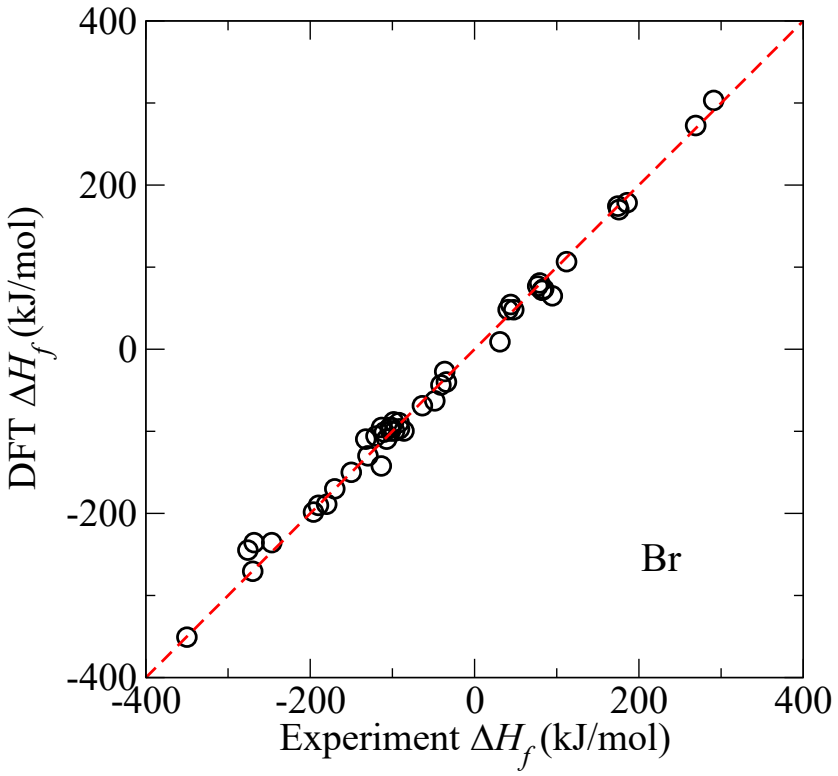

Figure S70. Correlation plot for ΔH_f computed using the extended atom equivalent energy model vs standard reference data for 34 CHNO+Br compounds.

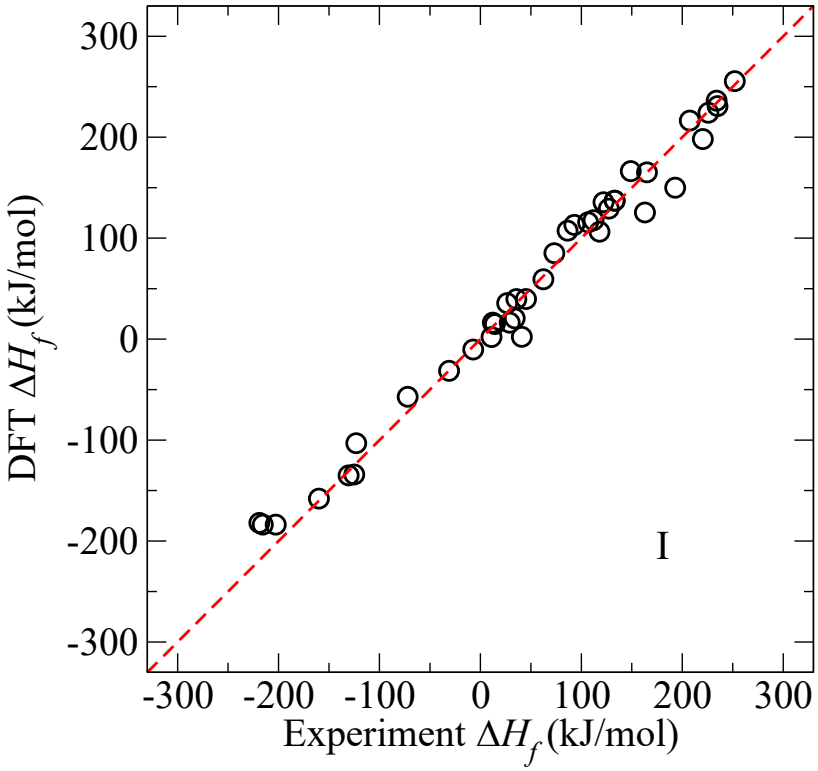

Figure S71. Correlation plot for ΔH_f computed using the extended atom equivalent energy model vs standard reference data for 40 CHNO+I compounds.

Single Crystal X-Ray Diffraction:

Single crystals retrieved from concentrated EtOH solutions were mounted on a MiTeGen micromount with NVH immersion oil. The data were collected on a Bruker D8 VENTURE Duo PHOTON 3 or a Rigaku XtaLAB Mini II (**PEDN-I_2**). Samples were maintained at 250 K (**PEMN-Cl_3**), 293 K (**PEDN-I_2**), 296 K (**PETriN-Cl**, **PEDN-Cl_2**, **PETriN-Br**, **PEMN-Br_3**, **PEMN-I_3**, **PETriN-Me**) using an Oxford Cyrostreams 800 low-temperature device or at ambient 305 K (**PEDN-Br_2**, **PETriN-I**). The D8 VENTURE was equipped with a microfocus tube and a graphite monochromatized Mo Kα X-ray source (λ = 0.71073). A full sphere (**PETriN-Cl**, **PEDN-Cl_2**, **PETriN-Br**, **PEDN-Br_2**, **PETriN-I**, **PETriN-Me**) or hemisphere (**PEMN-Cl_3**, **PEMN-Br_3**, **PEDN-I_2**, **PEMN-I_3**) of data was collected using phi and omega scans. Data collection, initial indexing, and cell refinement were conducted using the Bruker Apex 4 suite [25], or by using CrysAlis Pro.[26] The data were corrected for absorption using redundant reflections and the SADABS program [25] (Apex 4) or by SCALE 3 ABSPACK (CrysAlis Pro).[26] Structures were solved by intrinsic phasing, and difference Fourier techniques were performed in Olex2.[27] Hydrogen atoms positions were idealized and allowed to ride on the attached carbon atom. *HKL* reflections with error/esd values ±10 were omitted from the models. The final refinement included anisotropic temperature factors on all non-hydrogen atoms. Structure solution and refinement were performed in Olex2 [27] using SHELXT,[28] and SHELXL,[29] respectively. Publication figures were generated using Mercury 4.0.[30]

Table 1.

	PETriN-Cl	PEDN-Cl_2	PEMN-Cl_3	PETriN-Br	PEDN-Br_2
Formula	$(C_5H_8ClN_3O_9)_2$	$C_5H_8Cl_2N_2O_6$	$(C_5H_8Cl_3NO_3)_2$	$(C_5H_8BrN_3O_9)_2$	$C_5H_8Cl_2N_2O_6$
FW (g mol^{-1})	579.19	263.03	472.95	668.11	351.95
Crystal system	Monoclinic	Monoclinic	Monoclinic	Orthorhombic	Monoclinic
Space group	$P2_1/c$	C2	Cc	$P2_12_12_1$	C2
a (Å)	12.5956(11)	14.7924(15)	12.074(4)	6.6728(9)	14.8421(4)
b (Å)	6.6449(6)	6.6138(6)	6.959(3)	12.5692(19)	6.7381(2)
c (Å)	27.335(2)	12.570(2)	22.562(9)	27.033(4)	12.6407(6)
α (deg)	90	90	90	90	90
β (deg)	102.653(5)	121.680(4)	90.017(13)	90	120.534(2)
γ (deg)	90	90	90	90	90
Volume ($Å^3$)	2232.3(3)	1046.5(2)	1895.7(12)	2267.3(6)	1088.86(7)
Z	4	4	4	4	4
ρ_{calc} (g cm^{-3})	1.723	1.669	1.657	1.957	2.147
μ (mm^{-1})	3.566	5.773	0.934	5.472	9.634
F (000)	1184	536	960	1328	680
θ range (deg)	3.314/74.20	4.13/73.80	3.375/24.88	3.269/69.45	4.060/70.00
R(int)	0.0414	0.0522	0.0828	0.0897	0.0809
data/restraints/parameters	4529/0/326	2021/1/137	4626/2/217	4620/0/325	1960/1/138
GOF	1.094	1.065	1.057	1.036	1.132
R_1 [$I > 2\sigma(I)$][a]	0.0809	0.0258	0.0296	0.0336	0.0408
wR_2 (all data)[b]	0.2314	0.0618	0.0613	0.0785	0.0952
Ext. Coeff.	0.0040(7)	-	-	-	0.0010(2)
Largest peak/hole (e · $Å^{-3}$)	0.811/-0.367	0.151/-0.250	0.181/-0.152	0.546/-0.533	0.527/-0.555
Temp (K)	296(1)	296(1)	250(1)	296(1)	305(1)

a. $R_1 = \Sigma\, ||F_o|-|F_c|| \,/\, \Sigma|F_o|$ for reflections with $F_o^2 > 2\,\sigma(F_o^2)$ b. $wR_2 = [\sum w(F_o^2 - F_c^2)^2 \,/\, \sum(F_o^2)^2]^{1/2}$ for all reflections.

Table 2.

	PEMN-Br_3	PETriN-I	PEDN-I_2	PEMN-I_3	PETriN-Me
Formula	$C_5H_8Br_3NO_3$	$(C_5H_8IN_3O_9)_2$	$C_5H_8I_2N_2O_6$	$C_5H_8I_3NO_3$	$C_6H_{11}N_3O_9$
FW (g mol^{-1})	369.85	761.08	445.93	510.82	269.18
Crystal system	Monoclinic	Orthorhombic	Monoclinic	Orthorhombic	Monoclinic
Space group	$P2_1$	$P2_12_12_1$	$P2_1/c$	$P2_12_12_1$	$P2_1/n$
a (Å)	7.0321(3)	6.7370(4)	13.1616(8)	6.9671(2)	7.5161(2)
b (Å)	11.3862(5)	12.6197(7)	13.0126(8)	12.3623(5)	11.0417(3)
c (Å)	7.2912(3)	27.5521(14)	6.7544(4)	26.6682(12)	14.1414(3)
α (deg)	90	90	90	90	90
β (deg)	118.747(2)	90	98.802(5)	90	92.476(2)
γ (deg)	90	90	90	90	90
Volume ($Å^3$)	511.85(4)	2342.4(2)	1143.18(12)	2296.92(15)	1172.51(5)
Z	2	4	4	8	4
ρ_{calc} (g cm^{-3})	2.400	2.158	2.591	2.954	1.525
μ (mm^{-1})	11.792	21.997	5.513	8.139	1.297
F (000)	348	1468	824	1824	560
θ range (deg)	3.187/25.68	3.208/55.15	3.103/28.461	2.247/25.31	6.265/73.55
R(int)	0.0819	0.1302	0.0394	0.0807	0.0781
data/restraints/parameters	3376/1/109	4105/0/326	2337/0/137	6434/0/217	2102/0/165
GOF	1.013	0.976	1.054	1.027	1.026
R_1 [$I > 2\sigma(I)$][a]	0.0355	0.0503	0.0288	0.0376	0.0463
wR_2 (all data)[b]	0.0577	0.1120	0.0609	0.0828	0.1152
Ext. Coeff.	-	0.0020(2)	0.0076(3)	-	0.023(4)
Largest peak/hole (e · $Å^{-3}$)	0.353/-0.395	0.881/-0.655	1.207/-0.776	2.062/-0.650	0.235/-0.159
Temp (K)	296(1)	305(1)	293(1)	296(1)	296(1)

a. $R_1 = \Sigma\, |F_o|-|F_c| \,/\, \Sigma|F_o|$ for reflections with $F_o^2 > 2\,\sigma(F_o^2)$ b. $wR_2 = [\sum w(F_o^2 - F_c^2)^2 \,/\, \sum(F_o^2)^2]^{1/2}$ for

References:

1. Mondanaro, K. R.; Dailey, W. P. *Organic Syntheses, Coll. Vol. 10, p.212 (2004); Vol. 75, p.89 (1998).*2.
2. (a) G. C. Shaw, D. L. Seaton, *J. Org. Chem.* **1961**, 5227-5228. (b) M. E. Hill, F. Taylor, Jr. *J. Org. Chem.* **1960**, 1037-1038. (c) W. M. Koppes, H. G. Adolph, M. E. Sitzmann, *U. S. Patent 4,173,591*, November 6, 1979.
3. (a) A. A. DeFusco, Jr., A. T. Nielsen, R. L. Atkins, *U. S. Patent 4,434,304*, February 28, 1984. (b) T. M. Benziger, *U. S. Patent 4,032,377*, June 28, 1977.
4. Zeman, S.; Jungova, M., Sensitivity and Performance of Energetic Materials. *Explos. Pyrotech.* **2016**, *41*, 426-451.
5. Politzer, P.; Murray, J. S., Impact Sensitivity and the Maximum Heat of Detonation. *J. Mol. Model.* **2015**, *21*.
6. Kinney, G. F.; Graham, K. J., *Explosive Shocks in Air*, 2nd ed.; Springer-Verlag, 1985.
7. Mathieu, D., Sensitivity of Energetic Materials: Theoretical Relationships to Detonation Performance and Molecular Structure. *Ind. Eng. Chem. Res.* **2017**, *56*, 8191-8201.
8. Politzer, P.; Murray, J. S., High Performance, Low Sensitivity: Conflicting or Compatible? . *Propellants Explos. Pyrotech.* **2016**, *41*, 414.
9. Xiong, X.; He, W.; Xiong, Y.; Xue, X.; Yang, H.; Zhang, C., Correlation between the Self-Sustaining Ignition Ability and the Impact Sensitivity of Energetic Materials. *Energetic Materials Frontiers* **2020**, *1*, 40-49.
10. Curtiss, L. A.; Raghavachari, K.; Redfern, P. C.; Pople, J. A., Assessment of Gaussian-2 and Density Functional Theories for the Computation of Enthalpies of Formation. *J. Chem. Phys.* **1997**, *106*, 1063-1079.
11. Curtiss, L. A.; Raghavachari, K.; Redfern, P. C.; Pople, J. A., Assessment of Gaussian-3 and Density Functional Theories for a Larger Experimental Test Set. *J. Chem. Phys.* **2000**, *112*, 7374-7383.
12. Ohlinger, W. S.; Klunzinger, P. E.; Deppmeier, B. J.; Hehre, W. J., Efficient Calculation of Heats of Formation. *J. Phys. Chem. A* **2009**, *113*, 2165-2175.
13. Mathieu, D., Atom Pair Contribution Method: Fast and General Procedure to Predict Molecular Formation Energies. *J. Chem. Inf. Model.* **2018**, *58*, 12-26.
14. Guthrie, J. P., Heats of Formation from DFT Calculations: An Examination of Several Parameterizations. *J. Phys. Chem. A* **2001**, *105*, 9196-9202.
15. Cawkwell, M. J.; Burch, A. C.; Ferreira, S. R.; Lease, N.; Manner, V. W., Atom Equivalent Energies for the Rapid Estimation of the Heat of Formation of Explosive Molecules from Density Functional Tight Binding Theory. *J. Chem. Inf. Model.* **2021**, *61*, 3337-3347.
16. Byrd, E. F. C.; Rice, B. M., Improved Prediction of Heats of Formation of Energetic Materials Using Quantum Mechanical Calculations. *J. Phys. Chem. A* **2006**, *110*, 1005-1013
17. Becke, A. D., Density Functional Thermochemistry. III. The Role of Exact Exchange. *J. Chem. Phys.* **1993**, *98*, 5648.
18. Frisch, M. J., et al. *Gaussian 16 Rev. C.01*, Wallingford, CT, 2016.
19. Mayer, I., Charge, Bond Order and Valence in the Ab Initio Scf Theory. *Chem. Phys. Lett.* **1983**, *97*, 270.
20. Wiberg, K. B., Application of the Pople-Santry-Segal Cndo Method to the Cyclopropylcarbinyl and Cyclobutyl Cation and to Bicyclobutane. *Tetrahedron* **1968**, *24*, 1083.
21. Elstner, M.; Porezag, D.; Jungnickel, G.; Elsner, J.; Haugk, M.; Frauenheim, T.; Suhai, S.; Seifert, G., Self-Consistent-Charge Density-Functional Tight-Binding Method for Simulations of Complex Materials Properties. *Phys. Rev. B* **1998**, *58*, 7260-7268.
22. Cawkwell, M. J.; Perriot, R., Transferable Density Functional Tight Binding for Carbon, Hydrogen, Nitrogen, and Oxygen: Application to Shock Compression. *J. Chem. Phys.* **2019**, *150*, 024107.
23. Burgess, D. R., Thermochemical Data. In *NIST Chemistry Webbook, Nist Standard Reference Database Number 69*, Lindstrom, P. J.; Mallard, W. G., Eds. National Institute of Standards and Technology: Gaithersburg MD, 2022.
24. O'Boyle, N. M., Banck, M., James, C. A., Morley, C., Vandermeersch, T., and Hutchinson, G. R., Open Babel: An open chemical toolbox, *J. Cheminf.*, **3**, 33 (2011).
25. Bruker (2021). *APEX4*. Bruker AXS Inc., Madison, Wisconsin, USA.

26. Agilent (2014). *CrysAlis PRO*. Agilent Technologies Ltd, Yarnton, Oxfordshire, England.
27. Dolomanov, O. V., Bourhis, L. J., Gildea, R. J., Howard, J. A. K.; Puschmann, H. OLEX2: a complete structure solution, refinement and analysis program. *J. Appl. Crystallogr.* **2009**, *42*, 339– 341, DOI: 10.1107/s0021889808042726.
28. Sheldrick, G. M. SHELXT- Integrated space-group and crystal-structure determination. *Acta Crystallogr., Sect. A: Found. Adv.* **2015**, *71*, 3-8. DOI:10.1107/s2053273314026370.
29. Sheldrick, G. M. Crystal structure refinement withSHELXL. *Acta Crystallogr., Sect. C: Struct. Chem.* **2015**, *71*, 3-8. DOI: 10.1107/s2053229614024218.
30. C. F. Macrae, I. Sovago, S. J. Cottrell, P. T. A. Galek, P. McCabe, E. Pidcock, M. Platings, G. P. Shields, J. S. Stevens, M. Towler and P. A. Wood, Mercury 4.0: from visualization to analysis, design and prediction. *J. Appl. Cryst.*, **53**, 226-235, 2020. DOI: 10.1107/S1600576719014092.